

**Pre-biotic molecules and dynamics in  
the ionosphere of Titan: a space  
weather station perspective**

**Licentiate thesis**

Oleg Shebanits

January 28th, 2014



## Abstract

Saturn's largest moon Titan (2575 km radius) is the second largest in the Solar system. Titan is the only known moon with a fully developed nitrogen-rich atmosphere with ionosphere extending to ~2000 km altitude, hosting complex organic chemistry. One of the main scientific interests of Titan's atmosphere and ionosphere is the striking similarity to current theories of those of Earth ~3.5 billion years ago. The Cassini spacecraft has been in orbit around Saturn since 2004 and carries a wide range of instruments for investigating Titan's ionosphere, among them the Langmuir probe, a "space weather station", manufactured and operated by the Swedish Institute of Space Physics, Uppsala.

This thesis reviews the first half of the PhD project on the production of pre-biotic molecules in the atmosphere of Titan and early Earth, focusing on the ion densities and dynamics in Titan's ionosphere derived from the *in-situ* measurements by the Cassini Langmuir probe.

One of the main results is the detection of significant, up to  $\sim 2300 \text{ cm}^{-3}$ , charge densities of heavy (up to  $\sim 13000 \text{ amu}$ ) negative ions in Titan's ionosphere below 1400 km altitude. On the nightside of the ionosphere at altitudes below 1200 km, the heavy negative ion charge densities are comparable to the positive ion densities and are in fact the main negative charge carrier, making this region of the ionosphere exhibit properties of dusty plasma. The overall trend is the exponential increasing of the negative ion charge densities towards lower altitudes.

Another important result is the detection of ion drifts that between 880-1100 km altitudes in Titan's ionosphere translate to neutral winds of 0.5-5.5 km/s. Ion drifts define three regions by altitude, the top layer (above  $\sim 1600 \text{ km}$  altitude) where the ions are frozen into the background magnetic field, the dynamo region (1100 – 1600 km altitudes) where the ions are drifting in partly opposing directions due to ion-neutral collisions in the presence of the magnetic and electric fields and the bottom layer (below 1100 km altitude) of the ionosphere, where the ions are coupled to neutrals by collisions.

*If you try and take a cat apart to see how it works, the first thing you have on your hands is a non-working cat.*

— Douglas Adams



## List of Papers

This thesis is based on the following papers, which are referred to in the text by their Roman numerals.

- I **Shebanits, O.**, J.-E. Wahlund, K. Mandt, K. Ågren, N. J. T. Edberg, and J. H. Waite (2013), Negative ion densities in the ionosphere of Titan–Cassini RPWS/LP results, *Planetary and Space Science*, 84, 153-162
- II **Shebanits O.**, Wahlund, J.-E., Edberg, N. J. T., Andrews, D. J., Crary, F. J., Wellbrock, A., Coates, A. J., Mandt, K. E., Waite Jr, J. H., On Ion Drifts and Neutral Winds in Titan’s Thermosphere. To be submitted to *Journal of Geophysical Research*.

All reprints were made with permission from the respective publishers.

## Papers not included in the thesis

Edberg, N.J.T., Andrews, D.J., **Shebanits, O.**, Ågren, K., Wahlund, J.E., Opgenoorth, H.J., Cravens, T.E., Girazian, Z., 2013a. Solar cycle modulation of Titan's ionosphere. *Journal of Geophysical Research: Space Physics* 118, 5255-5264.

Edberg, N.J.T., Andrews, D.J., **Shebanits, O.**, Agren, K., Wahlund, J.E., Opgenoorth, H.J., Roussos, E., Garnier, P., Cravens, T.E., Badman, S.V., Modolo, R., Bertucci, C., Dougherty, M.K., 2013b. Extreme densities in Titan's ionosphere during the T85 magnetosheath encounter. *Geophysical Research Letters* 40, 2879-2883.

Vigren, E., Galand, M., **Shebanits, O.**, Wahlund, J.E., Geppert, W.D., Lavvas, P., Vuitton, V., Yelle, R.V., 2014a. Increasing Positive Ion Number Densities Below the Peak of Ion-Electron Pair Production in Titan's Ionosphere. *The Astrophysical Journal* 786, 69.

Vigren, E., Galand, M., Yelle, R.V., Wellbrock, A., Coates, A.J., Snowden, D., Cui, J., Lavvas, P., Edberg, N.J.T., **Shebanits, O.**, Wahlund, J.E., Vuitton, V., Mandt, K., 2014b. Ionization balance in Titan's nightside ionosphere. *Icarus* 248, 539-546.

# Contents

Abbreviations.....	viii
Introduction.....	ix
1 Titan .....	11
1.1 Magnetospheric environment .....	11
1.2 Ionosphere: a temporal perspective .....	13
1.2.1 Previously on Titan... ..	13
1.2.2 Recent RPWS/LP results.....	16
1.2.3 In the not-so-distant future .....	18
2 Measurements .....	19
2.1 Langmuir probe theory .....	19
2.2 Spacecraft-Plasma interactions .....	21
2.3 Details of ion measurements.....	23
3 Summary of publications .....	29
3.1 Paper I.....	29
3.2 Paper II.....	30
3.3 Papers not included in this thesis:.....	31
4 Bibliography .....	32

# Abbreviations

CAPS	Cassini Plasma Spectrometer
DC	Direct current
ELS	Electron Spectrometer
ENA	Energetic Neutral Atom
EUV	Extreme Ultra-Violet
IBS	Ion Beam Spectrometer
INMS	Ion and Neutral Mass Spectrometer
JPL	Jet Propulsion Laboratory (NASA)
LP	Langmuir Probe
MSSL	Mullard Space Science Laboratory
OML	Orbital Motion Limited
PAH	Polycyclic Aromatic Hydrocarbon
RPWS	Radio and Plasma Wave Science
s/c	Spacecraft
SKR	Saturn Kilometric Radiation
SLT	Saturn Local Time
SZA	Solar Zenith Angle
SWRI	Southwest Research Institute

# Introduction

Saturn and its moons are a miniature model of a solar system. Interaction of its magnetospheric plasma with its moons resembles that of solar wind and planets, its rings offer insights into protoplanetary disks and two of its moons, Titan and Enceladus, may push our definitions of habitability.

Titan is the second biggest moon in our solar system and the only one with a fully formed dense atmosphere (pressure  $\sim 1.6 \times$  Earth's at the surface) that extends to more than half its radius above the surface, consisting to 97% of nitrogen and up to 2.7% of methane (Niemann et al., 2005; Waite et al., 2005; Coustenis et al., 2007). The atmosphere is primarily ionized by the solar EUV/X-rays, with lesser contributions from Saturn's magnetospheric particles and cosmic radiation (Cravens et al., 2005; Wahlund et al., 2005; Ågren et al., 2007; Galand et al., 2010; Shebanits et al., 2013). The ionization triggers complex organic chemistry, forming heavier organics (hydrocarbons), which are thought to be precursors to aerosols (tholins<sup>1</sup>) responsible for the orange haze of the moon (Sagan et al., 1993; Coates et al., 2007; Waite et al., 2007; Vuitton et al., 2009; Lavvas et al., 2013). The atmospheric composition along with chemistry has been compared to the models of Earth  $\sim 3.5$  Myrs ago (Pavlov et al., 2003; Tian et al., 2008).

All this leads us to the overarching scientific interest, beginning with the two papers included in this thesis: production of pre-biotic molecules in the atmosphere of Titan and early Earth. We approach the topic from the space physics point of view, focusing on plasma densities and drifts derived from the *in-situ* measurements by the Cassini spacecraft (*s/c*).

The Cassini *s/c* has been in orbit around Saturn since 2004 and has completed 107 targeted flybys of Titan until the end of 2014. A total of 127 are planned until the end of the mission in 2017. The *in-situ* measurements used in the papers I & II are primarily from the Radio and Plasma Wave Science Langmuir Probe (RPWS/LP), complemented by data from the Cassini Plasma Spectrometer package, Electron Spectrometer (CAPS/ELS) and Ion Beam Spectrometer (CAPS/IBS) as well as the Ion and Neutral Mass Spectrometer (INMS) and the magnetometer (MAG).

---

<sup>1</sup> From Greek “θόλος” meaning “muddy”, introduced by Sagan, C., Khare, B.N., 1979. Tholins: organic chemistry of interstellar grains and gas. *Nature* 277, 102-107.

Section 1 gives an overview of Titan's ionosphere and highlights the relevant processes. The basic principles of the instruments are covered in Section 2. Publications are summarized in Section 3. All figures are used with permission from respective publishers.

# 1 Titan

## 1.1 Magnetospheric environment

As mentioned above, Titan’s atmosphere is partly ionized by the impacts of Kronian<sup>2</sup> magnetospheric energetic particles, perhaps one of the smallest influences of the giant planet’s magnetospheric environment. The ionosphere is highly conductive and interacts with Saturn’s magnetic field and the magnetospheric plasma it carries, inducing a magnetosphere around Titan complete with an elongated tail and causing exospheric escape of neutrals by charge exchange collisions (Johnson et al., 2010; Strobel et al., 2014, and references therein) and ion escape (Edberg et al., 2011). This interaction resembles that between the solar wind and the ionospheres of Mars and Venus (Nagy et al., 2004). There are two differences though: the direction of incoming magnetospheric plasma is not the same as the Sun-ward direction for Titan, and the Kronian magnetospheric plasma is sub-magnetosonic - no bow shock is formed at Titan (Wahlund et al., 2014). This interaction (shown in Figure 1) influences chemistry in Titan’s ionosphere by energy inputs (energetic particles, collisional heating, plasma waves), introduction of traces of watergroup ions, ion pickup outflows and bulk plasma wake outflows (see e.g. Coustenis et al., 2007; Sittler et al., 2009; Sittler et al., 2010; Wahlund et al., 2014) and may be driving neutral winds in Titan’s thermosphere (Paper II).

The magnetospheric plasma flow at Titan varies periodically ( $\sim 10.7$  h) with Saturn Kilometric Radiation (SKR), the dynamic pressure of the solar wind which causes “flapping” of the plasma sheet (see e.g. Arridge et al. (2008); Morooka et al. (2009) and the references therein) and the seasons of Saturn due to changing inclination of the plasma sheet. Additionally, since Titan’s orbit is at  $\sim 20$  Saturn Radii ( $R_S$ ), the moon may be subjected to the shocked solar wind plasma in Saturn’s magnetosheath (or even solar wind itself) – based on a magnetosphere model, the probability to “catch” Titan outside Saturn’s magnetosphere between Saturn and the Sun has been calculated to 5.5% (Arridge et al., 2006; Achilleos et al., 2008). Such excursion events have indeed been observed during three Titan flybys to date, T32, T85 and T96 (e.g. Bertucci et al., 2008; Garnier et al., 2009; Edberg et al., 2013b;

---

<sup>2</sup> Saturnian, from *Κρόνος*, the Greek name of Saturn

Bertucci et al., 2014 (submitted) – out of 101, consistent with the theoretical estimate mentioned above. For all other flybys Titan has been inside the magnetosphere, bracing the impact of  $\sim 120$  km/s corotational plasma flow of Saturn's magnetodisk (Thomsen et al., 2010; Arridge et al., 2012). The magnetospheric plasma also carries with it Saturn's magnetic field of  $\sim 5$  nT at Titan's orbit, directed mainly vertically southwards (Bertucci et al., 2009). The influence of the magnetic field and magnetospheric flux on the ionospheric currents (including neutral winds) is further discussed in the summary of Paper II (Section 3.2).

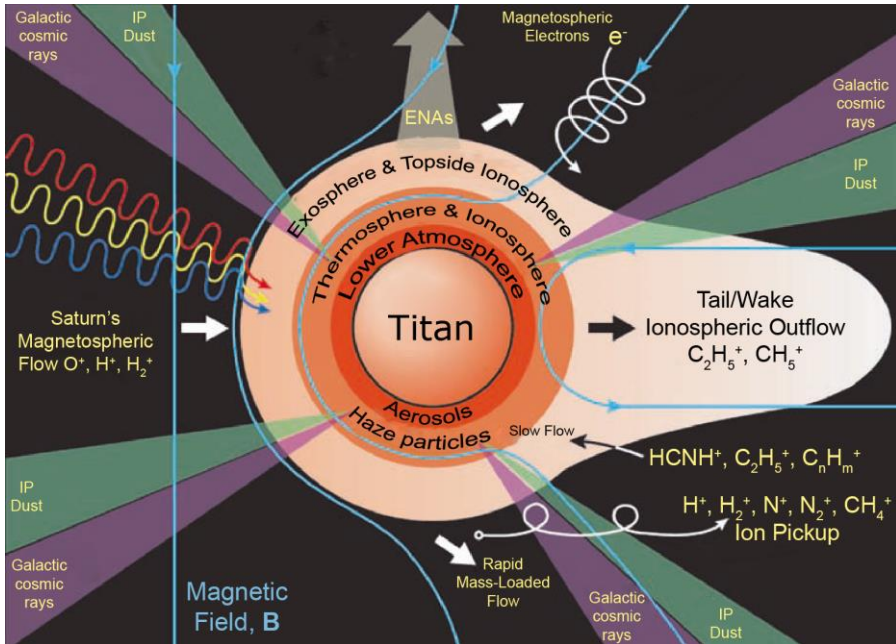


Figure 1. Schematic representation of the Saturn's magnetospheric particle and energy input, draping of the magnetic field due to Titan's induced magnetosphere and energetic neutral atom (ENA) emissions from charge transfer collisions between magnetospheric ions and ionospheric neutrals. Red, yellow and blue waves represent energy inputs from solar IR, visible and UV radiation, resp. From (Sittler et al., 2010), in turn adapted from (Waite et al., 2004).

## 1.2 Ionosphere: a temporal perspective

*If I have seen further it is by standing  
on the shoulders of Giants.*

— Isaac Newton

### 1.2.1 Previously on Titan...

The investigation of Titan's ionosphere began with its detection during the first targeted flyby of the moon by Voyager I in 1980, coming as close as 4403 km altitude (Bird, 1997). Two decades before the arrival of Cassini there was only a very limited knowledge of the composition of the atmosphere and ionosphere (Coustenis et al., 2010; Cravens et al., 2010b and references therein). Laboratory experiments suggested the tholins in Titan's signature orange haze to form from the chemically "close relatives" of methane and nitrogen like polycyclic aromatic hydrocarbons (PAHs) – relatively simple molecules – in the atmosphere around altitudes of few hundred kilometres, where the haze layers were observed by the Voyager (Sagan et al., 1993; Thompson et al., 1994). A big surprise came after arrival of Cassini: the discovery of the negative ions by the *in-situ* CAPS/ELS measurements (Coates et al., 2007). Due to the extreme mass/charge ratios of the negative ions (up to 13800 amu/q) they were gradually accepted as more suitable candidates for aerosol/tholin precursors. Thus the observations of positive and negative ions (Wahlund et al., 2005; Waite et al., 2007; Crary et al., 2009; Sittler et al., 2009; Wahlund et al., 2009b; Coates et al., 2010) and the models based on measurements have led to the current idea: the ionization of the atmosphere initiates the reactions in the top layers of the ionosphere (~1600-1800 km altitude), the ions gradually grow and precipitate, forming aerosols already around ~1000 km altitude, in the lower ionosphere as illustrated in Figure 2. The negative ion masses and densities showed a dependence on altitudes and local time at Titan (Coates et al., 2009; Shebanits et al., 2013; Wellbrock et al., 2013), with stronger presence of higher mass groups towards lower altitudes, which further strengthened the concept.

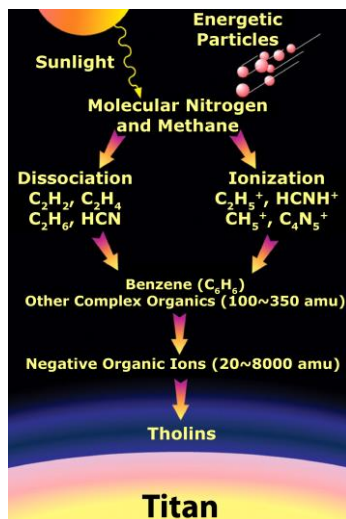


Figure 2. Aerosol/tholin formation in Titan's ionosphere. Adapted from Waite et al. (2007)

The formation region of the aerosols and/or their precursors turned out to be situated in Titan's ionosphere, neatly within reach of the *in-situ* measurements by particle/plasma instruments of Cassini, which can derive a wide set of plasma properties. The measurements relevant for this thesis include: the charge densities of electrons and ions and electron temperatures from the RPWS/LP, neutral densities and masses from the INMS, positive and negative ion mass profiles from the CAPS/ELS and CAPS/IBS. As Cassini accumulated flybys of Titan and with it the data, the shape of its ionosphere was mapped, reflecting the "fluffiness" of the atmosphere of the moon (Figure 3). The ionosphere of Titan extends to about 1800 km altitude (0.7 Titan radii). The RPWS/LP-derived electron density peaks at altitudes around 1050 km dayside and 1150 km nightside (Ågren et al., 2009). Positive ion density peaks at ~1000 km while negative ion density peaks have been observed only occasionally at ~1000 km on dayside and are expected to be below the closest approach altitudes (Shebanits et al., 2013). Negative ion charge density profile from T40 flyby was found to be remarkably similar to aerosol density profile (at ~50 km lower altitude) from an aerosol growth model by Lavvas et al. (2013) for the same flyby, further supporting the scenario of aerosols forming from a mixture of complex organic ions.

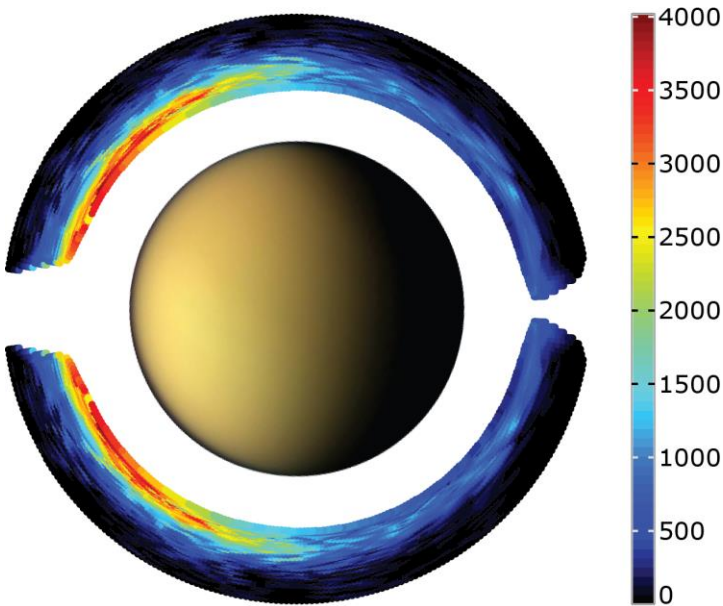


Figure 3. Titan's ionosphere (Sun to the left). Colour-coded: Solar Zenith Angle (SZA) & altitude fit to electron densities (colour-coded,  $\text{cm}^{-3}$ ), horizontally mirrored in the figure for illustrative purpose. The “holes” are due to lack of SZA coverage below  $20^\circ$  and close to  $180^\circ$  by the Cassini s/c. Image of Titan is a courtesy of NASA JPL archive<sup>3</sup>.

Interpretation of the RPWS/LP data (particularly the ion part of the current-voltage sweep characteristics) has come a long way in the last decade. The analysis tools and methods are constantly polished as the software is updated, even though the basic principles do not change. The most “game-changing” events for the analysis of Titan’s ionosphere data were the RPWS/LP measurements of the negative ions and dust (Ågren et al., 2012; Shebanits et al., 2013) and the ion drifts (Paper II). After the discovery of the negative ions by the CAPS/ELS (Coates et al., 2007), their influence was seen in the RPWS/LP measurements already during the first targeted flyby of Titan (Wahlund et al., 2005). However, only after accumulating the RPWS/LP data from a number of flybys could their substantial presence be revealed, more or less forcing their inclusion in the models, measurements and discussions of Titan’s ionosphere (Shebanits et al., 2013). The same extensive dataset was also needed to pinpoint the ion drift effects. These recent findings are summarized in the next section.

---

<sup>3</sup> <http://saturn.jpl.nasa.gov/photos/index.cfm>

### 1.2.2 Recent RPWS/LP results

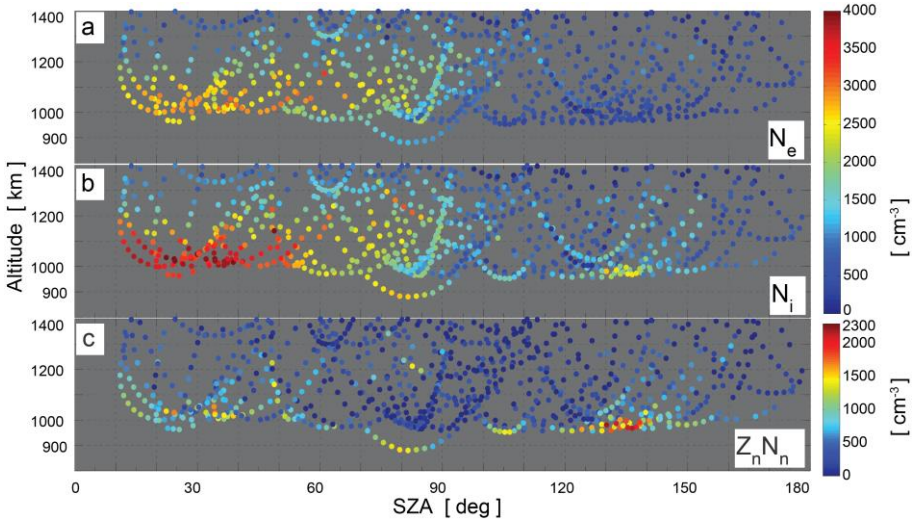


Figure 4. Altitude vs SZA map of charge densities (colour-coded) in Titan's ionosphere: (a) electrons, (b) positive ions, (c) negative ions. Note the separate colour scale for the negative ions. Adapted from Paper I (Shebanits et al., 2013). Includes flybys TA-T84.

The solar EUV is the main ionization source and as expected, the plasma densities in the ionosphere vary significantly with solar illumination (day-side/nightside and solar cycle) and altitude (Ågren et al., 2009; Edberg et al., 2013a; Edberg et al., 2013b; Shebanits et al., 2013). Typical plasma densities can be inferred from Figure 4, which shows the general structure of the ionosphere:

- on the dayside ( $SZA < 70^\circ$ ), the ionosphere is clearly dominated by electrons and positive ions; negative ions are present already at  $\sim 1200$  km altitudes
- over the terminator region ( $70^\circ < SZA < 110^\circ$ ) the overall charge densities gradually decrease while the peaks of the positive ion and electron densities move upwards in altitudes (see also Figure 3)
- on the nightside ( $SZA > 110^\circ$ ) the electron densities drop to  $\sim 500 \text{ cm}^{-3}$ , the ionosphere is dominated by positive and negative ions, exhibiting properties of dusty plasma at altitudes below 1100 km (Shebanits et al., 2013)

With measurements of the mean masses of ions (CAPS/ELS, CAPS/IBS), the magnetic field strength (MAG) and estimation of electric field upper limit of  $\sim 3 \mu\text{V/m}$  (Ågren et al., 2011), the ionosphere can be divided into another three regions by altitude (Figure 5, Paper II):

1. ions are frozen into the magnetic field (negligible collisions,  $\vec{E} \times \vec{B}$ -drifting magnetospheric ions, yellow-shaded);
2. dynamo region with positive and negative ions drifting in partly opposite directions due to collisions with neutrals in the presence of electric and magnetic fields (red-shaded);
3. collision-dominated region where ions and neutrals move together (blue-shaded in the zoom-in).

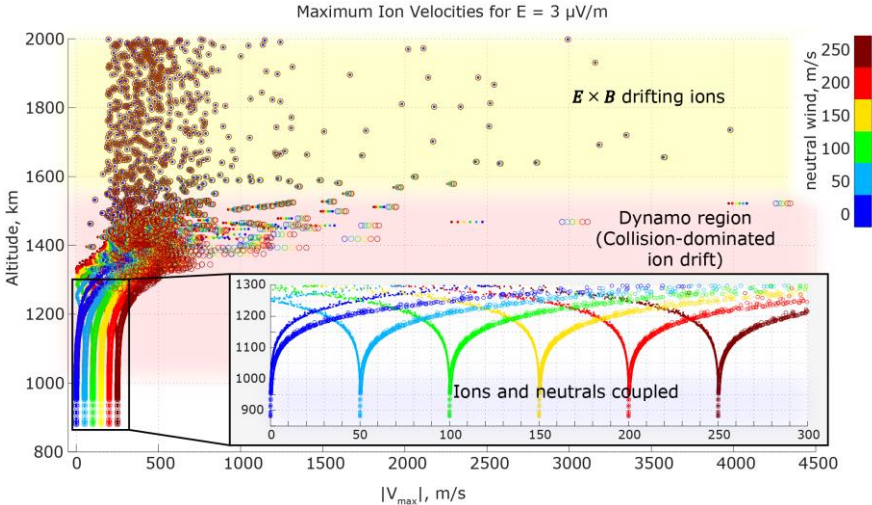


Figure 5. Color-coded: Maximum ion speed dependence on altitude and neutral winds for  $E = 3 \mu\text{V/m}$ . Dots and circles represent negative and positive ion velocities, resp. Simulated neutral winds of 0-250 m/s demonstrate the coupling of ions and neutrals in the collision-dominated region. Adapted from Paper II.

The ion drifts are relevant for this thesis because they influence the ion transport and (by the continuity equation) the chemistry in Titan's ionosphere. If the ion drifts in Cassini's reference frame are directed headwinds (or tailwinds), the ion fluxes measured by the RPWS/LP would increase (or decrease), which translates directly to an increase (or decrease) in the measured ion densities. Since the magnetic and electric fields are required, the ion drifts (and in the deep ionosphere, neutral winds) may be driven by the Kronian magnetospheric plasma flow. The strong collisional coupling between the ions and neutrals below 1100 km altitude has also been shown by Cravens et al. (2010a).

The ion drifts have been previously calculated from a global circulation model (Müller-Wodarg et al., 2008) and derived from a combined analysis of the line-of-sight INMS and CAPS/IBS data from 14 flybys of Titan (Crary et al., 2009) to a modest value of at most 240 m/s at altitudes of 1000-1200 km. However, the ionospheric ion fluxes continuously measured by RPWS/LP along the s/c trajectory during 55 flybys below 1400 km altitude (Paper II) required ion velocities approximately one magnitude larger, translating into

neutral winds of 0.5-2.5 km/s below altitudes of 1100 km (on average, as high as 5.5 km/s during T70). Ion velocities of similar magnitudes were also needed to explain the RPWS/LP measurements during T70 flyby (Ågren et al., 2012) and the dayside-to-nightside ion transport modelled by Cui et al. (2010) based on INMS, RPWS and MAG data. More detailed summary of Paper II results is given in Section 3.2.

### 1.2.3 In the not-so-distant future

The mean positive ion mass profiles used in analysis of RPWS/LP data were previously derived from measurements by the INMS, which (currently) is limited to particles of up to 100 amu. The CAPS/IBS has virtually no upper limit, but the CAPS instrument has been turned off since June 4<sup>th</sup> 2012<sup>4</sup>. Using the available data from both INMS and CAPS/IBS instruments, it is possible to introduce a correction for heavy-ions to the INMS dataset. Thus, data from CAPS/ELS, CAPS/IBS and RPWS/LP measurements may be combined to improve upon the existing ionospheric charge density profiles and to derive the average charge of the negative ions.

Cassini mission is planned to end in 2017 and will have toured Saturn's system for nearly half of a Kronian (and thus Titan) year (29.5 Earth years), providing a great opportunity to study seasonal changes of Titan's atmosphere and ionosphere. The beginning of the mission (2004) was during Titan's northern hemisphere spring, with equinox occurring during 2009. In the last years the northern hemisphere of the moon has had summer, which also coincided with solar maximum. The increased ionization by the solar EUV was seen in the measured electron densities in Titan's ionosphere (Edberg et al., 2013a).

Effect of solar EUV cycle on the ion densities and a multi-instrument case study are topics of ongoing investigations. The end goal of the project is the investigation of implications for the early Earth thermosphere and ionosphere. With the extreme EUV levels and stronger solar wind of a young Sun, the thermosphere of Earth would be extending to few Earth's radii (Tian et al., 2008), comparable with the weaker magnetosphere modelled by Tarduno et al. (2010) – similar to the interaction of Titan's ionosphere and induced magnetosphere with the Kronian magnetospheric plasma flow. With respect to its composition, Titan has very limited supply of water in the atmosphere (Kronian magnetospheric water group particles as mentioned above), compared to early Earth. Both environments seem to have the formation of the aerosols/tholins in the ionosphere (Raulin et al., 2010).

---

<sup>4</sup> <http://saturn.jpl.nasa.gov/news/significantevents/anomalies/>

## 2 Measurements

### 2.1 Langmuir probe theory

Electrostatic probes have been used for measurements of plasma properties for almost a century, based on the theory of current collectors in gaseous discharges (Mott-Smith and Langmuir, 1926). Two years after, the term “plasma” was introduced for a quasi-neutral<sup>5</sup> ionized gas (Langmuir, 1928). Here we review the probe theory for ion measurements in dense plasmas on the example of Titan’s ionosphere.

#### Orbital-Motion Limited theory

The Orbital-Motion Limited (OML) theory is based on independent trajectories of a particle speed distribution (Maxwellian for our purposes). The trajectories are defined by conservations of energy and (optionally) angular momentum (Laframboise and Parker, 1973).

Key points of the theory are **a**) no particle originates from the probe and **b**) the radius of the probe must be (much) smaller than one Debye length ( $\lambda_D$ , also called “screening length”) - otherwise there will be sheath effects and one should use the so-called Sheath Limited theory instead. The OML works fine for the ionospheric plasma of Titan where  $\lambda_D \sim 3 - 7$  cm.

The original equations by (Mott-Smith and Langmuir, 1926) for an isotropic plasma were upgraded by (Medicus, 1962) for space applications where the probe would be moving in plasma. For a spherical probe, the collected ion current  $I$  for a set probe potential  $U$  is:

$$I = -qn r_{ip}^2 \cdot \sqrt{\frac{\pi p k_b T}{2m}} \cdot \left[ e^{-A} \cdot \left( 1 - \frac{v_1}{v_{sc}} \right) + e^{-B} \cdot \left( 1 + \frac{v_1}{v_{sc}} \right) + \sqrt{\frac{2k_b T}{m v_{sc}^2}} \cdot \left( \frac{m v_{sc}^2}{k_b T} + 1 - \frac{2qU}{k_b T} \right) \cdot \sqrt{\pi} \left( \operatorname{erf}(\sqrt{A}) - \operatorname{erf}(\sqrt{B}) \right) \right] \quad (1)$$

where  $q$ ,  $n$ ,  $m$  and  $T$  are ion charge, density, mass and temperature resp.,  $k_b$  is the Boltzmann constant and  $v_{sc}$  is the spacecraft (s/c) speed relative to the plasma (SI units),  $A = \frac{m}{2k_b T} (v_1 + v_{sc})^2$ ,  $B = \frac{m}{2k_b T} (v_1 - v_{sc})^2$ ,  $\operatorname{erf}(x) = \frac{2}{\sqrt{\pi}} \int_0^x e^{-y^2} dy$ ,  $v_1$  is the minimum relative speed a particle needs to overcome

---

<sup>5</sup> *quasi-neutrality*: approximately (sufficiently) equal amounts of positive and negative charge carriers

the potential barrier defines as  $v_1 = \sqrt{2qU/m}$  for repelling potentials and  $v_1 = 0$  for attracting potentials.

OML theory is not locked to spherical probes as it can be applied to cylindrical and general geometry. Interested readers are referred to Laframboise and Parker (1973) who show that the expression for ideal spheres also holds for some deviations from the perfect shape, such a spherical probe on a boom. However, the ion current has been observed to be linear within the noise level of 100 pA, proving Equation ( 1 ) to be unnecessarily complicated. Instead, an approximation by Fahleson et al. (1974) is employed, giving currents as

$$I = \begin{cases} I_0(1 - \chi) & \text{for attracting potentials} \\ I_0e^{-\chi} & \text{for repelling potentials} \end{cases} \quad (2)$$

where

$$I_0 = -qnA_{LP} \sqrt{\frac{v^2}{16} + \frac{k_bT}{2\pi m}} \quad \text{and} \quad \chi = \frac{2q|U_{bias} + U_{float}|}{mv^2 + 2k_bT} \quad (3)$$

$U_{bias}$  is the probe potential and  $U_{float}$  is the s/c floating potential<sup>6</sup>, determined by s/c charging (see Section 2.2 below).

These equations give an extremely good approximation for ion and electron currents compared to the full Medicus (1962) expressions and are far easier to fit to data. For ions, the thermal energy component  $k_bT$  can often be neglected<sup>7</sup> (since they are heavy) in a fast flowing plasma (= fast flying s/c). Furthermore, for large negative ions  $\chi$  is small due to large mass (and for  $|U_{bias}| < 4$  V), thus the exponential can be approximated by  $1 - \chi$  (large ions give a nearly constant current) (Shebanits et al., 2013).

### Photoelectron current

An important effect to consider for Langmuir probe measurements in space is the photoelectron emission. Lab experiments by Grard (1973) have shown that although photoelectron current depends on the material, the energy distribution shape is similar and can be approximated by a double-Maxwellian (dominant peak at  $\sim 2$  eV). If the photoelectron sheaths of the probe and s/c are overlapping, a “stray” current may leak through.

On a side note, if the LP is mounted on a stub (e.g. Cassini, see Figure 7) rather than a wire boom (e.g. Cluster), the probe may shadow the stub and the s/c may shadow the probe, causing a dependence of the photoelectron current on the s/c attitude (Jacobsen et al., 2009; Morooka et al., 2009; Holmberg et al., 2012).

For Titan’s ionosphere, the photoelectron current is typically negligible, being  $\sim 0.1$  times the ion current at altitudes of 1600-1400 km and vanishing

---

<sup>6</sup> Defined for a certain *surface* on a s/c, not to be confused with the s/c potential

<sup>7</sup> This introduces errors of  $< 5.6\%$  for ion currents in Titan’s ionosphere below 1400 km altitudes ( $\sim 150$  K ions with s/c-relative velocities  $> 3000$  m/s), well below the RPWS/LP ion density measurement error of 10%

completely due to solar EUV extinction below  $\sim 1400$  km altitudes. Nevertheless, it is removed in the analysis as a standard procedure via an application of the solar EUV extinction model.

## 2.2 Spacecraft-Plasma interactions

An object immersed in plasma will be hit by the charge carriers, some giving it the charge and some taking it away. This means that an object in plasma will accumulate potential (in relation to plasma) until the net charge flux is zero. Naturally, for s/c applications it is called the spacecraft potential ( $U_{sc}$ ). In addition, s/c in sunlight will be “ionized” by solar photons (photoelectron emission) as well as impacting particles (secondary electron emission), which may add to the current balance for the s/c potential. These and other related issues are discussed below.

### Spacecraft charging

Awareness of s/c charging began with the first ionosphere measurements with rockets. Understanding of the phenomenon has been developing since the launch of Sputnik in 1957. The charging of an object in plasma usually depends only on the electron energies and densities, since the flux of light electrons is typically much larger than flux of much heavier ions. Furthermore, in a dense plasma ( $I_{ion}, I_e \gg I_{ph}$ )  $U_{sc}$  is only dependant on the electron temperature; in a tenuous plasma ( $I_{ion} \ll I_e \sim I_{ph}$ ) it may be used to derive the charge densities (Garrett and Whittlesey, 2000). In dusty plasmas (described below), the metallic plates of a s/c and/or an instrument are subject to triboelectric charging: a charge transfer from dust particles due to frictional contact or a difference in work functions of the dust and metal surfaces (Barjatya and Swenson, 2006), a yet another mechanism that influences the s/c potential. However, so far no extra charging has been detected in dust-rich environments like Enceladus’ plume (Morooka et al., 2011) and deep ionosphere of Titan (Wahlund et al., 2009b).

Potential of RPWS/LP on Cassini is defined relatively to  $U_{sc}$  so the latter can be measured “directly”. For Titan’s ionosphere, the Cassini s/c potential is typically very stable on the order of 0.5-1.5 V (Wahlund et al., 2005; Ågren et al., 2007) and the influence of the photoelectron current shifts it between dayside and nightside only by 0.1-0.2 V. Below 1600 km altitude  $U_{sc}$  has no impact on the RPWS/LP measurements because the instrument is mounted on a 1.5 m boom, which is much longer than the local Debye length of up to 8 cm. Generally though, the s/c charging is of great concern for all missions and must be taken into account at design stage – depending on the environment,  $U_{sc}$  can reach kilovolts (Eriksson and Wahlund, 2006). Usual practice is to make a surface of the s/c conductive so that it has the same potential, avoiding the potential differences that cause arc discharges and fry the electronics.

## Wake effects

A s/c in a plasma topic is not complete without discussing wake effects. A wake forms in a supersonic flow behind the s/c, that is when the kinetic energy of plasma ions  $m_i v_i^2/2$  exceeds their thermal energy  $k_b T_i$  (and the s/c potential  $eU_{sc}$ ). Electrons on other hand are subsonic in an ionosphere, which means that while ions are depleted in a wake, electrons fill it up, giving it a negative potential. If the ion kinetic energy is smaller than the s/c potential, the ions will not reach the s/c at all and an enhanced wake will form (Figure 6).

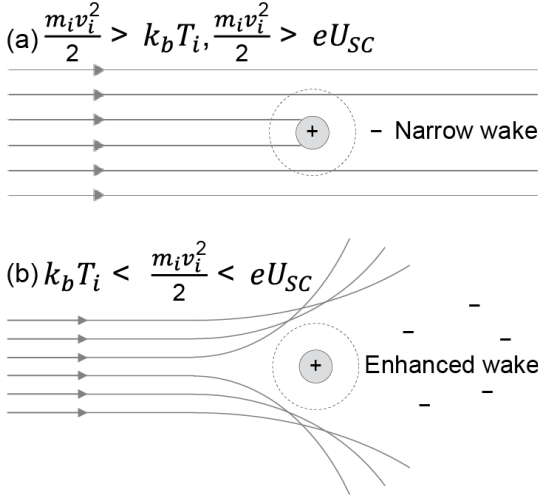


Figure 6. Wake formation in supersonic plasma. For Cassini case (a) is a typical wake in Titan's ionosphere while (b) is only relevant for tenuous magnetospheric plasma.

A usual practice is to adjust the s/c attitude as to avoid the wake with the plasma measurement instruments. Yet, however undesirable the wake artefacts may be, some plasma properties can be derived from wake formation - for instance combined measurements of two LP probes and an electron drift instrument can (with application of a simple model) give estimates of the flow velocity vector (Engwall et al., 2006).

During the RPWS/LP measurements of Titan's ionosphere, the probe was in the s/c wake during (so far) only three early flybys, T3, T8 and T13. T3 and T8 are outside the altitude range relevant for this work, T13 data has been removed from the dataset.

## Dusty plasma

Dusty plasmas have been observed in the noctilucent clouds and D-region of ionosphere on Earth (Havnes et al., 1996), Enceladus plume (Morooka et al., 2011), E-ring of Saturn (Kurth et al., 2006; Srama et al., 2006), deep ionosphere of Titan (Shebanits et al., 2013) and cometary comas. A dusty plasma is defined by the so-called dusty plasma condition,  $r_d \ll d \ll \lambda_D$ , i.e. the dust grain radius  $r_d$  must be small compared to the intergrain distance  $d$ , which in

turn must be smaller than Debye length  $\lambda_D$ . When this condition is met, the dust particles exhibit collective behaviour because they are coupled to the plasma, which is then called “dusty plasma”. Otherwise, the system is referred to as “dust in plasma” (Shukla, 2001; Morooka et al., 2011).

Dust particles in a plasma resemble tiny s/c:s: electrons will stick to them and charge them negatively in the same way (Horányi et al., 2004; Wahlund et al., 2009a). Density of electrons in such dusty plasma decreases with increasing dust density. For instance, a study by Morooka et al. (2011) shows that the depletion of electrons in Enceladus plume is nearly 100%. Although not so extreme, electron depletion is also the case in the deep (<1100 km altitude) ionosphere of Titan, reaching electron to positive ion density ratios of ~0.1 (Shebanits et al., 2013). In such cases, the dust particles become primary negative charge carriers.

Dusty plasma exhibits different properties than “normal” plasma because of the much heavier negative particles (compared to positive ions). Heavier ions have more inertia and their motion is less affected by the electromagnetic forces – but because of their charge they still influence the rest of plasma. An example of such different behaviour is Kronian E-ring, populated by the dust from Enceladus (Kurth et al., 2006, and references therein), where the dust velocities are tending towards Keplerian<sup>8</sup> motion rather than not following the corotation of the magnetospheric plasma.

## 2.3 Details of ion measurements

### **Langmuir Probe (RPWS/LP)**

Part of the Radio Plasma and Wave Science (RPWS) package of Cassini s/c, the Langmuir Probe has been built and is operated by the Swedish Institute of Space Physics. It is a spherical probe with diameter of 2.5 cm, mounted on a 1.5 m boom and has three modes of operation, voltage sweep, density and cleaning (for more detailed description, see Gurnett et al., 2004; Wahlund et al., 2009a; Morooka et al., 2011)

---

<sup>8</sup> Here: governed by gravity



Figure 7. RWPS/LP, engineering model. The red arrow marks the stub that has same potential as the probe.

Voltage sweeps measure the current to the probe for voltage ranges of  $\pm 32$  V or  $\pm 4$  V (for targeted flybys of moons) every 24 s, shifting the voltage in 512 steps under 0.5 s (for Titan flybys the speed of Cassini s/c is about 6 km/s, limiting the spatial resolution of the probe to  $\approx 3$  km). Targeted flybys usually have double-sweeps (down and up), giving 1024 points. Furthermore, to avoid capacitive charging effects<sup>9</sup>, the current is sampled twice, just after the voltage shift and just before the next shift (see Figure 8). Voltage sweep mode is used for simultaneous measuring of electron and ion characteristics.

For the density mode the probe is put at a constant voltage, allowing to sample the current with a high frequency (20 Hz). This mode is typically used for electron measurements. The cleaning mode is regularly used to remove any possible contamination of the probe surface. This is done by setting the probe to large negative potential (-100 V), thus sputtering the surface with high energy ions.

---

<sup>9</sup> Capacitors in the circuitry don't allow the current to instantly adapt to the voltage change

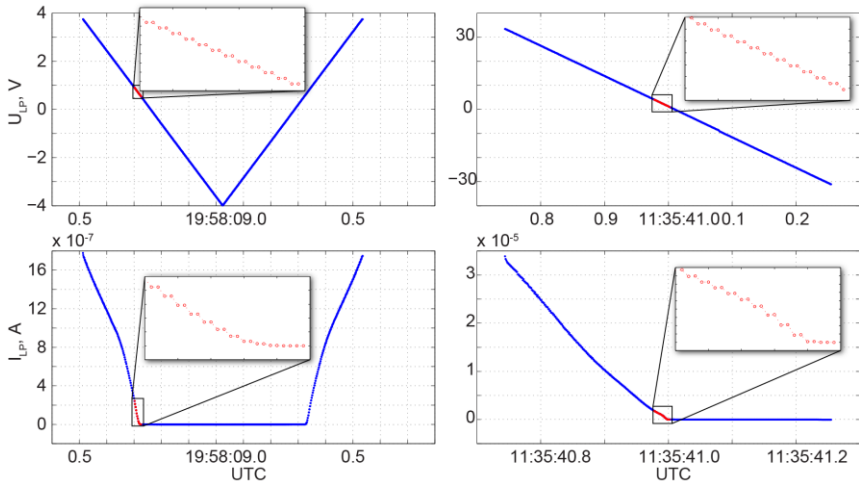


Figure 8. Examples of  $\pm 4$  V (left) and  $\pm 32$  V (right) voltage sweeps (top) with corresponding currents (bottom). Zoomed in areas show the double-sampling.

To derive ion parameters, analysis of sweep data is performed as follows:

1. The double-sampled current values are averaged and double-sweeps (if any) are folded into one to increase amount of data points.
2. The current is fitted to a linear curve  $m = a + U \cdot b (+I_{ph})$ , yielding the slope  $b$  and the DC-current  $a$ . The photoelectron current<sup>10</sup>  $I_{ph}$  can be removed in Titan's ionosphere by applying a simple solar extinction model for the dominant atmospheric species (Ågren et al., 2007).
3. Plasma densities, temperatures and speeds may be derived from the obtained fit parameters. Due to the “simplicity” of the ion current theory the analysis process can be largely automatized.

<sup>10</sup> As mentioned in Section 2.1, the photoelectron current is negligible in the ionosphere of Titan below 1400 km altitude as discussed in Section 2.1

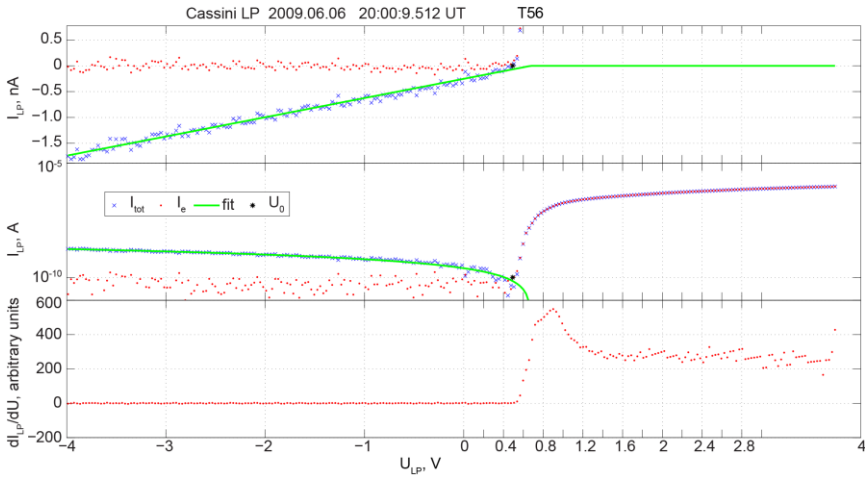


Figure 9. Current fit example from Titan flyby T56. Blue crosses show the total sampled current, red dots show the electron current for positive probe bias and the instrument noise for negative bias.

### Ion and Neutral Mass Spectrometer (INMS)

Built at NASA's Goddard Space Flight Centre's Planetary Atmospheres Laboratory and the University of Michigan's Space Physics Research Laboratory, INMS is a high-resolution particle instrument for measuring masses of neutral gas and ions up to 100 amu (Mandt et al., 2012). It has two modes of operation, closed ion source and open ion source (see Figure 10).

In *closed ion source*, the neutral gas collides with the walls of the spherical antechamber, attaining thermal equilibrium. Pressure gradient (created by the antechamber geometry) pushes the gas to the ion source, where it is ionized by electron guns and focused into the quadrupole mass analyser by electrostatic and quadrupole switching lenses.

In *open ion source*, the ions (or ionized neutrals) are again focused into the quadrupole mass analyser by the quadrupole switching lens. When neutrals are measured, ions are filtered out (trapped) by the deflectors in the cylindrical antechamber. When ions are measured, the neutrals are not ionized and do not react to the quadrupole switching lens. The charged particles are then processed by the quadrupole mass analyser that separates them by mass-to-charge ratios.

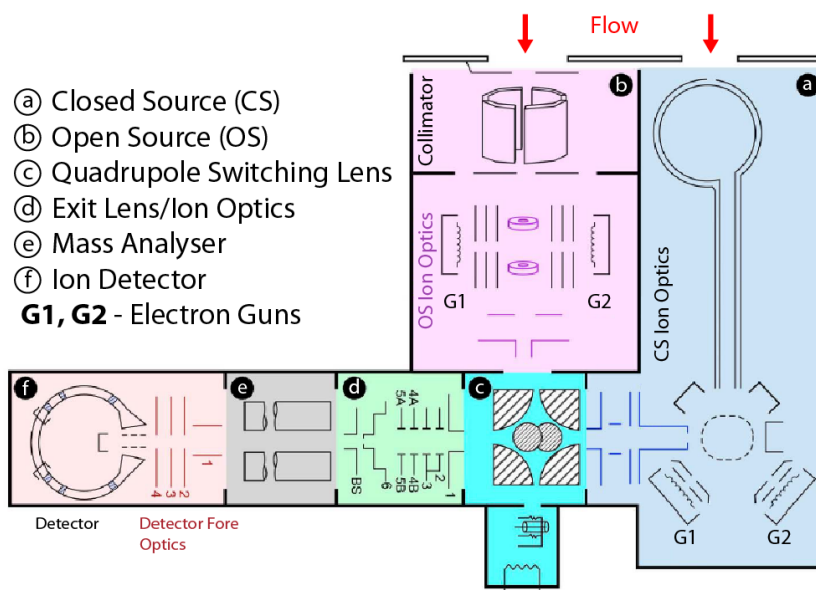


Figure 10. Schematic representation of INMS (adapted from Mandt et al., 2012)

### Electron Spectrometer (CAPS/ELS)

The Electron Spectrometer (ELS) is a part of Cassini Plasma Science package (Figure 11) manufactured by the Mullard Space Science Laboratory (MSSL). The instrument is a hemispherical top-hat electrostatic analyser, thus the angular and energy resolution is limited by its geometry and the micro-channel plate (8 anodes,  $20^\circ$  each). During a measurement, ELS sweeps through log-spaced voltages in accumulation intervals of 31.25 ms (for Titan, the default mode is used: 64 steps covering 0.6-28000 eV). Being an electrostatic analyser, ELS actually detects *energy/charge*, which is then converted to mass/charge. This must be kept in mind when looking at the negative ion data from ELS as the negative ions may have multiple charges – as the fact that the instrument was built to measure electrons, detection of negative ions was a major discovery for Titan (see e.g. Coates et al., 2007).

### Ion Beam Spectrometer (CAPS/IBS)

Similarly to CAPS/ELS, the Ion Beam Spectrometer (IBS) is a curved-electrode electrostatic analyser (Figure 11) made by the Southwest Research Institute (SWRI). It is designed for high-resolution measurements of positive ion flux over 0.6-28250 eV energy range. During operation the instrument performs a voltage scan in 255 steps over 2 s and can potentially cover 80% of all space (Young et al., 2004). Translating energy coverage to mass, IBS may provide mass/charge measurements up to  $\sim 1500$  amu, thus covering the vast majority of positive ion species in Titan's ionosphere.

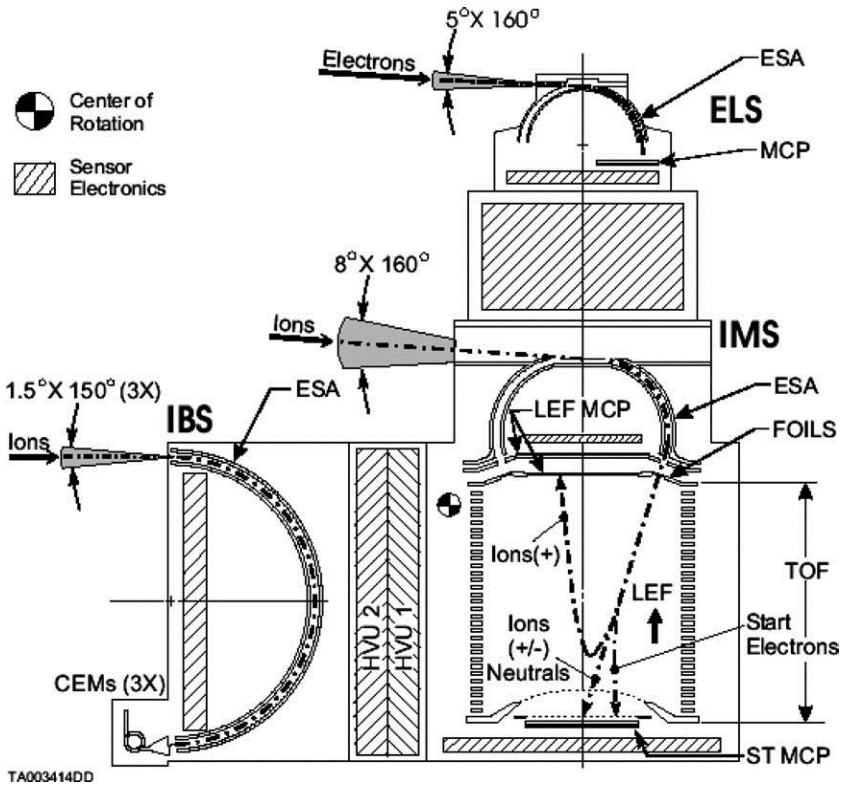


Figure 11. Cassini Plasma Spectrometer layout showing position and schematic representation of the IBS and ELS instruments. Adapted from (Young et al., 2004).

## 3 Summary of publications

### 3.1 Paper I

*Negative ion densities on the ionosphere of Titan – Cassini RPWS/LP results*

**Authors:**

O. Shebanits, J.-E. Wahlund, K. Mandt, K. Ågren, N.J.T. Edberg,  
J.H. WaiteJr

**Journal:**

Planetary and Space Science

**Status:**

Published

**Summary:**

In this paper we investigate the distribution of charge densities of positive and negative ions, as well as electrons, in Titan's ionosphere. A total of 47 flybys below 1400 km altitude were used, between Oct 2004 and July 2012. The charge densities were mapped to solar zenith angle and altitude, with main result being the significant amount of the negative ions, particularly on the nightside and below altitudes of 1000 km, where the free electrons are much less abundant than the ions ( $n_e/n_+ \sim 0.1 - 0.7$ ) - effectively increasing the ionization levels (typically based only on the electron densities).

Consistent with previous measurements, the main ionospheric peak is seen at altitudes increasing towards the terminator region. Negative ion charge densities increase exponentially with decreasing altitudes (down to the lowest flown altitudes of 880 km), reaching up to  $2500 \text{ cm}^{-3}$ . Measured positive ion densities reach values of  $4200 \text{ cm}^{-3}$ . The depletion of electrons on the nightside, together with large negative ion charge densities, imply dusty plasma properties: the dominant negative charge carriers are the heavy negative ions, with  $10^4$ - $10^6$  ions/Debye cube. Negative ions are predicted to have 1-2 charges.

Lower negative ion charge densities around the ecliptic polar regions as compared to the ecliptic equatorial region are another confirmation of the importance of the solar EUV for the ion production. Magnetospheric plasma impacts on the ionization was also investigated but no correlation was found.

### **My contribution to Paper I:**

I performed the RPWS/LP ion data analysis and had the main responsibility for writing the paper.

## 3.2 Paper II

*On Ion Drifts and Neutral Winds in Titan's Thermosphere*

### **Authors:**

O. Shebanits, J.-E. Wahlund, N.J.T. Edberg, D.J. Andrews, F.J. Crary, A. Wellbrock, A.J. Coates, K.E. Mandt, J.H. Waite Jr

### **Journal:**

Journal of Geophysical Research

### **Status:**

To be submitted

### **Summary:**

In this paper we investigate apparent deviations from the charge neutrality condition measured by Cassini RPWS/LP in the ionosphere of Titan at altitudes below 1400 km. The dataset used for this study consists of 55 flybys. Total ion current measured by the instrument consists of positive and negative ion fluxes, which if added together must match the independently measured electron flux. As mentioned in Section 1.2.2, the ion drifts affect the ion fluxes measured by the RPWS/LP. In Paper I this effect has been circumvented by using the electron density derived independently from the electron characteristics instead of the total ion density derived from the ion characteristics.

The resulting *differential ion flux* is defined as *the difference between the positive and negative ion fluxes to the probe*. Ionospheric origin of the differential ion flux is evident as it is only measured in deeper parts of Titan's ionosphere, below ~1400 km.

The collisions with neutrals become more important with decreasing altitude. Based on measurements of the positive and negative ion average masses, neutral densities and magnetic field, one of the results of this study is division of the ionosphere into three layers: above 1600 km, the ions are frozen into

magnetic field; between 1100 and 1600 km (dynamo region), collisions with neutrals in the presence of electric and magnetic fields force the ions to drift in opposite directions; below 1000-1100 km, ions are moving with neutrals, the measured differential ion flux at these altitudes therefore translates into the neutral winds with strength averaging to 0.5-1.5 km/s on the dayside and 1.5-2.5 km/s on the nightside (up to 5.5 km/s during T70 flyby), the main result of this study. Most fluctuations of the differential ion current in the dynamo region are measured near the north polar part of Titan's ionosphere and may be explained by currents closing into Saturn's corotational magnetospheric plasma flows. There is (yet) no flyby coverage near the south polar part of the ionosphere, where a similar picture is expected.

**My contribution to Paper II:**

I planned the study, performed the RPWS/LP ion data analysis, contributed to the method development and had the main responsibility for writing the paper.

### 3.3 Papers not included in this thesis:

I performed the RPWS/LP ion data analysis.

## 4 Bibliography

- Achilleos, N., Arridge, C.S., Bertucci, C., Jackman, C.M., Dougherty, M.K., Khurana, K.K., Russell, C.T., 2008. Large-scale dynamics of Saturn's magnetopause: Observations by Cassini. *Journal of Geophysical Research* 113.
- Ågren, K., Andrews, D.J., Buchert, S.C., Coates, A.J., Cowley, S.W.H., Dougherty, M.K., Edberg, N.J.T., Garnier, P., Lewis, G.R., Modolo, R., Opgenoorth, H., Provan, G., Rosenqvist, L., Talboys, D.L., Wahlund, J.E., Wellbrock, A., 2011. Detection of currents and associated electric fields in Titan's ionosphere from Cassini data. *Journal of Geophysical Research* 116.
- Ågren, K., Edberg, N.J.T., Wahlund, J.E., 2012. Detection of negative ions in the deep ionosphere of Titan during the Cassini T70 flyby. *Geophysical Research Letters* 39.
- Ågren, K., Wahlund, J.E., Garnier, P., Modolo, R., Cui, J., Galand, M., Müller-Wodarg, I., 2009. On the ionospheric structure of Titan. *Planetary and Space Science* 57, 1821-1827.
- Ågren, K., Wahlund, J.E., Modolo, R., Lummerzheim, D., Galand, M., Müller-Wodarg, I., Canu, P., Kurth, W.S., Cravens, T.E., Yelle, R.V., Waite, J.H., Coates, A.J., Lewis, G.R., Young, D.T., Bertucci, C., Dougherty, M.K., 2007. On magnetospheric electron impact ionisation and dynamics in Titan's ram-side and polar ionosphere - a Cassini case study. *Annales Geophysicae* 25, 2359-2369.
- Arridge, C.S., Achilleos, N., Dougherty, M.K., Khurana, K.K., Russell, C.T., 2006. Modeling the size and shape of Saturn's magnetopause with variable dynamic pressure. *Journal of Geophysical Research* 111.
- Arridge, C.S., André, N., McAndrews, H.J., Bunce, E.J., Burger, M.H., Hansen, K.C., Hsu, H.W., Johnson, R.E., Jones, G.H., Kempf, S., Khurana, K.K., Krupp, N., Kurth, W.S., Leisner, J.S., Paranicas, C., Roussos, E., Russell, C.T., Schippers, P., Sittler, E.C., Smith, H.T., Thomsen, M.F., Dougherty, M.K., 2012. Mapping Magnetospheric Equatorial Regions at Saturn from Cassini Prime Mission Observations. *Space Science Reviews* 164, 1-83.
- Arridge, C.S., Khurana, K.K., Russell, C.T., Southwood, D.J., Achilleos, N., Dougherty, M.K., Coates, A.J., Leinweber, H.K., 2008. Warping of Saturn's magnetospheric and magnetotail current sheets. *Journal of Geophysical Research* 113.
- Barjatya, A., Swenson, C.M., 2006. Observations of triboelectric charging effects on Langmuir-type probes in dusty plasma. *J Geophys Res-Space* 111.

- Bertucci, C., Achilleos, N., Dougherty, M.K., Modolo, R., Coates, A.J., Szego, K., Masters, A., Ma, Y., Neubauer, F.M., Garnier, P., Wahlund, J.E., Young, D.T., 2008. The magnetic memory of Titan's ionized atmosphere. *Science* 321, 1475-1478.
- Bertucci, C., Hamilton, D.C., Kurth, W.S., Hospodarsky, G.B., Mitchell, D., Dougherty, M.K., 2014 (submitted). Titan's Supersonic Interaction with the Solar Wind. *Science*.
- Bertucci, C., Sinclair, B., Achilleos, N., Hunt, P., Dougherty, M.K., Arridge, C.S., 2009. The variability of Titan's magnetic environment. *Planetary and Space Science* 57, 1813-1820.
- Bird, M., 1997. Detection of Titan's Ionosphere from Voyager 1 Radio Occultation Observations. *Icarus* 130, 426-436.
- Coates, A.J., Crary, F.J., Lewis, G.R., Young, D.T., Waite, J.H., Sittler, E.C., 2007. Discovery of heavy negative ions in Titan's ionosphere. *Geophysical Research Letters* 34.
- Coates, A.J., Wellbrock, A., Lewis, G.R., Jones, G.H., Young, D.T., Crary, F.J., Waite, J.H., 2009. Heavy negative ions in Titan's ionosphere: Altitude and latitude dependence. *Planetary and Space Science* 57, 1866-1871.
- Coates, A.J., Wellbrock, A., Lewis, G.R., Jones, G.H., Young, D.T., Crary, F.J., Waite, J.H., Johnson, R.E., Hill, T.W., Sittler, E.C., 2010. Negative ions at Titan and Enceladus: recent results. *Faraday Discussions* 147, 293-305.
- Coustenis, A., Achterberg, R.K., Conrath, B.J., Jennings, D.E., Marten, A., Gautier, D., Nixon, C.A., Flasar, F.M., Teanby, N.A., Bezdard, B., Samuelson, R.E., Carlson, R.C., Lellouch, E., Bjoraker, G.L., Romani, P.N., Taylor, F.W., Irwin, P.G.J., Fouchet, T., Hubert, A., Orton, G.S., Kunde, V.G., Vinatier, S., Mondellini, J., Abbas, M.M., Courtin, R., 2007. The composition of Titan's stratosphere from Cassini/CIRS mid-infrared spectra. *Icarus* 189, 35-62.
- Coustenis, A., Lellouch, E., Sicardy, B., Roe, H., 2010. Earth-Based Perspective and Pre-Cassini–Huygens Knowledge of Titan, In: Brown, R., Lebreton, J.-P., Waite, J.H. (Eds.), *Titan from Cassini-Huygens*. Springer Netherlands, pp. 9-34.
- Crary, F.J., Magee, B.A., Mandt, K., Waite, J.H., Westlake, J., Young, D.T., 2009. Heavy ions, temperatures and winds in Titan's ionosphere: Combined Cassini CAPS and INMS observations. *Planetary and Space Science* 57, 1847-1856.
- Cravens, T.E., Richard, M., Ma, Y.J., Bertucci, C., Luhmann, J.G., Ledvina, S., Robertson, I.P., Wahlund, J.E., Agren, K., Cui, J., Muller-Wodarg, I., Waite, J.H., Dougherty, M., Bell, J., Ulusen, D., 2010a. Dynamical and magnetic field time constants for Titan's ionosphere: Empirical estimates and comparisons with Venus. *J Geophys Res-Space* 115.
- Cravens, T.E., Robertson, I.P., Clark, J., Wahlund, J.E., Waite, J.H., Ledvina, S.A., Niemann, H.B., Yelle, R.V., Kasprzak, W.T., Luhmann, J.G., McNutt, R.L., Ip, W.H., De La Haye, V., Muller-Wodarg, I., Young,

- D.T., Coates, A.J., 2005. Titan's ionosphere: Model comparisons with Cassini Ta Data. *Geophysical Research Letters* 32.
- Cravens, T.E., Yelle, R.V., Wahlund, J.E., Shemansky, D.E., Nagy, A.F., 2010b. Composition and Structure of the Ionosphere and Thermosphere, In: Brown, R., Lebreton, J.-P., Waite, J.H. (Eds.), *Titan from Cassini-Huygens*. Springer Netherlands, pp. 259-295.
- Cui, J., Galand, M., Yelle, R.V., Wahlund, J.E., Ågren, K., Waite, J.H., Dougherty, M.K., 2010. Ion transport in Titan's upper atmosphere. *Journal of Geophysical Research* 115.
- Edberg, N.J.T., Ågren, K., Wahlund, J.E., Morooka, M.W., Andrews, D.J., Cowley, S.W.H., Wellbrock, A., Coates, A.J., Bertucci, C., Dougherty, M.K., 2011. Structured ionospheric outflow during the Cassini T55–T59 Titan flybys. *Planetary and Space Science* 59, 788-797.
- Edberg, N.J.T., Andrews, D.J., Shebanits, O., Ågren, K., Wahlund, J.E., Opgenoorth, H.J., Cravens, T.E., Girazian, Z., 2013a. Solar cycle modulation of Titan's ionosphere. *Journal of Geophysical Research: Space Physics* 118, 5255-5264.
- Edberg, N.J.T., Andrews, D.J., Shebanits, O., Agren, K., Wahlund, J.E., Opgenoorth, H.J., Roussos, E., Garnier, P., Cravens, T.E., Badman, S.V., Modolo, R., Bertucci, C., Dougherty, M.K., 2013b. Extreme densities in Titan's ionosphere during the T85 magnetosheath encounter. *Geophysical Research Letters* 40, 2879-2883.
- Engwall, E., Eriksson, A.I., André, M., Dandouras, I., Paschmann, G., Quinn, J., Torkar, K., 2006. Low-energy (order 10 eV) ion flow in the magnetotail lobes inferred from spacecraft wake observations. *Geophysical Research Letters* 33.
- Eriksson, A.I., Wahlund, J.E., 2006. Charging of the Freja Satellite in the Auroral Zone. *IEEE Transactions on Plasma Science* 34, 2038-2045.
- Fahleson, U., Falthamm, Cg, Pedersen, A., 1974. Ionospheric Temperature and Density-Measurements by Means of Spherical Double Probes. *Planetary and Space Science* 22, 41-66.
- Galand, M., Yelle, R., Cui, J., Wahlund, J.E., Vuitton, V., Wellbrock, A., Coates, A., 2010. Ionization sources in Titan's deep ionosphere. *J Geophys Res-Space* 115.
- Garnier, P., Wahlund, J.E., Rosenqvist, L., Modolo, R., Ågren, K., Sergis, N., Canu, P., Andre, M., Gurnett, D.A., Kurth, W.S., Krimigis, S.M., Coates, A., Dougherty, M., Waite, J.H., 2009. Titan's ionosphere in the magnetosheath: Cassini RPWS results during the T32 flyby. *Annales Geophysicae* 27, 4257-4272.
- Garrett, H.B., Whittlesey, A.C., 2000. Spacecraft charging, an update. *Ieee Transactions on Plasma Science* 28, 2017-2028.
- Grard, R.J.L., 1973. Properties of the satellite photoelectron sheath derived from photoemission laboratory measurements. *Journal of Geophysical Research* 78, 2885-2906.
- Gurnett, D.A., Kurth, W.S., Kirchner, D.L., Hospodarsky, G.B., Averkamp, T.F., Zarka, P., Lecacheux, A., Manning, R., Roux, A., Canu, P.,

- Cornilleau-Wehrlin, N., Galopeau, P., Meyer, A., Bostrom, R., Gustafsson, G., Wahlund, J.E., Ahlen, L., Rucker, H.O., Ladreiter, H.P., Macher, W., Woolliscroft, L.J.C., Alleyne, H., Kaiser, M.L., Desch, M.D., Farrell, W.M., Harvey, C.C., Louarn, P., Kellogg, P.J., Goetz, K., Pedersen, A., 2004. The Cassini radio and plasma wave investigation. *Space Science Reviews* 114, 395-463.
- Havnes, O., Næsheim, L.I., Hartquist, T.W., Morfill, G.E., Melandsø, F., Schleicher, B., Trøim, J., Blix, T., Thrane, E., 1996. Meter-scale variations of the charge carried by mesospheric dust. *Planetary and Space Science* 44, 1191-1194.
- Holmberg, M.K.G., Wahlund, J.E., Morooka, M.W., Persoon, A.M., 2012. Ion densities and velocities in the inner plasma torus of Saturn. *Planetary and Space Science* 73, 151-160.
- Horányi, M., Hartquist, T.W., Havnes, O., Mendis, D.A., Morfill, G.E., 2004. Dusty plasma effects in Saturn's magnetosphere. *Reviews of Geophysics* 42.
- Jacobsen, K.S., Wahlund, J.E., Pedersen, A., 2009. Cassini Langmuir probe measurements in the inner magnetosphere of Saturn. *Planetary and Space Science* 57, 48-52.
- Johnson, R.E., Tucker, O.J., Michael, M., Sittler, E.C., Smith, H.T., Young, D.T., Waite, J.H., 2010. Mass Loss Processes in Titan's Upper Atmosphere, In: Brown, R., Lebreton, J.-P., Waite, J.H. (Eds.), *Titan from Cassini-Huygens*. Springer Netherlands, pp. 373-391.
- Kurth, W.S., Averkamp, T.F., Gurnett, D.A., Wang, Z., 2006. Cassini RPWS observations of dust in Saturn's E Ring. *Planetary and Space Science* 54, 988-998.
- Laframboise, J.G., Parker, L.W., 1973. Probe Design for Orbit-Limited Current Collection. *Physics of Fluids* 16, 629-636.
- Langmuir, I., 1928. Oscillations in Ionized Gases. *Proceedings of the National Academy of Sciences of the United States of America* 14, 627-637.
- Lavvas, P., Yelle, R.V., Koskinen, T., Bazin, A., Vuitton, V., Vigren, E., Galand, M., Wellbrock, A., Coates, A.J., Wahlund, J.E., Crary, F.J., Snowden, D., 2013. Aerosol growth in Titan's ionosphere. *Proceedings of the National Academy of Sciences of the United States of America* 110, 2729-2734.
- Mandt, K.E., Gell, D.A., Perry, M., Waite, J.H., Crary, F.A., Young, D., Magee, B.A., Westlake, J.H., Cravens, T., Kasprzak, W., Miller, G., Wahlund, J.E., Agren, K., Edberg, N.J.T., Heays, A.N., Lewis, B.R., Gibson, S.T., de la Haye, V., Liang, M.C., 2012. Ion densities and composition of Titan's upper atmosphere derived from the Cassini Ion Neutral Mass Spectrometer: Analysis methods and comparison of measured ion densities to photochemical model simulations. *J Geophys Res-Planet* 117.
- Medicus, G., 1962. Spherical Langmuir Probe in Drifting and Accelerated Maxwellian Distribution. *Journal of Applied Physics* 33, 3094-3100.
- Morooka, M.W., Modolo, R., Wahlund, J.E., Andre, M., Eriksson, A.I., Persoon, A.M., Gurnett, D.A., Kurth, W.S., Coates, A.J., Lewis, G.R.,

- Khurana, K.K., Dougherty, M., 2009. The electron density of Saturn's magnetosphere. *Annales Geophysicae* 27, 2971-2991.
- Morooka, M.W., Wahlund, J.E., Eriksson, A.I., Farrell, W.M., Gurnett, D.A., Kurth, W.S., Persoon, A.M., Shafiq, M., Andre, M., Holmberg, M.K.G., 2011. Dusty plasma in the vicinity of Enceladus. *J Geophys Res-Space* 116.
- Mott-Smith, H., Langmuir, I., 1926. The Theory of Collectors in Gaseous Discharges. *Physical Review* 28, 727-763.
- Müller-Wodarg, I.C.F., Yelle, R.V., Cui, J., Waite, J.H., 2008. Horizontal structures and dynamics of Titan's thermosphere. *Journal of Geophysical Research* 113.
- Nagy, A.F., Winterhalter, D., Sauer, K., Cravens, T.E., Brecht, S., Mazelle, C., Crider, D., Kallio, E., Zakharov, A., Dubinin, E., Verigin, M., Kotova, G., Axford, W.I., Bertucci, C., Trotignon, J.G., 2004. The plasma Environment of Mars. *Space Science Reviews* 111, 33-114.
- Niemann, H.B., Atreya, S.K., Bauer, S.J., Carignan, G.R., Demick, J.E., Frost, R.L., Gautier, D., Haberman, J.A., Harpold, D.N., Hunten, D.M., Israel, G., Lunine, J.I., Kasprzak, W.T., Owen, T.C., Paulkovich, M., Raulin, F., Raen, E., Way, S.H., 2005. The abundances of constituents of Titan's atmosphere from the GCMS instrument on the Huygens probe. *Nature* 438, 779-784.
- Pavlov, A.A., Hurtgen, M.T., Kasting, J.F., Arthur, M.A., 2003. Methane-rich Proterozoic atmosphere? *Geology* 31, 87.
- Raulin, F., McKay, C., Lunine, J., Owen, T., 2010. Titan's Astrobiology, In: Brown, R., Lebreton, J.-P., Waite, J.H. (Eds.), *Titan from Cassini-Huygens*. Springer Netherlands, pp. 215-233.
- Sagan, C., Khare, B.N., 1979. Tholins: organic chemistry of interstellar grains and gas. *Nature* 277, 102-107.
- Sagan, C., Khare, B.N., Thompson, W.R., McDonald, G.D., Wing, M.R., Bada, J.L., Vo-Dinh, T., Arakawa, E.T., 1993. Polycyclic aromatic hydrocarbons in the atmospheres of Titan and Jupiter. *Astrophys J* 414, 399-405.
- Shebanits, O., Wahlund, J.-E., Mandt, K., Ågren, K., Edberg, N.J.T., Waite, J.H., 2013. Negative ion densities in the ionosphere of Titan–Cassini RPWS/LP results. *Planetary and Space Science* 84, 153-162.
- Shukla, P.K., 2001. A survey of dusty plasma physics. *Physics of Plasmas* 8, 1791-1803.
- Sittler, E., Hartle, R.E., Bertucci, C., Coates, A., Cravens, T., Dandouras, I., Shemansky, D., 2010. Energy Deposition Processes in Titan's Upper Atmosphere and Its Induced Magnetosphere, In: Brown, R., Lebreton, J.-P., Waite, J.H. (Eds.), *Titan from Cassini-Huygens*. Springer Netherlands, pp. 393-453.
- Sittler, E.C., Ali, A., Cooper, J.F., Hartle, R.E., Johnson, R.E., Coates, A.J., Young, D.T., 2009. Heavy ion formation in Titan's ionosphere: Magnetospheric introduction of free oxygen and a source of Titan's aerosols? *Planetary and Space Science* 57, 1547-1557.

- Srama, R., Kempf, S., Moragas-Klostermeyer, G., Helfert, S., Ahrens, T.J., Altobelli, N., Auer, S., Beckmann, U., Bradley, J.G., Burton, M., Dikarev, V.V., Economou, T., Fechtig, H., Green, S.F., Grande, M., Havnes, O., Hillier, J.K., Horanyi, M., Igenbergs, E., Jessberger, E.K., Johnson, T.V., Krüger, H., Matt, G., McBride, N., Mocker, A., Lamy, P., Linkert, D., Linkert, G., Lura, F., McDonnell, J.A.M., Möhlmann, D., Morfill, G.E., Postberg, F., Roy, M., Schwehm, G.H., Spahn, F., Svestka, J., Tschernjawski, V., Tuzzolino, A.J., Wäsch, R., Grün, E., 2006. In situ dust measurements in the inner Saturnian system. *Planetary and Space Science* 54, 967-987.
- Strobel, D.F., Cui, J., Strobel, D.F., Cui, J., 2014. Titan's upper atmosphere/exosphere, escape processes, and rates  
Titan. Cambridge University Press.
- Tarduno, J.A., Cottrell, R.D., Watkeys, M.K., Hofmann, A., Doubrovine, P.V., Mamajek, E.E., Liu, D., Sibeck, D.G., Neukirch, L.P., Usui, Y., 2010. Geodynamo, solar wind, and magnetopause 3.4 to 3.45 billion years ago. *Science* 327, 1238-1240.
- Thompson, W.R., McDonald, G.D., Sagan, C., 1994. The Titan haze revisited: magnetospheric energy sources and quantitative tholin yields. *Icarus* 112, 376-381.
- Thomsen, M.F., Reisenfeld, D.B., Delapp, D.M., Tokar, R.L., Young, D.T., Crary, F.J., Sittler, E.C., McGraw, M.A., Williams, J.D., 2010. Survey of ion plasma parameters in Saturn's magnetosphere. *Journal of Geophysical Research* 115.
- Tian, F., Solomon, S.C., Qian, L.Y., Lei, J.H., Roble, R.G., 2008. Hydrodynamic planetary thermosphere model: 2. Coupling of an electron transport/energy deposition model. *J Geophys Res-Planet* 113.
- Vuitton, V., Lavvas, P., Yelle, R.V., Galand, M., Wellbrock, A., Lewis, G.R., Coates, A.J., Wahlund, J.E., 2009. Negative ion chemistry in Titan's upper atmosphere. *Planetary and Space Science* 57, 1558-1572.
- Wahlund, J.-E., Modolo, R., Bertucci, C., Coates, A.J., 2014. Titan's magnetospheric and plasma environment, In: Ingo Müller-Wodarg, Caitlin A. Griffith, Emmanuel Lellouch, Cravens, T.E. (Eds.), Titan. Cambridge University Press, Cambridge, pp. 419-458.
- Wahlund, J.E., André, M., Eriksson, A.I.E., Lundberg, M., Morooka, M.W., Shafiq, M., Averkamp, T.F., Gurnett, D.A., Hospodarsky, G.B., Kurth, W.S., Jacobsen, K.S., Pedersen, A., Farrell, W., Ratynskaia, S., Piskunov, N., 2009a. Detection of dusty plasma near the E-ring of Saturn. *Planetary and Space Science* 57, 1795-1806.
- Wahlund, J.E., Bostrom, R., Gustafsson, G., Gurnett, D.A., Kurth, W.S., Pedersen, A., Averkamp, T.F., Hospodarsky, G.B., Persoon, A.M., Canu, P., Neubauer, F.M., Dougherty, M.K., Eriksson, A.I., Morooka, M.W., Gill, R., Andre, M., Eliasson, L., Muller-Wodarg, I., 2005. Cassini measurements of cold plasma in the ionosphere of Titan. *Science* 308, 986-989.

- Wahlund, J.E., Galand, M., Muller-Wodarg, I., Cui, J., Yelle, R.V., Crary, F.J., Mandt, K., Magee, B., Waite, J.H., Young, D.T., Coates, A.J., Garnier, P., Agren, K., Andre, M., Eriksson, A.I., Cravens, T.E., Vuitton, V., Gurnett, D.A., Kurth, W.S., 2009b. On the amount of heavy molecular ions in Titan's ionosphere. *Planetary and Space Science* 57, 1857-1865.
- Waite, J.H., Jr., Lewis, W.S., Kasprzak, W.T., Anicich, V.G., Block, B.P., Cravens, T.E., Fletcher, G.G., Ip, W.H., Luhmann, J.G., McNutt, R.L., Niemann, H.B., Parejko, J.K., Richards, J.E., Thorpe, R.L., Walter, E.M., Yelle, R.V., 2004. The Cassini Ion and Neutral Mass Spectrometer (INMS) Investigation. *Space Science Reviews* 114, 113-231.
- Waite, J.H., Jr., Niemann, H., Yelle, R.V., Kasprzak, W.T., Cravens, T.E., Luhmann, J.G., McNutt, R.L., Ip, W.H., Gell, D., De La Haye, V., Muller-Wordag, I., Magee, B., Borggren, N., Ledvina, S., Fletcher, G., Walter, E., Miller, R., Scherer, S., Thorpe, R., Xu, J., Block, B., Arnett, K., 2005. Ion neutral mass spectrometer results from the first flyby of Titan. *Science* 308, 982-986.
- Waite, J.H., Jr., Young, D.T., Cravens, T.E., Coates, A.J., Crary, F.J., Magee, B., Westlake, J., 2007. The process of tholin formation in Titan's upper atmosphere. *Science* 316, 870-875.
- Wellbrock, A., Coates, A.J., Jones, G.H., Lewis, G.R., Waite, J.H., 2013. Cassini CAPS-ELS observations of negative ions in Titan's ionosphere: Trends of density with altitude. *Geophysical Research Letters*.
- Young, D.T., Berthelier, J.J., Blanc, M., Burch, J.L., Coates, A.J., Goldstein, R., Grande, M., Hill, T.W., Johnson, R.E., Kelha, V., McComas, D.J., Sittler, E.C., Svenes, K.R., Szegö, K., Tanskanen, P., Ahola, K., Anderson, D., Bakshi, S., Baragiola, R.A., Barraclough, B.L., Black, R.K., Bolton, S., Booker, T., Bowman, R., Casey, P., Crary, F.J., Delapp, D., Dirks, G., Eaker, N., Funsten, H., Furman, J.D., Gosling, J.T., Hannula, H., Holmlund, C., Huomo, H., Illiano, J.M., Jensen, P., Johnson, M.A., Linder, D.R., Luntama, T., Maurice, S., McCabe, K.P., Mursula, K., Narheim, B.T., Nordholt, J.E., Preece, A., Rudzki, J., Ruitberg, A., Smith, K., Szalai, S., Thomsen, M.F., Viherkanto, K., Vilppola, J., Vollmer, T., Wahl, T.E., Wüest, M., Ylikorpi, T., Zinsmeyer, C., 2004. Cassini Plasma Spectrometer Investigation. *Space Science Reviews* 114, 1-112.



## Negative ion densities in the ionosphere of Titan–Cassini RPWS/LP results



O. Shebanits<sup>a,b,\*</sup>, J.-E. Wahlund<sup>b</sup>, K. Mandt<sup>c</sup>, K. Ågren<sup>b</sup>, N.J.T. Edberg<sup>b</sup>, J.H. Waite Jr<sup>c</sup>

<sup>a</sup> Department of Physics and Astronomy, Uppsala University, Box 516, SE 751 20 Uppsala, Sweden

<sup>b</sup> Swedish Institute of Space Physics, Box 537, SE 751 21 Uppsala, Sweden

<sup>c</sup> Space and Science Engineering Division, Southwest Research Institute (SWRI), 6220 Culebra Road, San Antonio, TX 78238, USA

### ARTICLE INFO

#### Article history:

Received 15 February 2013

Received in revised form

30 April 2013

Accepted 28 May 2013

Available online 5 June 2013

#### Keywords:

Titan

Ionospheric physics

Cassini

Negative ions

Dust–plasma interaction

### ABSTRACT

The Cassini spacecraft Radio and Plasma Wave Science (RPWS) Langmuir Probe (LP) provides in-situ measurements of Titan's ionosphere. We present here data from 47 deep flybys in the time period October 2004–July 2012 of charge densities of positive and negative ions as well as electrons. These densities have been mapped with respect to altitude and solar zenith angle (SZA) in an altitude range of 880–1400 km. The inferred electron number densities are consistent with earlier presented observational results. Negative ion charge densities exhibit a trend that exponentially increases towards lower altitudes within the covered altitude range. This is especially evident on the nightside of Titan (SZA > 110°). The negative ion charge densities at the lowest traversed altitudes (near 960 km) are inferred to be in the range 300–2500 cm<sup>-3</sup>. The results show that very few free electrons ( $n_e/n_i \sim 0.1\text{--}0.7$ ) exist in the deepest regions (880–1050 km) of Titan's nightside ionosphere. Instead the deep nightside part of Titan's ionosphere is dominated by both negatively and positively charged heavy (> 100 amu) organic ions. We therefore believe a dust/aerosol-ion plasma exists here, similar to what is found in noctilucent clouds in Earth's mesosphere.

© 2013 Elsevier Ltd. All rights reserved.

### 1. Introduction

Saturn's largest moon Titan hosts an atmosphere with complex organic chemistry (Waite et al., 2007) which may be similar to that of early Earth. The Kronian system and Titan in particular are being explored by the Cassini spacecraft, which has been in orbit around Saturn since 2004 and has carried out 86 flybys of Titan by July 2012.

Titan's nitrogen-rich atmosphere is partially ionized into an ionosphere primarily by solar EUV/X-ray radiation, whereas ionization by cosmic radiation and energetic particles from the Kronian magnetosphere becomes important at lower altitudes and on the nightside of Titan (e.g., Wahlund et al., 2005; Ågren et al., 2009; Galand et al., 2010). These sources of energy provide a basis for the complex ion chemistry, leading to aerosol (tholin) formation as suggested by e.g., Sagan and Khare (1979) and Waite et al. (2007).

Positive ions of up to 350 amu/q and negative ions of up to 10,000 amu/q, the building blocks of aerosols, were indeed

detected by the CAPS instrument on Cassini (Coates et al., 2007, 2010; Waite et al., 2007); these heavy species are dominating the ionosphere below 1000 km (Crarty et al., 2009; Wahlund et al., 2009). The composition of the ionosphere has been studied by e.g., Cravens et al. (2006) and the chemical reactions at work have been extensively modelled for both positive and negative ions by Vuitton et al. (2009), classifying chemistry pathways and ion types. Heavy negative ions were also detected by the Cassini Radio and Plasma Wave Science Langmuir Probe (RPWS/LP) instrument (Ågren et al., 2012).

Here we present electron as well as positively and negatively charged ion profiles of Titan's ionosphere based on Cassini RPWS/LP in-situ measurements during 47 deep (below 1400 km) flybys in the time period between Oct 2004 and July 2012. Section 2 covers the experiment and analysis method together with error estimation. Observations and results are presented in Section 3 and discussed in Section 4. The conclusions are found in Section 5.

### 2. Experiment and analysis method description

The RPWS LP is a titanium nitride coated titanium sphere of 2.5 cm radius, installed on a boom so that the sensor is 1.5 m from nearest spacecraft surface (Gurnett et al., 2004). During Titan flybys the LP samples the plasma current to the probe each 24 s

\* Corresponding author at: Swedish Institute of Space Physics, Box 537, SE 751 21 Uppsala, Sweden. Tel.: +46 184715944, mobile: +46 735933269; fax: +46 184715905.

E-mail address: [oleg.shebanits@irfu.se](mailto:oleg.shebanits@irfu.se) (O. Shebanits).

by sweeping the voltage in 512 or 1024 steps between  $\pm 4$  V (or  $\pm 32$  V for flybys not reaching below 1400 km) in 0.5 or 1 s respectively. These measurements yield electron and ion number densities along with other plasma parameters (see e.g., Wahlund et al., 2009; Morooka et al., 2011; Holmberg et al., 2012).

The sweep data constitute samples of current as a function of probe voltage and the output parameters (e.g., see Eq. (A7)) are derived by fitting a curve to the data using the Orbital Motion Limited (OML) theory (Mott-Smith and Langmuir, 1926; Medicus, 1962). The total current for a negative bias voltage applied to the LP can be written as a sum of sampled ram and thermal currents from positive ( $I_i$ ) and negative ( $I_n$ ) ions in the surrounding plasma together with the photoelectron current due to solar EUV radiation:

$$I_{tot} = I_i + I_n + I_{ph} \quad (1)$$

In the dense ionospheric conditions of Titan the small contribution of the photoelectron current ( $I_{ph}$ ) is removed using a model for atmospheric EUV extinction (see Appendix A for details). Any secondary electron currents from energetic (250–450 eV) electron impacts are negligible at Titan (Garnier et al., 2012). A numerically convenient approximation for the sampled ion currents ( $U < 0$ ) has been given by Fahleson et al. (1974) as  $I_i = I_{i0}(1 - \chi_i)$  for a positive ion current and  $I_n = I_{n0}\exp(\chi_n)$  for a negative ion current, where

$$\begin{cases} I_0 = -ZnA_{LP}\sqrt{\frac{v^2}{16} + \frac{eT[eV]}{2\pi m}} \\ \chi = \frac{U}{mv^2/2e + T[eV]} \end{cases} \quad (2)$$

Here,  $A_{LP}$  is the probe surface area,  $U = U_{bias} + U_{float}$  is the sum of the probe bias voltage and floating potential (spacecraft potential at the probe),  $e$  is the electron charge,  $n$ ,  $v$ ,  $T$ ,  $m$  and  $Z$ , are the number density, drift speed, temperature, mass and charge of ions, respectively. The ion current is negative for positive ions and positive for negative ions.

Observations by CAPS/IBS and ELS as well as INMS indicate that the negatively charged ions reach much larger masses (at least an order of magnitude) than positively charged ions (Coates et al., 2009; Crary et al., 2009; Mandt et al., 2012). Also the observed LP characteristic for negative bias voltages very seldom deviates significantly from the linear fit line. Only the T70 data from the deepest parts of Titan's ionosphere (see Ågren et al., 2012) show a slight bend of the LP characteristics towards zero bias voltage, and this bend was interpreted to be due to an ion drift. We consequently conclude that the average mass of negative ions ( $m_n$ ) must be large compared to the average mass of positive ions ( $m_i$ ) also from RPWS/LP observations, and it is safe to assume that  $m_n \geq 10m_i$ .

The speed of the Cassini spacecraft through Titan's ionosphere is around 6 km/s and we can thus assume a rigid ionosphere (no drift,  $v_{sc} \approx v_i \approx v_n$ ). Further, we assume quasineutrality ( $n_e + Z_n n_n \approx n_i$ ) and singly-charged positive ions (Thissen et al., 2011). With these assumptions, an expression for the charge density of negative ions is derived from Eqs. (1) and (2) as

$$Z_n n_n \approx -\frac{4}{eA_{LP}} \left( \frac{a}{v_{sc}} - \frac{bv_{sc}m_i}{2e} \right) \quad (3)$$

where  $a$  and  $b$  are the parameters extracted from a linear fit to data (an example of such is shown in Fig. 1). A detailed derivation is given in Appendix A. The residual (red dots in Fig. 1) after taking away the linear fit (green line in Fig. 1) shows that the instrument noise level (pre-amp) of the observed LP characteristic is slightly under 100 pA, well below the measured ion currents of 0.5–1 nA for  $U_{bias} < -1$  V. The instrument noise level results in a maximum error in the inferred values for  $a$  and  $b$  of less than 10%. INMS mean ion mass profile (from which  $m_i$  is derived) has 27% error (Mandt et al., 2012). These error sources combine into a total error in  $Z_n n_n$

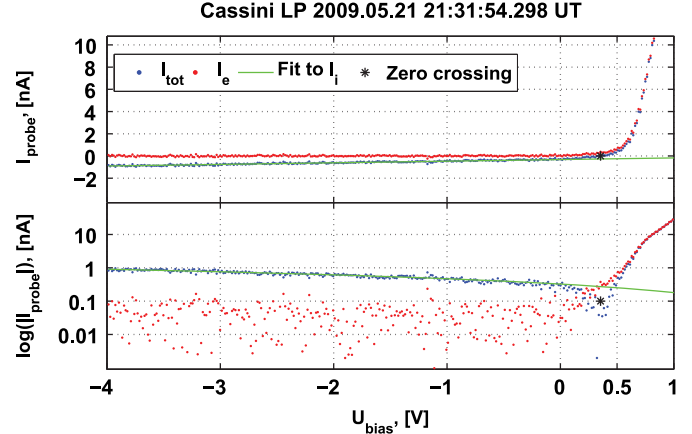


Fig. 1. Ion part of a Langmuir Probe sweep (blue) taken at 1400 km altitude and  $115^\circ$  SZA during egress of T55 flyby. Electron current (pre-amp instrument noise,  $\sim 100$  pA residual after subtracting the linear fit) is shown in red and the fit to data in green. Star marks potential of zero current. (For interpretation of references to colour in this figure, the reader is referred to the web version of this article.)

that corresponds to a general worst-case error margin of  $-100$  to  $+300$   $\text{cm}^{-3}$  (independent of altitude and SZA), with an asymmetry due to the underestimated positive ion masses inferred from INMS measurements because of the instrument upper limit of 100 amu.

The electron number density is derived from  $a$  (A8), and the ion number density is found from the quasineutrality condition ( $n_e + Z_n n_n = n_i$ ). In the case where no negative ions can be found the positive ion number density is simply equal to the electron density ( $n_e = n_i$ ).

We have used RPWS/LP data from 47 flybys of Titan below an altitude of 1400 km in the time frame August 2004–July 2012 (TA-T84) for our analysis. The flybys T7, T11, T37, T45 and T60 were excluded due to bad or missing data. Additionally, T83, T84 and T85 were excluded for further investigation due to unusually high ionospheric plasma densities, and are in preparation for a future study. INMS data are used from 14 flybys (T5, T17, T18, T21, T26, T32, T36, T39, T40, T48, T50, T51, T57 and T59) in order to produce altitude and SZA profiles of the average mass of positively charged ions ( $m_i$ ). These are, in turn, used to construct  $m_i$  values (through an exponential altitude and SZA fit to the INMS values) for each LP sweep.

### 3. Observations

The derived electron number densities ( $n_e = n_i - Z_n n_n$ ) from the RPWS/LP sweep characteristics for negative bias voltages (ion sampling side) are shown in Fig. 2. The altitude of each individual measurement is plotted as a function of SZA and marked with a white dot; the density is linearly interpolated onto a uniform grid and colour coded. The resulting plot of the ionospheric electron density is in good agreement with previously reported electron number densities from the RPWS/LP sweep characteristics for positive bias voltages (electron sampling side; e.g., Ågren et al., 2009; Edberg et al., 2011); with a clear maximum of dayside electron number densities (reaching  $3800$   $\text{cm}^{-3}$ ), due mostly to solar EUV radiation, a rising dayside ionospheric peak shifting to higher altitudes with increasing SZA, and weaker nightside peak densities reaching at most  $1100$ – $1200$   $\text{cm}^{-3}$  for SZA  $> 130^\circ$ . However, the presented data set in Fig. 2 contains a much larger number of flybys and therefore offers a better statistical result.

In order to give further credit to the inferred charge densities of negatively charged ions presented here, we have made a combined analysis of electron densities estimated from Langmuir probe

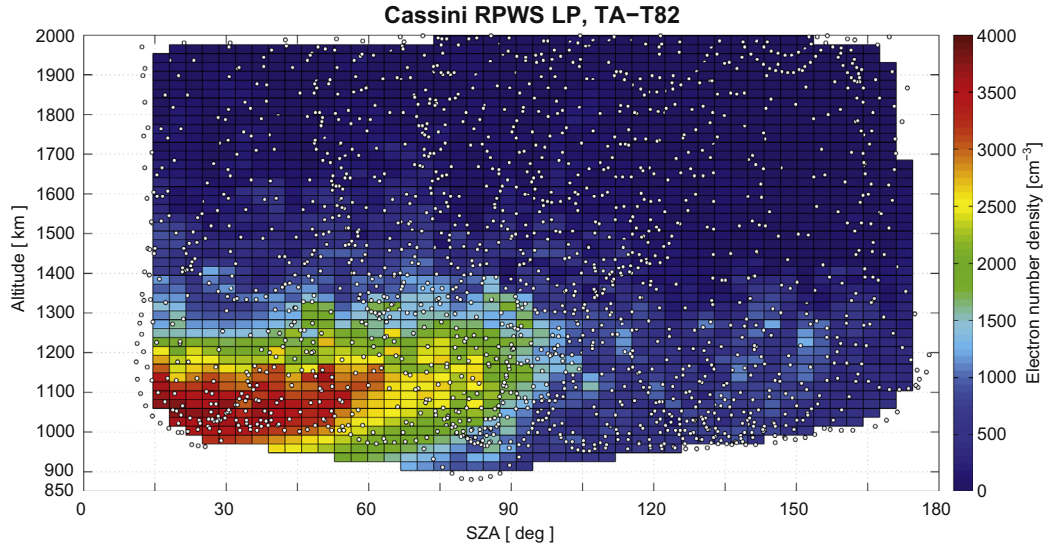


**Fig. 2.** Linear interpolation of Titan's ionosphere electron densities from 47 flybys as function of altitude and SZA. White dots are the actual measurement points. The hole near midday (SZA < 11°) is due to poor flyby coverage. (Figure in colour is available in the web version of this article.)

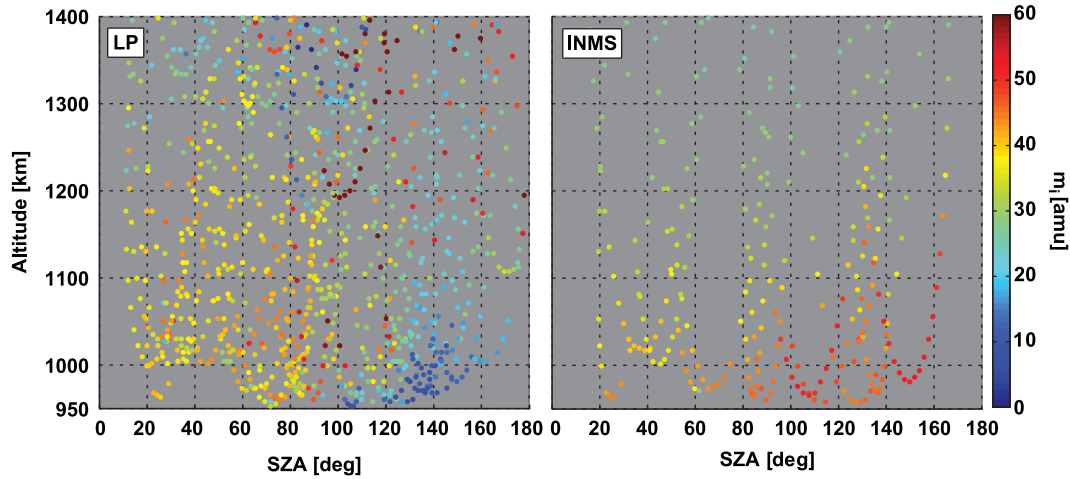


**Fig. 3.** LP (left) and INMS (right) positive ion masses as a function of altitude and SZA, interpolated to the measurement points (white dots). Large mass fluctuations above 1200 km altitude are due to ion winds ( $v_{sc} \neq v_i$ ). (Figure in colour is available in the web version of this article.)

sweeps using the full sweep bias range (both ion and electron sampling sides) as well as electron densities estimated from the upper hybrid emissions ( $f_{UH} \approx f_p = 8980 \sqrt{n_e}$ ) detected by the RPWS antenna in Titan's ionosphere.

To illustrate the necessity to incorporate the negative ions into the RPWS/LP sweep analysis we present the following comparison between the average mass of positively charged ions ( $m_i$ ) calculated from the RPWS/LP sweep characteristics (assuming that no negatively charged ions were present) and corresponding  $m_i$  inferred from the INMS measurements. Fig. 3 shows the former in the left panel and the latter in the right panel. The INMS derived average ion masses show an exponential increase towards the nightside below 1200 km and towards lower altitudes, while the LP derived average ion masses show a decrease for SZA > 100° to clearly inconsistent values below 20 amu. The LP derived average ion mass is sensitive to whether negatively charged ions are present in the analysis (Appendix A) or not (Appendix B) and this is the cause of the inconsistency. We therefore conclude that substantial amounts of negatively charged ions cannot be neglected in the LP analysis, at least not on the nightside below 1400 km. The sporadically deviating LP values above 1200 km in Fig. 3 are due to significant ion convection occurring with respect to the spacecraft

trajectory (the analysis assumes zero ion drift) and should be disregarded in the comparison. It should be noted that in order to include the negative ions in the analysis, mean positive ion mass data from the INMS instrument is used for  $m_i$ .

The full analysis of the LP sweep-characteristics including negatively charged ions is presented in Fig. 4, where the inferred electron number densities ( $n_e$ , panel a) and number densities of the positively charged ions ( $n_i$ , panel b) as well as the charge densities of negatively charged ions ( $Z_n n_n$ , panel c) are shown. The data is colour coded onto a SZA-altitude map. Substantial charge densities of negatively charged ions are detected below 1100 km for all covered SZA. Although charge densities of negatively charged ions commonly reach 500–1000  $\text{cm}^{-3}$  below 1100 km, more pronounced abundances (reaching 2000  $\text{cm}^{-3}$ ) are detected between 130° and 140° SZA. In these altitude regions, because of the quasi-neutrality condition ( $n_i \approx n_e + Z_n n_n$ ), the number densities of positively charged ions (Fig. 4, panel b) become larger than the electron number densities (Fig. 4, panel a). The dominance of positively charged ions could be one explanation for the discrepancy between previously reported electron densities and modelled ionospheric densities from Titan (Cravens et al., 2009). On the nightside below an altitude of 1100 km, the comparable

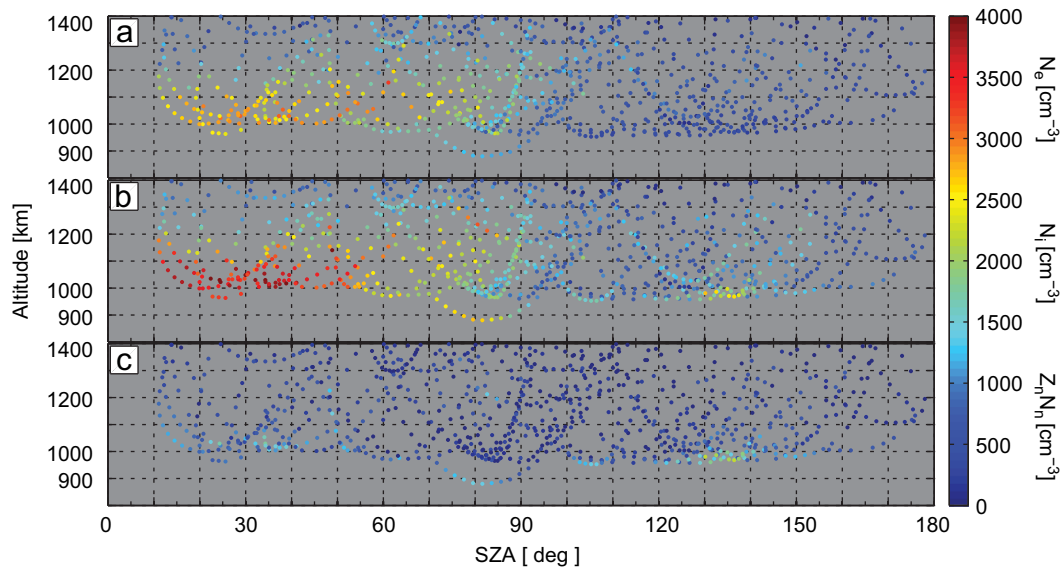


**Fig. 4.** Cassini RPWS LP electron number densities (a), positive ion number densities (b) and negative ion charge densities (c) as functions of altitude and SZA. Each point is one measurement. (Figure in colour is available in the web version of this article.)

amount of electrons becomes small, and the ionosphere is here dominated by ions. This may explain the lack of observed ionospheric electrons as compared to the levels predicted by previous model calculations of ionization by impacting magnetospheric electrons on the nightside (e.g., Ågren et al., 2007; Cravens et al., 2009). Future ionization model calculations need to take into account the effect of negatively charged ions in the charge balance of Titan's ionosphere. The apparent minimum of large ion densities of positively charged ions (Fig. 4, panel b) around  $90\text{--}120^\circ$  SZA is due to flybys being mostly in the ecliptic polar regions of Titan's terminator (see Fig. 7, panel b).

The superimposed altitude profiles for all used Titan flybys of the charge density of negatively charged ions ( $Z_n n_n$ ) are shown in Fig. 5 for dayside ( $\text{SZA} < 70^\circ$ , panel a), terminator region ( $70^\circ < \text{SZA} < 100^\circ$ , panel b) and nightside ( $\text{SZA} > 100^\circ$ , panel c). Since the errors are between  $-100$  and  $300 \text{ cm}^{-3}$ , the small difference between  $n_i$  and  $n_e$  (see (A11) in Appendix A) in the high altitude parts of Titan's ionosphere makes it difficult to be confident in  $Z_n n_n$  above  $\sim 1200$  km. This also contributes to the spread in the data points from one flyby to the next. Nevertheless, the derived data points presented here from the T70 flyby below  $950$  km (compare with Ågren et al., 2012; see also Appendix C) follow the overall trend, exponentially increasing towards lower altitudes (best fits shown as dashed lines). Due to the overlapping uncertainties in  $n_e$  and  $n_i$  some of the  $Z_n n_n$  end up negative, which is of course physically impossible. This is addressed by the error estimation of  $Z_n n_n$  and discussed in Section 4. Also, the nightside values (Fig. 5, panel c) below  $1100$  km are more confident due to the significantly lower electron densities ( $\sim 500 \text{ cm}^{-3}$ ) compared to ion densities here, and a more prominent exponential trend with decreasing altitude is evident in panel c with mean negative ion charge densities close to  $700\text{--}800 \text{ cm}^{-3}$  near  $1000$  km. The exponential increase with decreasing altitude is still distinguishable on the dayside (Fig. 5, panel a). For example  $Z_n n_n$  reaches  $1000 \text{ cm}^{-3}$  at  $950\text{--}1000$  km compared to  $3000\text{--}3500 \text{ cm}^{-3}$  for  $n_e$  and  $3500\text{--}4200 \text{ cm}^{-3}$  for  $n_i$  at the same altitude (see Fig. 4, panels a and b). Still, we cannot be certain whether the dayside peak at  $1025$  km and the terminator region peak at  $1200$  km are indeed peaks in negative ion charge density, as the highest  $Z_n n_n$  values come from 3 flybys on dayside (T20, T23 and T43) that do not show peaks and the outbound leg of TA flyby for the terminator case, where a  $Z_n n_n$  peak cannot be identified due to large variations in electron

densities. The uncertainty also applies to the larger values of  $Z_n n_n$  at higher altitudes on the dayside compared to the terminator and nightside. However, the horizontal spread in data points represents real variation between flybys, as explained in the following example.

A set of individual altitude profiles of charge densities for negative ions ( $Z_n n_n$ ) from four flybys with different SZAs (T16, T40, T42 and T50) is displayed in Fig. 6, panels a, b, c and d, respectively. For comparison, the corresponding positive ion ( $n_i$ ) and electron ( $n_e$ ) number density profiles are superimposed, together with panels showing the SZA coverage for each flyby. By comparing the different profiles it is clear that the horizontal spread of  $Z_n n_n$  data points in Fig. 5 is not due to a random error, but is in fact a variation in profiles from flyby to flyby. This may either be due to a real variation, a systematic error, or both. We argue here that it is due to the real variation between flybys. T40 and T42 are dayside flybys, T16 traverses both terminator (outbound) and nightside (inbound) regions and T50 is a pure nightside event. The dayside profiles (Fig. 6 b and c) show a large difference in the electron ( $n_e$ ) and positive ion ( $n_i$ ) number densities that increases towards lower altitudes. This difference is more than  $1000 \text{ cm}^{-3}$  below  $1100$  km (T40, Fig. 6b) and below  $1200$  km (T42, Fig. 6c) and is much larger than the error estimations ( $-100$  to  $+300 \text{ cm}^{-3}$ ). It should be kept in mind that the electron number density is a result of three different estimation methods (see above), which are all in agreement within the error margin. We conclude that large charge densities of negatively charged ions ( $Z_n n_n \approx 500\text{--}2000 \text{ cm}^{-3}$ ) exist on the dayside below altitudes of  $1100\text{--}1200$  km. The same conclusion can be made for the nightside case of T50 (Fig. 6d), below an altitude of  $1030$  km. For T50 it is also evident that both  $Z_n n_n$  and  $n_i$  reach  $2000\text{--}2500 \text{ cm}^{-3}$  at the lowest measured altitudes, while  $n_e \approx 400 \text{ cm}^{-3}$ . There are therefore very few “free” electrons and the plasma primarily consists of only ions. The LP cannot discriminate between types of ions; the given ion number densities represent total charge densities and may therefore include charged aerosol particles. The flyby T16 (Fig. 6a) shows similar trends as T50, with  $Z_n n_n$  and  $n_i$  reaching  $1000\text{--}1500 \text{ cm}^{-3}$  at the lowest measured altitudes below  $1000$  km, while  $n_e$  is  $400\text{--}800 \text{ cm}^{-3}$  and decreases with altitude. Generally, the  $Z_n n_n$  data become more reliable as the negative ion charge density approaches its peak towards lower altitudes and the difference between positive ion and electron

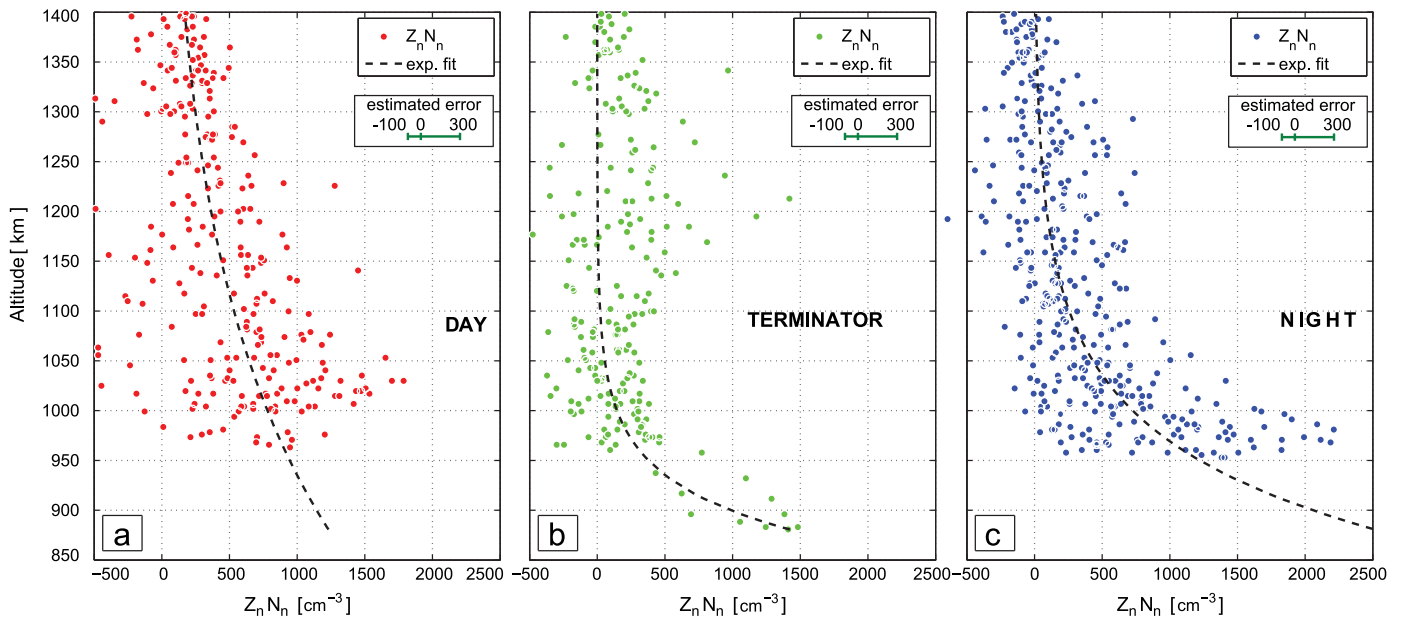


**Fig. 5.** Altitude profiles of negative ion charge densities separated into three SZA intervals. Dayside,  $SZA < 80^\circ$  (a), terminator,  $80^\circ < SZA < 110^\circ$  (b) and nightside,  $SZA > 110^\circ$  (c). Dashed lines are least-square exponential fits to the data:  $f(x) = 3.548E4 \times e^{-3.816E-3x}$  (a),  $f(x) = 2.626E10 \times e^{-1.9E-2x}$  (b),  $f(x) = 2.407E7 \times e^{-1.041E-2x}$  (c), where  $f(x)$  is  $Z_n n_n$ , as a function of altitude  $x$ . The error bar shows total estimated uncertainty, between  $-100$  and  $+300 \text{ cm}^{-3}$ .

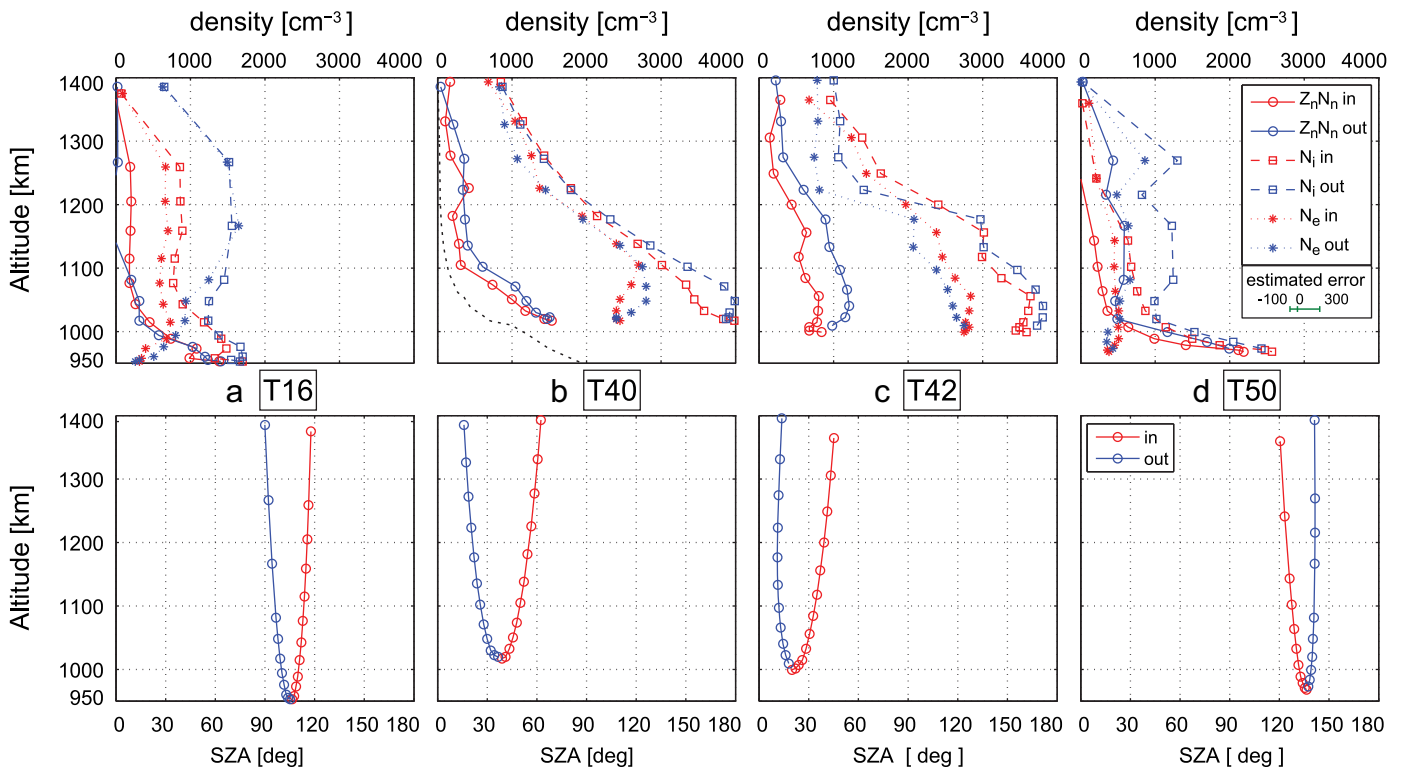


**Fig. 6.** Altitude profiles of electron number density ( $n_e$ ), positive ion number density ( $n_i$ ) and negative ion charge density ( $Z_n n_n$ ) for four individual flybys, T16 (a), T40 (b), T42 (c) and T50 (d), together with corresponding SZA profiles. Red colour shows the ingress data, blue colour shows the egress data. Error bar shows total estimated uncertainty, between  $-100$  and  $+300 \text{ cm}^{-3}$ . The dashed black line superimposed on T40 (b) is the sum of theoretical small-mass negative ion densities and negatively charged aerosol densities adapted from Lavvas et al. (2013). (For interpretation of references to colour in this figure legend, the reader is referred to the web version of this article.)

densities becomes significant. For T16 and T50 (Fig. 6a and d), the regions with most reliable data are below 1000 km and 1020 km altitudes; for T40 and T42 (Fig. 6b and c) such regions are below 1100 km and 1200 km. The nightside negative ion charge densities exhibit a very clear exponential trend already at 1000 km altitude and are the most significant results. Together with the dayside results, this sets constraints on heavy negative ion production and

day-to-night ion chemistry and precipitation. Model results (sum of small-mass negative ion and aerosol densities) from Lavvas et al. (2013) are superimposed onto T40 data (Fig. 6b), replicating the exponential trend of the measured  $Z_n n_n$ . This supports the importance of heavy negative ions for aerosol formation in Titan's ionosphere with a process akin to the one described in Lavvas et al. (2013).

## 4. Discussion

### 4.1. Model assumptions behind derived parameters

The assumption that the plasma impacts the LP with the spacecraft speed ( $v_i \approx v_n \approx v_{sc}$ ) may not be valid for the analysed data set in the ionospheric region of concern. The spacecraft speed relative to Titan is approximately 6 km/s and varies slightly from flyby to flyby, and significant ion drift speeds in the ionosphere may influence the derived densities presented here. If so they need to explain the difference between mean positive ion mass values inferred from the LP and the INMS measurements respectively (see Fig. 3), and to remove the discrepancy the required ion drift speeds relative the spacecraft need to be 3–4 km/s below 1200 km altitude for  $SZA > 100^\circ$  (nightside). However, collisions with the neutral atmosphere are frequent here and such ion drift speeds cannot be explained by convection electric fields (Cravens et al., 2010; Galand et al., in press; Wahlund et al., in press). Also, the observed ion drift speeds along the spacecraft trajectory do not exceed 260 m/s at these lower altitudes (Crary et al., 2009), and estimated neutral wind speeds are not larger (Müller-Wodarg et al., 2006, 2008).

The reported RPWS/LP observations of negative ions during the unique T70 deep flyby to an altitude of 880 km required a differential drift between the positively and negatively charged ions (Ågren et al., 2012), and the results were based on a detailed analysis of selected RPWS/LP voltage sweeps. We therefore present such a case in Appendix C using  $v_{i,n} = v_{sc} \pm 260$  m/s along the Cassini trajectory. This scenario yields an average  $\pm 500 \text{ cm}^{-3}$  shift in  $Z_n n_n$  for most flybys, and we conclude that a differential ion drift may indeed affect the magnitude of the derived charge density of negative ions presented here. Unfortunately, Cassini does not carry an instrument for direct measurements of the DC electric field, and CAPS/IBS did not carry out measurements during the T70 flyby, which would have allowed an estimate of this effect.

An important parameter for our negative ion charge density calculation, the mean positive ion mass ( $m_i$ , see Eq. (3)) is based on INMS data. At least in the deep nightside ionosphere ( $< 1200$  km and  $SZA > 110^\circ$ )  $m_i$  is most likely larger than measured by INMS due to the instrument's measurement limit of 100 amu. The positive ion number densities ( $n_i$ ) and negative ion charge densities ( $Z_n n_n$ ) presented here should therefore be considered as minima. This effect is linearly proportional for  $n_i$ , but  $Z_n n_n$  also depends on the LP sweep measurements ( $a$  and  $b$  parameters)

thus scaling differently for each value. As an example, a factor two increase of  $m_i$  (a likely scenario on the nightside) at altitudes 950–1100 km increases  $Z_n n_n$  by 2400–3500  $\text{cm}^{-3}$  on the dayside and by 700–1200  $\text{cm}^{-3}$  on the nightside.

At the terminator, an apparent decrease (compared to dayside and nightside) in negative ion charge densities at altitudes below 1200 km may instead point to a possible minimum in the ecliptic polar regions of Titan. This is shown in Fig. 7, panel b. Only three flybys passed the Titan ecliptic latitudes of up to  $\pm 30^\circ$  at low altitudes in the terminator region; these three flybys occurred near 6 h Titan Local Time (LT), and show lower densities than other data in the ecliptic latitude belt. If negative ion production is determined by solar EUV radiation, we would expect to find lower  $Z_n n_n$  values near 6 h LT compared to 18 h LT because of the moon's rotation and the time spent during illuminated conditions; also the midday peak of  $Z_n n_n$  should be shifted towards 14 h LT. Unfortunately, no flybys near 18 h LT near Titan's ecliptic plane have taken place so far. The LT and altitude dependence of the presented data shown in Fig. 7 (panel a) is consistent with a scenario where the production starts on the dayside close to the ecliptic belt, and due to Titan's rotation time (16 days) these produced negative ions are slowly moved into the nightside (if no planet-wide drifts are assumed), meanwhile drifting towards lower altitudes and growing into larger particles. The particle sedimentation velocity of 200 cm/s suggested by Wahlund et al. (2009) fits well into the time frame of Titan's rotation period in such a scenario. Horizontal plasma transport could further enhance this picture, and explain why similar heavy ions are detected on both the dayside and nightside hemispheres (Cui et al., 2009).

### 4.2. Charge level of negative ions

Using the Cassini spacecraft potential measured by the LP it is possible to estimate negative ion charge with dusty plasma theory. The measured spacecraft potential ( $U_{sc}$ ) is usually between  $-1$  and  $-0.5$  V, reaching  $-1.5$  V on a few occasions (Wahlund et al., 2009). Dust grain charge is given by Horányi et al. (2004) and Waite et al. (2007) as

$$q_d = 4\pi\epsilon_0 r_d \phi_s \quad (4)$$

where  $q_d$  is the dust grain charge,  $\epsilon_0$  is the vacuum permittivity,  $r_d$  is the radius of a dust grain (assumed to be spherical) and  $\phi_s$  is the surface potential, for which we use as a proxy the spacecraft surface potential ( $U_{sc}$ ) measured by the LP. The dust grain radius is

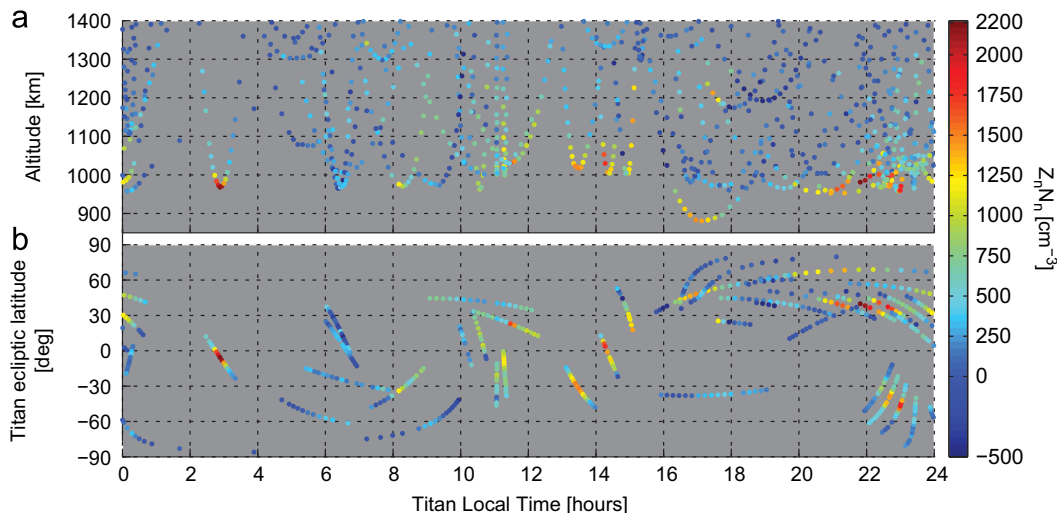


**Fig. 7.** Titan Local Time (LT) dependence of the negative ion charge density  $Z_n n_n$  (panel a). Cassini coverage of Titan in ecliptic coordinates (panel b). Data has been cut above 1200 km for clarity. Note: Time interval of 24 h LT corresponds to one Titan rotation period (16 days). (Figure in colour is available in the web version of this article.)

related to the density and mass of a dust grain as  $r_d^3 = (3m_d/4\pi\rho_d)$ . We assume the density of a dust grain to be  $\approx 0.5 \text{ g/cm}^3$ . Comparing these calculations to heavy negative ions with  $\sim 10,000 \text{ amu/q}$  detected by the CAPS/ELS instrument (Coates et al., 2007, 2009) suggests that the heavy negative ions may have 1 or 2 charges. Additionally, due to the stochastic nature of the dust charging processes for the smallest (nm-sized) grains, the charge is expected to fluctuate around these values depending on the charging mechanism (Horányi et al., 2004).

#### 4.3. Dusty plasma

Dusty behaviour of Titan's nightside low-altitude ionosphere ( $\text{SZA} > 110^\circ$  at altitudes below 1100 km) is suggested by the dominance of ions over “free” electrons, as seen in Fig. 4. To test this hypothesis we use the dusty plasma condition  $r_d \ll d \ll \lambda_D$ , where  $r_d$  is the dust grain radius,  $d$  is the distance between grains and  $\lambda_D$  is the Debye length (Morooka et al., 2011). For the specified region of the ionosphere, with electron densities less than  $500 \text{ cm}^{-3}$  (see Fig. 4, panel a) and electron temperature 300–700 K (Edberg et al., 2010),  $\lambda_D$  is in the range of  $\sim 4\text{--}8 \text{ cm}$ . Assuming negative ions with one or two charges, the distance  $d$  between dust grains is simply inverse cubic root of the negative ion number density  $n_n$ , thus between 0.77 and 2 mm (decreasing towards lower altitude). This gives  $10^4\text{--}10^6$  particles per Debye-cube. Finally, using Eq. (4) we set the radius limit of a spherical dust grain to approximately 3 nm for the heaviest detected negative ions (Coates et al., 2009). Therefore the nightside ( $\text{SZA} > 110^\circ$ ) ionospheric plasma of Titan satisfies the dusty plasma condition at altitudes below 1100 km. Since the peak of the negative ion charge density is not detected most of the time at the lowest measured altitudes on the nightside, it is reasonable to assume that the condition is also fulfilled at altitudes below our current observational limit.

## 5. Conclusions

We present Cassini RPWS/LP ionosphere data based on 47 flybys (94 altitude profiles) of the moon Titan between 880 km and 1400 km altitude, and investigate the distribution of charge particles of positively and negatively charged ions (or aerosol precursors) as well as “free” electrons. In the analysis we make use of the INMS derived average ion mass from 14 of those flybys. The main result is that the total charge densities of negative ions can indeed be estimated with this measurement technique and that Titan harbours substantial amounts of such ions in its ionosphere. Below an altitude of 1000 km on the nightside, the ionosphere is dominated by a mixture of positive and negative ions with few “free” electrons. Our results seem to be consistent with estimates of charge densities of negatively charged ions by the CAPS/ELS instrument (Wellbrock et al., submitted for publication; Coates et al., 2011), there are also interesting similarities in negative ion density trends but a detailed comparison is required to draw conclusions. This is to be investigated in future studies.

The total ionization level in the ionosphere of Titan is therefore larger than previously thought based on measurements of electron number densities alone, and ionospheric ionization models need to take the new results presented here into account in the future. For example, it may provide an explanation for an additional loss process of electrons to charged aerosols as suggested by Vignen et al. (2013). Moreover, the results support the view that the aerosol particle formation starts in the ionosphere of Titan as suggested by several authors (Waite et al., 2007; Coates et al., 2009; Wahlund et al., 2009; 2010; Ågren et al., 2012; Lavvas et al., 2013).

In summary, our results presented here for Titan's ionosphere are:

- The derived electron number densities are consistent with earlier measurements (e.g., Wahlund et al., in press; Wahlund et al., 2005; Ågren et al., 2007, 2009; Edberg et al., 2010), and confirm the characteristics of typical day- and nightside altitude profiles and variation with SZA. Solar EUV dominates the production of the dayside ionosphere. The altitude of the main ionospheric peak rises with increased SZA on the dayside (Fig. 2).
- Negatively charged ions increase exponentially towards lower altitudes down to 880 km. Charge densities of these ions reach up to  $2500 \text{ cm}^{-3}$ . Positively charged ion number densities reach  $4200 \text{ cm}^{-3}$ . On the nightside below 1000 km, the electron number densities are much lower than the ion densities; the positive and negative ion plasma components dominate (Figs. 4 and 6).
- A minimum of negative ion densities is detected around 6 h Titan LT, while a maximum is detected just after 12 h, where also the negative ions are detected at the highest altitudes (up to at least 1200 km). The nightside negative ions are detected mostly below 1000 km (Figs. 4, 6 and 7). We interpret these observations as consistent with a dayside initial production solar EUV and a drift of long-lived heavy negative ions towards lower altitudes during the dusk and night. The ecliptic polar regions show lower negative ion charge densities as compared to dayside ecliptic equatorial belt, further indicating that solar EUV is important for the production.
- The effect of the Kronian magnetosphere particle impact ionization was investigated from a ram angle point-of-view on nightside, but no obvious relationship to the derived negative ion charge densities could be found in this study.
- The deepest part of the ionosphere ( $< 1000 \text{ km}$ ) shows properties of a dusty plasma, with a dominant part of the negative charges carried by heavy negative ions rather than “free” electrons. There are  $10^4\text{--}10^6$  heavy negative ions per Debye-cube, and each of the aerosol-precursor negatively charged particle is predicted to have at most 1–2 charges.

## Acknowledgements

OS, J-EW, NJTE, KÅ were supported by the Swedish National Space Board (SNSB); KM and JHW were supported by NASA funding for the Cassini project. SNSB supports the RPWS/LP instrument on board Cassini.

## Appendix A. Derivation of the negative ion charge density

Analysis of the negative bias voltage current characteristics of the LP revealed that the presence of negative ions is necessary to fully describe Titan's ionosphere, specifically at altitudes below 1200 km and in the deep nightside ionosphere. Here we present the full derivation of ionosphere plasma characteristics from the LP theory.

Using the Orbital Motion Limited (OML) theory (Mott-Smith and Langmuir, 1926; Medicus, 1962), the total current to the LP is fitted to the sum of measured currents from positive and negative ions in the ionosphere:

$$I_{\text{tot}} = I_i + I_n \quad (\text{A1})$$

Here  $I_i$  and  $I_n$  are the positive and the negative ion currents, respectively. To avoid contamination from the electron current, a negative voltage one magnitude larger than the ambient electron temperature ( $< 0.1 \text{ eV}$ , Ågren et al., 2009) is used, i.e.  $U_{\text{bias}} < -1 \text{ V}$  ( $\pm 4 \text{ V}$  sweeps) and  $U_{\text{bias}} < -5 \text{ V}$  ( $\pm 32 \text{ V}$  sweeps). For these

voltages, the numerically convenient approximation of the positive ion current for single-charged positive ions (Fahleson et al., 1974) is

$$I_i = I_{i0}(1 - \chi_i); \quad \begin{cases} I_{i0} = -en_i A_{LP} \sqrt{\frac{v_i^2}{16} + \frac{eT_i[eV]}{2\pi m_i}} \\ \chi_i = \frac{|U_{bias} + U_{float}|}{m_i v_i^2 / 2e + T_i[eV]} \end{cases} \quad (A2)$$

and the approximation for the negative ion current is

$$I_n = I_{n0} \exp(\chi_n); \quad \begin{cases} I_{n0} = +eZ_n n_n A_{LP} \sqrt{\frac{v_n^2}{16} + \frac{eT_n[eV]}{2\pi m_n}} \\ \chi_n = \frac{|U_{bias} + U_{float}|}{m_n v_n^2 / 2e + T_n[eV]} \end{cases} \quad (A3)$$

where  $e$  is the electron charge,  $n_x$ ,  $m_x$ ,  $T_x$  and  $v_x$  are the ion density, mass, temperature and speed, respectively and  $Z_n$  is the negative ion charge number.

As mentioned in Section 2, spacecraft speed at Titan is  $\approx 6$  km/s. This gives typical ram energies of the ions towards the probe in excess of 5 eV, while the dense and cold plasma of Titan's ionosphere has been observed to have thermal energies less than 0.1 eV below an altitude of 1500 km (e.g., Wahlund et al., 2005; Cray et al., 2009; Edberg et al., 2010). The thermal current to the LP for the case of a negative applied voltage is therefore negligible compared to the ram current, so we can approximate with  $\frac{eT[eV]}{2\pi m} \ll \frac{v^2}{16}$  and  $T[eV] \ll \frac{m v^2}{2e}$ . These approximations introduce errors of 0.024% and 0.02%, respectively, in the worst case scenario of lightest ions (molecular nitrogen) and largest ion temperature (0.1 eV). Doubly-charged positive ions are modelled to have negligible peak densities on the order of magnitude of  $10^{-2} \text{ cm}^{-3}$  (Thissen et al., 2011).

The total negative bias voltage current to the LP can then be written as

$$I_{tot} \approx -\frac{1}{4} en_i A_{LP} |v_i| \left(1 - \frac{2eU}{m_i v_i^2}\right) + \frac{1}{4} eZ_n n_n A_{LP} |v_n| \exp\left(\frac{2eU}{m_n v_n^2}\right) \quad (A4)$$

Relying on the fact that the negative ions are heavier than positive ions (Coates et al., 2009; Cray et al., 2009; Mandt et al., 2012) we approximate the exponential term in the negative ion current with a Taylor expansion,  $\exp\left(\frac{2eU}{m_n v_n^2}\right) \approx 1 + \frac{2eU}{m_n v_n^2}$  and assume an order of magnitude difference between negative ( $m_n$ ) and positive ( $m_i$ ) ion mass,  $m_n \geq 10m_i$ . This approximation does not introduce errors larger than the measurement noise of the LP (10%) and indeed we do not see exponential behaviour in our data except for the extremely deep T70 flyby. The total negative bias voltage current then takes simpler form:

$$I_{tot} \approx -\frac{1}{4} en_i A_{LP} |v_i| \left(1 - \frac{2eU}{m_i v_i^2}\right) + \frac{1}{4} eZ_n n_n A_{LP} |v_n| \left(1 + \frac{2eU}{m_n v_n^2}\right) \quad (A5)$$

Using the quasineutrality  $n_e + Z_n n_n \approx n_i$  and assuming no ion drift,  $v_i \approx v_n \approx v_{sc}$ , the total current is simplified further into

$$I_{tot} \approx -\frac{1}{4} eA_{LP} v_{sc} n_e + \frac{e^2 A_{LP}}{2v_{sc}} \left(\frac{Z_n n_n}{m_n} + \frac{n_i}{m_i}\right) U. \quad (A6)$$

Or, in terms of the linear fit to the current measured by the LP,

$$m = a + b \dots U + I_{ph} \quad (A7)$$

where the ‘‘DC’’ level is

$$a \approx -\frac{1}{4} eA_{LP} v_{sc} n_e \quad (A8)$$

and the slope is

$$b \approx -\frac{dI_{tot}}{dU} = -\frac{e^2 A_{LP}}{2v_{sc}} \left(\frac{Z_n n_n}{m_n} + \frac{n_i}{m_i}\right) \quad (A9)$$

Before  $a$  and  $b$  are extracted, the photoelectron current  $I_{ph}$  is removed from the data. This is done by using a simple density model for the dominant atmospheric species  $N_2$  and  $CH_4$  (Ågren et al., 2007), which gives values consistent with Yelle et al. (2006). Together with EUV absorption cross-section, the densities yield the EUV flux and ultimately the photoelectron current along the Cassini trajectory.

Using the assumption  $m_n \geq 10m_i$  we can simplify (A9):

$$b \approx -\frac{e^2 A_{LP}}{2v_{sc} m_i} (n_e + Z_n n_n) \quad (A10)$$

Substituting the electron density derived from (A8) (cross-referenced with the measured electron density from the positive bias voltage LP characteristics and the electron density obtained from the frequency upper-hybrid emissions) we receive the negative ion charge density:

$$Z_n n_n \approx -\frac{4}{eA_{LP}} \left(\frac{a}{v_{sc}} - \frac{bv_{sc} m_i}{2e}\right) \quad (A11)$$

The first term on the right side then corresponds to electron number density and the second term corresponds to the positive ion number density because of quasineutrality. Incidentally, it is worth mentioning that in a case of  $m_n \sim m_i$ , which may affect ionosphere above 1200 km, the derived  $Z_n n_n$  would decrease by a factor of two, which is well within our error margin at these altitudes. However, there is so far no support in the literature for such a case.

## Appendix B. Sweep analysis without negative ions

A simpler model of Titan's ionosphere (as seen by the LP) includes only electrons and positive ions. This model provides simple analysis with less assumptions and generally reliable data at altitudes of 1200–1400 km, where the negative ions appear in small or negligible quantities, such as upper dayside and terminator ionosphere.

Considering only positive ions, the total current approximation for a negative applied bias voltage to the LP, derived from the OML (Mott-Smith and Langmuir, 1926; Medicus, 1962) and LP theories (Fahleson et al., 1974), is simply:

$$I_{tot} \approx -\frac{1}{4} en_i A_{LP} |v_i| \left(1 - \frac{2eU}{m_i v_i^2}\right) \quad (B1)$$

The linear fit to the measured current from which the ion current is derived is again

$$m = a + b \cdot U + I_{ph} \quad (B2)$$

The ‘‘DC’’ current level and the slope are now significantly simpler compared to the full model:

$$a \approx -\frac{1}{4} eA_{LP} |v_i| n_i \quad (B3)$$

$$b \approx -eA_{LP} n_i \frac{e}{2m_i |v_i|} \quad (B4)$$

The positive ion density ( $n_i$ ), the positive ion speed ( $v_i$ ) and the average positive ion mass ( $m_i$ ) can be derived from (B3) and (B4) and according to

$$a \times b \propto n_i^2, m_i^{-1} \quad (B5)$$

$$\frac{a}{b} \propto v_i^2, m_i \quad (B6)$$

Since the system is underdetermined with two equations and three unknowns, either  $v_i$  or  $m_i$  is needed to calculate the other two. If  $v_i \approx v_{sc}$  (no ion drift) is assumed,  $n_i$  (Fig. 2) and  $m_i$  (Fig. 3, left) can be calculated. This is valid for ionosphere in an altitude range

of 1200–1400 km, where the ion drift is negligible or its contribution is less than the measurement noise. As the model was upgraded with the addition of negative ions it has become apparent that the ionospheric profile shown in Fig. 2 is in fact a sum of positive ion and negative ion charge densities, matching electron densities by the means of quasineutrality.

### Appendix C. Ion charge density error due to the zero ion drift assumption

Whether the negative ions are included in the model (Appendix A) or not (Appendix B), the calculations rely on the zero ion drift assumption. For some flybys, the ion drift has been estimated to be up to 260 m/s (Müller-Wodarg et al., 2006, 2008; Crary et al., 2009). Unfortunately the Cassini spacecraft does not carry any instruments on-board to directly measure winds speed and so the ion drifts must be calculated or otherwise derived indirectly. If the ion drift is assumed to be powered by neutral winds, it is sufficient to add an error estimation to the earlier assumption of zero drift ( $v_i \approx v_n \approx v_{sc}$ ). Another scenario is the generation of ion drift by an electric field. In this case the positive and negative ions have the same drift speed ( $v_d$ ) in opposite directions, and the total current given in Eq. (A5) can be written as:

$$I_{tot} \approx -\frac{1}{4} e n_i A_{LP} (v_{i0} + v_d) \left( 1 - \frac{2eU}{m_i (v_{i0} + v_d)^2} \right) + \frac{1}{4} e Z_n n_n A_{LP} (v_{n0} - v_d) \left( 1 + \frac{2eU}{m_n (v_{n0} - v_d)^2} \right) \quad (C1)$$

The zero drift speed assumption now applies to the “rest speed” of the ions,  $v_{i0} \approx v_{n0} \approx v_{sc}$ . Then, using

$$v_i \approx \frac{v_{sc}}{K} \approx v + \Delta v \quad (C2)$$

and

$$v_n \approx v_{sc} \cdot K \approx v_{sc} - \Delta v \quad (C3)$$

where  $\Delta v$  is between 0 and 260 m/s along Cassini trajectory, with  $K \in [0.957; 1]$ , the ion drift can be factorized and the total current can be rewritten as

$$I_{tot} \approx \frac{e A_{LP}}{4} v_{sc} \left[ Z_n n_n K - \frac{n_i}{K} + \frac{2eU}{m_i v_{sc}^2} \left( n_e K + \left( \frac{0.1}{K} + K \right) Z_n n_n \right) \right] \quad (C4)$$

Applying the fit

$$m = a + b \cdot U + I_{ph} \quad (C5)$$

we get parameters  $a$  and  $b$  affected by the ion drift:

$$a \approx -\frac{1}{4} e A_{LP} v_{sc} \left( Z_n n_n K - \frac{n_i}{K} \right) \approx -\frac{1}{4} e A_{LP} v_{sc} \frac{n_e}{K^2} \quad (C6)$$

$$b \approx -\frac{e^2 A_{LP}}{2 v_{sc} m_i} \left( n_e K + \left( \frac{0.1}{K} + K \right) Z_n n_n \right) \approx -\frac{e^2 A_{LP}}{2 v_{sc} m_i} (n_e + Z_n n_n) K \quad (C7)$$

Substituting  $n_e$  from (C6) into (C7) yields the negative ion charge density:

$$Z_n n_n \approx \frac{2}{e A_{LP}} \left( \frac{2a K^2}{v_{sc}} - \frac{b v_{sc} m_i}{e K} \right) \quad (C8)$$

Comparing with Eq. (A11), the electron component has been scaled up by  $K^2$  and the positive ion component has been scaled down by  $K$ . Since  $K \in [0.957; 1]$ , this means that the electron positive ion number densities got roughly decreased by up to 10% and increased by up to 5.3%, introducing an average error in  $Z_n n_n$  of approximately 10%. However, application of this formula requires wind data or estimate for each flyby individually. Therefore, it is

presently not possible to account for ion drifts with other than general and quite rough error estimation.

### References

- Ågren, K., Edberg, N.J.T., Wahlund, J.E., 2012. Detection of negative ions in the deep ionosphere of Titan during the Cassini T70 flyby. *Geophysical Research Letters*, 39.
- Ågren, K., Wahlund, J.E., Garnier, P., Modolo, R., Cui, J., Galand, M., Müller-Wodarg, I., 2009. On the ionospheric structure of Titan. *Planetary and Space Science*, 57, 1821–1827.
- Ågren, K., Wahlund, J.E., Modolo, R., Lummerzheim, D., Galand, M., Müller-Wodarg, I., Canu, P., Kurth, W.S., Cravens, T.E., Yelle, R.V., Waite, J.H., Coates, A.J., Lewis, G. R., Young, D.T., Bertucci, C., Dougherty, M.K., 2007. On magnetospheric electron impact ionisation and dynamics in Titan's ram-side and polar ionosphere—a Cassini case study. *Annales Geophysicae* 25, 2359–2369.
- Coates, A.J., Crary, F.J., Lewis, G.R., Young, D.T., Waite, J.H., Sittler, E.C., 2007. Discovery of heavy negative ions in Titan's ionosphere. *Geophysical Research Letters*, 34.
- Coates, A.J., Wahlund, J.E., Ågren, K., Edberg, N., Cui, J., Wellbrock, A., Szego, K., 2011. Recent results from Titan's ionosphere. *Space Science Reviews* 162, 85–111.
- Coates, A.J., Wellbrock, A., Lewis, G.R., Jones, G.H., Young, D.T., Crary, F.J., Waite, J.H., 2009. Heavy negative ions in Titan's ionosphere: altitude and latitude dependence. *Planetary and Space Science* 57, 1866–1871.
- Coates, A.J., Wellbrock, A., Lewis, G.R., Jones, G.H., Young, D.T., Crary, F.J., Waite, J.H., Johnson, R.E., Hill, T.W., Sittler, E.C., 2010. Negative ions at Titan and Enceladus: recent results. *Faraday Discussions* 147, 293–305.
- Crary, F.J., Magee, B.A., Mandt, K., Waite, J.H., Westlake, J., Young, D.T., 2009. Heavy ions, temperatures and winds in Titan's ionosphere: combined Cassini CAPS and INMS observations. *Planetary and Space Science* 57, 1847–1856.
- Cravens, T.E., Richard, M., Ma, Y.J., Bertucci, C., Luhmann, J.G., Ledvina, S., Robertson, I.P., Wahlund, J.E., Ågren, K., Cui, J., Müller-Wodarg, I., Waite, J.H., Dougherty, M., Bell, J., Ulusen, D., 2010. Dynamical and magnetic field time constants for Titan's ionosphere: empirical estimates and comparisons with Venus. *Journal of Geophysical Research: Space Physics*, 115.
- Cravens, T.E., Robertson, I.P., Waite, J.H., Yelle, R.V., Kasprzak, W.T., Keller, C.N., Ledvina, S.A., Niemann, H.B., Luhmann, J.G., McNutt, R.L., Ip, W.H., De La Haye, V., Mueller-Wodarg, I., Wahlund, J.E., Anicich, V.G., Vuitton, V., 2006. Composition of Titan's ionosphere. *Geophysical Research Letters*, 33.
- Cravens, T.E., Robertson, I.P., Waite, J.H., Yelle, R.V., Vuitton, V., Coates, A.J., Wahlund, J.E., Ågren, K., Richard, M.S., La Haye, V., Wellbrock, A., Neubauer, F.M., 2009. Model-data comparisons for Titan's nightside ionosphere. *Icarus* 199, 174–188.
- Cui, J., Galand, M., Yelle, R.V., Vuitton, V., Wahlund, J.E., Lavvas, P.P., Müller-Wodarg, I.C.F., Cravens, T.E., Kasprzak, W.T., Waite, J.H., 2009. Diurnal variations of Titan's ionosphere. *Journal of Geophysical Research: Space Physics*, 114.
- Edberg, N.J.T., Ågren, K., Wahlund, J.E., Morooka, M.W., Andrews, D.J., Cowley, S.W. H., Wellbrock, A., Coates, A.J., Bertucci, C., Dougherty, M.K., 2011. Structured ionospheric outflow during the Cassini T55–T59 Titan flybys. *Planetary and Space Science* 59, 788–797.
- Edberg, N.J.T., Wahlund, J.E., Ågren, K., Morooka, M.W., Modolo, R., Bertucci, C., Dougherty, M.K., 2010. Electron density and temperature measurements in the cold plasma environment of Titan: implications for atmospheric escape. *Geophysical Research Letters*, 37.
- Fahleson, U., Faltham, Cg, Pedersen, A., 1974. Ionospheric temperature and density-measurements by means of spherical double probes. *Planetary and Space Science* 22, 41–66.
- Galand, M., Coates, A.J., Cravens, T.E., Wahlund, J.-E., 2012. Titan's ionosphere. In: Müller-Wodarg, I., Griffith, C., Lellouch, E., Cravens, T.E. (Eds.), *Titan: Surface, Atmosphere and Magnetosphere*. Cambridge University Press. (in press).
- Galand, M., Yelle, R., Cui, J., Wahlund, J.-E., Vuitton, V., Wellbrock, A., Coates, A., 2010. Ionization sources in Titan's deep ionosphere. *J. Geophys. Res.* 115, A07312 10.1029/2009JA015100.
- Garnier, P., et al., 2012. The detection of energetic electrons with the Cassini Langmuir probe at Saturn. *J. Geophys. Res.* 117, A10202 10.1029/2011JA017298.
- Gurnett, D.A., Kurth, W.S., Kirchner, D.L., Hospodarsky, G.B., Averkamp, T.F., Zarka, P., Lecacheux, A., Manning, R., Roux, A., Canu, P., Cornilleau-Wehrin, N., Galopeau, P., Meyer, A., Bostrom, R., Gustafsson, G., Wahlund, J.E., Ahlen, L., Rucker, H.O., Ladreiter, H.P., Macher, W., Woolliscroft, L.J.C., Alleyne, H., Kaiser, M.L., Desch, M.D., Farrell, W.M., Harvey, C.C., Louarn, P., Kellogg, P.J., Goetz, K., Pedersen, A., 2004. The Cassini radio and plasma wave investigation. *Space Science Reviews* 114, 395–463.
- Holmberg, M.K.G., Wahlund, J.E., Morooka, M.W., Persoon, A.M., 2012. Ion densities and velocities in the inner plasma torus of Saturn. *Planetary and Space Science* 73, 151–160.
- Horányi, M., Hartquist, T.W., Havnes, O., Mendis, D.A., Morfill, G.E., 2004. Dusty plasma effects in Saturn's magnetosphere. *Reviews of Geophysics*, 42.
- Lavvas, P., Yelle, R.V., Koskinen, T., Bazin, A., Vuitton, V., Vigren, E., Galand, M., Wellbrock, A., Coates, A.J., Wahlund, J.E., Crary, F.J., Snowden, D., 2013. Aerosol growth in Titan's ionosphere. *Proceedings of the National Academy of Sciences of the United States of America*.
- Mandt, K.E., et al., 2012. Ion densities and composition of Titan's upper atmosphere derived from the Cassini Ion Neutral Mass Spectrometer: analysis methods and comparison of measured ion densities to photochemical model simulations. *J. Geophys. Res.* 117, E10006 10.1029/2012JE004139.

- Medicus, G., 1962. Spherical langmuir probe in drifting and accelerated Maxwellian distribution. *Journal of Applied Physics* 33, 3094.
- Morooka, M.W., Wahlund, J.E., Eriksson, A.I., Farrell, W.M., Gurnett, D.A., Kurth, W.S., Persoon, A.M., Shafiq, M., Andre, M., Holmberg, M.K.G., 2011. Dusty plasma in the vicinity of Enceladus. *Journal of Geophysical Research: Space Physics*, 116.
- Mott-Smith, H., Langmuir, I., 1926. The theory of collectors in gaseous discharges. *Physical Review* 28, 727–763.
- Müller-Wodarg, I.C.F., Yelle, R.V., Borggren, N., Waite, J.H., 2006. Waves and horizontal structures in Titan's thermosphere. *Journal of Geophysical Research* 111.
- Müller-Wodarg, I.C.F., Yelle, R.V., Cui, J., Waite, J.H., 2008. Horizontal structures and dynamics of Titan's thermosphere. *Journal of Geophysical Research* 113.
- Sagan, C., Khare, B.N., 1979. Tholins: organic chemistry of interstellar grains and gas. *Nature* 277, 102–107.
- Thissen, R., Witasse, O., Dutuit, O., Wedlund, C.S., Gronoff, G., Lilensten, J., 2011. Doubly-charged ions in the planetary ionospheres: a review. *Physical Chemistry Chemical Physics: PCCP* 13, 18264–18287.
- Vigren, E., Galand, M., Yelle, R.V., Cui, J., Wahlund, J.E., Ågren, K., Lavvas, P.P., Mueller-Wodarg, I.C.F., Strobel, D.F., Vuitton, V., Bazin, A., 2013. On the thermal electron balance in Titan's sunlit upper atmosphere. *Icarus* 223, 234–251.
- Vuitton, V., Lavvas, P., Yelle, R.V., Galand, M., Wellbrock, A., Lewis, G.R., Coates, A.J., Wahlund, J.E., 2009. Negative ion chemistry in Titan's upper atmosphere. *Planetary and Space Science* 57, 1558–1572.
- Wahlund, J.-E., Modolo, R., Bertucci, C., Coates, A.J., ?Titan's magnetospheric and plasma environment. In: Mueller-Wodarg, I., Griffith, C., Lellouch, E., Cravens, T. E. (Eds.), *Titan: Surface, Atmosphere and Magnetosphere*. Cambridge University Press. (in press).
- Wahlund, J.E., Bostrom, R., Gustafsson, G., Gurnett, D.A., Kurth, W.S., Pedersen, A., Averkamp, T.F., Hospodarsky, G.B., Persoon, A.M., Canu, P., Neubauer, F.M., Dougherty, M.K., Eriksson, A.I., Morooka, M.W., Gill, R., Andre, M., Eliasson, L., Muller-Wodarg, I., 2005. Cassini measurements of cold plasma in the ionosphere of Titan. *Science* 308, 986–989.
- Wahlund, J.E., Galand, M., Muller-Wodarg, I., Cui, J., Yelle, R.V., Crary, F.J., Mandt, K., Magee, B., Waite, J.H., Young, D.T., Coates, A.J., Garnier, P., Agren, K., Andre, M., Eriksson, A.I., Cravens, T.E., Vuitton, V., Gurnett, D.A., Kurth, W.S., 2009. On the amount of heavy molecular ions in Titan's ionosphere. *Planetary and Space Science* 57, 1857–1865.
- Waite Jr., J.H., Young, D.T., Cravens, T.E., Coates, A.J., Crary, F.J., Magee, B., Westlake, J., 2007. The process of tholin formation in Titan's upper atmosphere. *Science* 316, 870–875.
- Wellbrock, A., Coates, A.J., Jones, G.H., Lewis, G.R., Waite, J.H., ?Cassini CAPS-ELS observations of negative ions in Titan's ionosphere: trends of density with altitude. *Geophysical Research Letters*. (submitted for publication).
- Yelle, R.V., Borggren, N., de la Haye, V., Kasprzak, W.T., Niemann, H.B., Müller-Wodarg, I., Waite, J.H., 2006. The vertical structure of Titan's upper atmosphere from Cassini Ion Neutral Mass Spectrometer measurements. *Icarus* 182, 567–576.

# On Ion Drifts and Neutral Winds in Titan's Thermosphere

---

Oleg Shebanits, Swedish Institute of Space Physics, Uppsala, Sweden and Department of Physics and Astronomy, Uppsala University, Uppsala, Sweden

Jan-Erik Wahlund, Niklas J. T. Edberg, David J. Andrews, Swedish Institute of Space Physics, Uppsala, Sweden

Frank J. Crary, University of Colorado, Boulder, Massachusetts, USA

Anne Wellbrock and Andrew J. Coates, Mullard Space Science Laboratory, University College London, Dorking, UK and Centre for Planetary Sciences, University College London/Birkbeck, London, UK

Kathleen E. Mandt & J. Hunter Waite Jr., Space Science and Engineering Division, Southwest Research Institute, San Antonio, Texas, USA

Corresponding author: O. Shebanits, Swedish Institute of Space Physics, Box 537, SE 751 21 Uppsala, Sweden. ([oleg.shebanits@irfu.se](mailto:oleg.shebanits@irfu.se))

## Key points

- Differential ion flux measured by Cassini RPWS/LP
- Ion drifts in Titan's ionosphere
- Neutral winds in Titan's thermosphere
- Kronian Magnetosphere – Titan's Ionosphere plasma interaction

## Index

6281 Titan

2409 Current systems (2721)

2431 Ionosphere/magnetosphere interactions (2736)

2427 Ionosphere/atmosphere interactions (0335)

7849 Plasma interactions with dust and aerosols (2461)

Key words: ionosphere drifts

## Abstract

Saturn's largest moon Titan hosts an atmosphere with complex organic chemistry initiated partly in the ionosphere. The nightside chemistry may be influenced by the ion transport from the dayside ionosphere. In turn, ion transport (ion drifts) may be affected by the neutral winds, which cannot be measured directly by Cassini. In this study we derive the ion drifts along the spacecraft trajectories based on analysis of *in-situ* measurements of electron and ion fluxes, mean masses of positive and negative ions and the magnetic field. Data from Titan flybys TA to T100 (Oct 2005 - Apr 2014) is included in this study, 55 flybys are below 1400 km and 48 are below 1200 km altitude. Based on the measurements, three regions of the ionosphere were defined by altitude: **1**) above 1600 km, ions are  $\mathbf{E} \times \mathbf{B}$ -drifting (frozen into the magnetic field), **2**) 1100-1600 km, dynamo-region, ions drift partly in opposite directions (perpendicular to  $\mathbf{B}$ ) and **3**) below 1100 km (upper limit depends on convection electric field strength), ions are following neutrals and ion drifts translate to neutral winds of 0.5-2.5 km/s with weaker winds on the dayside of Titan's ionosphere. The measured neutral wind speed reaches 5.3 km/s during T70, with average values between is 0.5-1.5 km/s on the dayside and 1.5-2.5 km/s on the nightside.

## 1 Introduction

Since the arrival of Cassini mission, Saturn's moon Titan has attracted scientific interest with its one-of-a-kind dense organically rich atmosphere of nitrogen and methane [Waite *et al.*, 2005; Cravens *et al.*, 2006; Magee *et al.*, 2009; Cravens *et al.*, 2010b; Mandt *et al.*, 2012]. Titan's atmosphere and ionosphere has become famous for its complex organic chemistry [Waite *et al.*, 2007; Vuitton *et al.*, 2009] that produces hydrocarbons, nitriles and ultimately its orange haze aerosols [Niemann *et al.*, 2005; Coates *et al.*, 2007; Waite *et al.*, 2007; Lavvas *et al.*, 2013]. This process begins in the ionosphere with energy inputs by the solar EUV/X-rays, magnetospheric particles of Saturn and cosmic radiation, in the order of significance [Wahlund *et al.*, 2005; Ågren *et al.*, 2009; Galand *et al.*, 2010]. Instruments on-board Cassini s/c allowed extensive studies of Titan's ionosphere with *in-situ* measurements of ion densities [Ågren *et al.*, 2009; Shebanits *et al.*, 2013; Wellbrock *et al.*, 2013] and composition [Waite *et al.*, 2005; Cravens *et al.*, 2006; Magee *et al.*, 2009; Cravens *et al.*, 2010b; Mandt *et al.*, 2012]. Ion drifts have been modelled and derived from measurements by e.g. Müller-Wodarg *et al.* [2008]; Crary *et al.* [2009]; Cravens *et al.* [2010a] but such slow ion drifts could not account for the similar ion composition in the nightside and dayside ionosphere [Cui *et al.*, 2010]. Ion drifts are difficult to estimate because Cassini does not carry an instrument for direct measurement of neutral wind velocities and instead require a combination of simultaneous independent measurements. This study aims to extend and complement the previously presented ion drift derivations and models [Müller-Wodarg *et al.*, 2008; Crary *et al.*, 2009; Cravens *et al.*, 2010a]. To that end we analyse the difference in measured electron densities and apparent total ion densities (which may be affected by ion drifts) during all flybys of Titan from October 2004 to April 2014 and interpret it as an effect of the ion drifts measured by the Radio and Plasma Wave Science (RPWS) Langmuir probe (LP) instrument. Flybys TA to T100 were included, of which 55 were below 1400 km and 48 below 1200 km altitude. Section 2 covers the analysis, the results are presented and discussed in Section 3 and conclusions are summarized in Section 4.

## 2 Method and Instrumentation

### 2.1 Instrument methods

The Langmuir Probe on board Cassini s/c is a sphere of 2.5 cm radius covered in titanium nitride and placed on a rigid boom approximately 1.5 m from the s/c [Gurnett *et al.*, 2004]. The basic principle of operation is collection of plasma current for defined voltages (typical voltage sweep for Titan flybys is  $\pm 4$  V every 24 s), yielding a current-voltage characteristic that depends on ion and electron densities, speeds and temperatures. The analysis of the RPWS/LP ion current is based on the Orbital-Motion Limited (OML) theory described by *Medicus* [1962] and *Mott-Smith and Langmuir* [1926] and has been covered in i.e. *Edberg et al.* [2011]; *Morooka et al.* [2011]; *Shebanits et al.* [2013]. In this study we also used measurements of mean ion mass from Ion and Neutral Mass Spectrometer (INMS) [Waite *et al.*, 2004; Mandt *et al.*, 2012], Cassini Plasma Spectrometer [CAPS, Young *et al.*, 2004] Ion Beam Spectrometer (IBS) Crary *et al.* [2009] and Electron Spectrometer (ELS) Coates *et al.* [2010]; Wellbrock *et al.* [2013], and magnetic field measurements from Cassini Magnetometer (MAG) [Dougherty *et al.*, 2004]. Here we will give a brief summary of the RPWS/LP methods and concentrate on the part relevant for the study.

The OML theory gives an approximation [Fahleson *et al.*, 1974] of the total ion current to the probe moving in plasma [Shebanits *et al.*, 2013, Appendix] as:

$$I = \begin{cases} I_0(1 - \chi) & \text{for attracting potentials} \\ I_0 e^{-\chi} & \text{for repelling potentials} \end{cases} \quad (1)$$

with

$$I_0 = -q_{\pm} n_{\pm} A_{LP} |v_{sc} + v_{\pm}| \quad \text{and} \quad \chi = \frac{2q_{\pm} |U_{bias} + U_{float}|}{m_{\pm} (v_{sc} + v_{\pm})_{\pm}^2} \quad (2)$$

$A_{LP}$  is the LP surface area,  $v_{sc}$  is the s/c speed,  $q$ ,  $n$ ,  $m$  and  $v$  are the ion charges, densities, mean masses and *velocity projections* on s/c trajectory, resp. (indexed plus for positive and minus for negative ions) and  $U_{float} + U_{bias}$  is the sum of the floating and bias potentials of the probe. Inserting (2) into (1) for positive and negative ions we have the expression for the total ion current measured by the LP:

$$I_{tot} = \frac{q_e A_{LP}}{4} \left[ Z_- n_- |v_{sc} + v_-| - n_+ |v_{sc} + v_+| + 2q_e (U_{float} + U_{bias}) \cdot \left( \frac{n_+}{m_+ |v_{sc} + v_+|} + \frac{Z_- n_-}{Z_- |v_{sc} + v_-|} \right) \right] \quad (3)$$

where  $q_e$  is the electron charge,  $Z_-$  is the mean neg. ion charge (pos. ions assumed single-charged). This current is linearly dependent on the voltage and is therefore fitted in the analysis by

$$I_{tot} = a + b \cdot U_{bias} + I_{ph} \quad (4)$$

The photoelectron current  $I_{ph}$  is subtracted in the processing. Identifying with Equation (3) gives parameters  $a$  and  $b$ :

$$a = -\frac{q_e A_{LP}}{4} \left( \overbrace{(n_+ - Z_- n_-)}^{=n_e} v_{sc} + n_+ v_+ - Z_- n_- v_- \right) = -\frac{q_e A_{LP}}{4} (n_e v_{sc} + n_+ v_+ - Z_- n_- v_-) \quad (5)$$

$$b = -\frac{dI_{\text{tot}}}{dU} = -\frac{q_e^2 A_{\text{LP}}}{2V_{\text{sc}}} \cdot \left( \frac{n_+}{m_+(v_{\text{sc}}+v_+)} + \frac{Z_- n_-}{Z_- (v_{\text{sc}}+v_-)} \right) \quad (6)$$

where  $n_e$  is the electron density (replacing  $n_+ - Z_- n_-$  by charge quasineutrality) and we assume that  $|v_{\pm}| < v_{\text{sc}}$  (valid below  $\approx 1400$  km, see Figure 3). The calculation of mean ion masses is not straightforward: as CAPS instrument has been powered off since June 4, 2012<sup>1</sup> it is not possible to get mean ion masses for flybys of Titan past T83. INMS is still functional but has an upper measurement limit of 100 amu. However, the heavier positive and negative ions are all ultimately formed from the lighter positive ions (and neutrals) which implies an altitude dependence. This dependence can be exploited by fitting IBS and ELS mean ion masses (heavy and light ions) to the INMS mean ion masses (light ions). An altitude-SZA fit of INMS data described in *Shebanits et al.* [2013] is used for this purpose, effectively expanding the IBS/ELS-derived mean ion mass datasets to all flybys.

Charge neutrality implies that the total ion charge densities derived from the ion current must match electron densities derived from the electron current. For Titan flybys this is not always the case and  $n_+ - Z_- n_-$  frequently differs from  $n_e$  by more than the RPWS/LP measurement error of 10% (Figure 1) and has been observed for the majority of Titan flybys. The measured ion current is directly proportional to the ion charge flux to the probe and as such is affected by ion drifts: motion of the ions in the spacecraft frame, either headwinds or tailwinds, would respectively increase or decrease the measured ion charge flux, and therefore the ion current, while the electrons are thermal and therefore not affected. In previous studies (e.g. *Shebanits et al.* [2013]) an attempt to circumvent it was made by using the independently measured electron densities  $n_e$  rather than the total ion charge density  $n_+ - Z_- n_-$ . Interpreting the discrepancy between  $n_+ - Z_- n_-$  and  $n_e$  as ion drift effect, we construct the *differential ion flux as the difference between the positive and negative ion fluxes to the probe* from Equation (5):

$$F_{\text{diff}} = n_+ v_+ - Z_- n_- v_- = \frac{\overbrace{n'_{\text{tot}} v_{\text{sc}}}^{4a}}{q_e A_{\text{LP}}} - n_e v_{\text{sc}} \quad (7)$$

where  $n'_{\text{tot}}$  is the *apparent total ion density*, or the total ion density in a stationary plasma ( $v_{\text{sc}} \approx v_{\text{plasma}}$ ,  $v_+ = v_- = 0$ ). In essence,  $F_{\text{diff}}$  is the difference between the apparent total ion density and the electron density, as illustrated in Figure 1. The assumption  $v_{\text{sc}} \approx v_{\text{plasma}}$  has been used in the earlier analysis, with support from Titan wind models and studies [*Müller-Wodarg et al.*, 2008; *Crary et al.*, 2009], estimating error from ion drifts up to 10% for negative ion densities [*Shebanits et al.*, 2013].

## 2.2 Ionospheric drifts

Ionospheric drifts and currents are described by the momentum equation for the ions:

$$n_{\pm} m_{\pm} \frac{dv_{\pm}}{dt} = q_{\pm} n_{\pm} (\mathbf{E} + \mathbf{v}_{\pm} \times \mathbf{B}) - n_{\pm} m_{\pm} \nu_{\pm n} (\mathbf{v}_{\pm} - \mathbf{v}_n) \quad (8)$$

where  $n_{\pm}$ ,  $m_{\pm}$ ,  $q_{\pm}$ , and  $v_{\pm}$  are number density, mean mass, charge and density of ions,  $\mathbf{v}_n$  is the neutral wind,  $\nu_{\pm n}$  is the frequency of ion collisions with neutrals,  $\mathbf{E}$  and  $\mathbf{B}$  are electric and magnetic

<sup>1</sup> <http://saturn.jpl.nasa.gov/news/significantevents/anomalies/>

fields. Horizontal effects of pressure gradient and gravity terms can be neglected [Cui *et al.*, 2010]. Assuming steady state, single-charged positive ions and setting the negative ion charge  $q_- = -Z_-q_e$ , we can derive the ion velocities from Equation ( 8 ) as functions of three parameters,  $v_{\pm n}/\Omega_{\pm}$ ,  $\mathbf{E}$  and  $\mathbf{B}$ :

$$\mathbf{v}_{\pm} = \frac{1}{1 + \left(\frac{v_{\pm n}}{\Omega_{\pm}}\right)^2} \left( \frac{\mathbf{E}}{B} \pm \frac{v_{\pm n}}{\Omega_{\pm}} \mathbf{v}_n \right) \times \left( \hat{\mathbf{B}} \pm \frac{v_{\pm n}}{\Omega_{\pm}} \right) \quad (9)$$

where  $\hat{\mathbf{B}}$  is the magnetic field direction,  $\Omega_+ = q_e B/m_+$  and  $\Omega_- = Z_-q_e B/m_-$  are the gyrofrequencies of respective species and  $v_{\pm n} = 2.6 \cdot 10^{-9} n_{N_2} \sqrt{2.59/\mu_{\pm}}$  is the ion-neutral collision frequency (Hz) [Banks and Kockarts, 1973], a function of neutral nitrogen's density ( $\text{cm}^{-3}$ ) from INMS measurements [Magee *et al.*, 2009] and ion-neutral reduced mass  $\mu_{\pm} = m_{\pm} m_n (m_{\pm} + m_n)^{-1}$  (amu). The deciding factor for the ion velocities is the ratio of the collision and gyrofrequencies [Rosenqvist *et al.*, 2009], which can be derived with INMS measurements of neutral densities, CAPS/ELS and CAPS/IBS mass measurements and MAG measurements of magnetic field – plotted in Figure 2. Above  $\sim 1500$  km the collision frequencies for positive and negative ions are approximately one magnitude smaller than the gyrofrequencies (in agreement with Cui *et al.* [2009]; Rosenqvist *et al.* [2009]) and the ions are expected to  $\mathbf{E} \times \mathbf{B}$ -drift. Below this limit the electric field and increasing collision rates force ions to drift in different directions. It should be noted that the mean ion mass and neutral density profiles are uncertain for altitudes above 1400 km due to very low particle densities and high ion velocities but can be extrapolated from the fits to measurements below 1400 km. For positive and negative mean ion masses we assume 27-28 amu above 1400 km, based on INMS measurements near this limit [Mandt *et al.*, 2012]. It should also be noted that the difference in the ratio at altitudes below 1400 km is due to the gyrofrequency for negative ions decreasing more with altitude compared to positive ions (with increasing mass), while the collision frequency remains almost the same for both species.

Using the magnitude of the ion velocities in Equation ( 9 ),

$$|\mathbf{v}_{\pm}| = \left| \frac{\mathbf{E}}{B} \pm \frac{v_{\pm n}}{\Omega_{\pm}} \mathbf{v}_n \right| \left( 1 + \left( \frac{v_{\pm n}}{\Omega_{\pm}} \right)^2 \right)^{-0.5} \quad (10)$$

we derive the maximum ( $\mathbf{E} \parallel \mathbf{v}_n$ ) drift speeds of ions. Electric field strength varies between 0.5-4  $\mu\text{V}/\text{m}^2$  for shown altitudes in Titan's ionosphere [Ågren *et al.*, 2011]. Lower limit case is shown in Figure 3 and upper limit case in Figure 4. Below 1000-1100 km the ions are following neutrals, therefore the neutral wind speeds along the Cassini trajectory can be derived from the differential ion flux measurements by substituting  $v_+ \approx v_- \approx v_n$  into Equation ( 7 ):

$$v_n = v_{sc} \left( \frac{n'_{tot}}{n_e} - 1 \right) \quad (11)$$

### 2.3 Electric field

Summing Equation ( 8 ) over positive and negative ions (again assuming steady state and single-charged positive ions) and using the ion current definition from Equation ( 7 ) we have

$$\mathbf{E} = \frac{1}{q_e n_e} \left[ -q_e \mathbf{F}_{diff} \times \mathbf{B} + n_+ m_+ v_{+n} (\mathbf{v}_+ - \mathbf{v}_n) + Z_- n_- \frac{m_-}{Z_-} v_{-n} (\mathbf{v}_- - \mathbf{v}_n) \right] \quad (12)$$

The measured  $\mathbf{F}_{\text{diff}}$  (Equation ( 7 )) is a projection on  $\hat{\mathbf{v}}_{sc}$  and can be used to constrain the minimum values of the  $\mathbf{E}$ -field. Without the neutral winds,  $\mathbf{F}_{\text{diff}} \times \mathbf{B}$  term is 1-2 magnitudes smaller than the collision terms below 1100 km.

### 3 Results & Discussion

With calculation results shown in Figure 3 and Figure 4, three regions of the ionosphere can be defined:

1. In the upper ionosphere (yellow-shaded, above 1600 km) both positive and negative ions are  $\mathbf{E} \times \mathbf{B}$ -drifting and stronger electric field corresponds to larger ion drift velocities.
2. In the middle part of the ionosphere (dynamo region, red-shaded, from 1000-1100 km to 1600 km) the ions drift in opposite directions  $\perp \mathbf{B}$  due to collisions with neutrals in the presence of the electric and magnetic fields. Positive ions move faster than negative, proportionally to the ratio between  $m_-/Z_-$  and  $m_+$ . The altitude borders of this region in these calculations are in agreement with the conductivity model results presented in Rosenqvist et al. [2009].
3. In the collision-dominated lower ionosphere (below 1000-1100 km) the ions follow neutral winds. Upper limit of this region depends on the electric field strength and varies between 1100 km for  $E = 0.5 \mu\text{V}/\text{m}^2$  and 1000 km for  $E = 4 \mu\text{V}/\text{m}^2$  (blue-shaded, in Figure 4 shown in the zoom-in insert for clarity). The magnitudes of ion velocities in the neutral wind frame of reference are in agreement with the single-fluid momentum equation calculations of Cravens et al. [2010a] and MHD simulations by [Ma et al., 2011, private communication]. The upper altitude limit for this region, defined to be 1300 km by Cravens et al. [2010a], is further constrained here to 1100 km (Figure 2), based on the minimum estimated electric field strength of  $0.5 \mu\text{V}/\text{m}^2$  from Ågren et al. [2011].

The differential ion flux can in principle be caused by a  $\sim 0.1$ - $0.2$  V change in s/c potential ( $U_{sc}$ ), which may affect the electron densities. This effect is noticeable in the current-voltage characteristics of RPWS/LP in the thinner magnetospheric plasma [Olson et al., 2010], where the Debye length may be comparable to the RPWS/LP boom length (1.5 m). In Titan's ionosphere the Debye length is less than 10 cm [Shebanits et al., 2013] and therefore the effects of the s/c potential are eliminated. This is further confirmed by the fact that the  $U_{sc}$  derived from the RPWS/LP (typically electron side of the current-voltage characteristics) is in excellent agreement with  $U_{sc}$  derived from CAPS/IBS and INMS [Crary et al., 2009], which both measure positive ions that are *attracted* by the negative s/c potential. Additionally, the RPWS/LP measurements of total ion and electron densities are in good agreement outside the ionosphere of Titan, as shown in the T77 example (Figure 1, the beginning and the end of the density profiles). In particular, the RPWS/LP derived electron densities are consistent with those derived from the upper hybrid emissions. The differential ion flux at altitudes below 1100 km cannot be explained by previous ion velocity estimates of  $\leq 250$  m/s [Müller-Wodarg et al., 2008; Crary et al., 2009]. It should also be noted that the values presented here are consistent across 48 flybys of Titan's ionosphere below 1200 km and agree with the ion velocities required by Ågren et al. [2012] to explain the LP measurements during the T70 flyby. In absence of other evidence, the ion drifts explanation is therefore most plausible.

To make the measurements of the differential ion flux  $F_{\text{diff}}$  independent of the s/c movement, a westward-positive  $\hat{F}_{\text{diff}}$  was defined by reversing all Cassini trajectories with a westward component (since  $\hat{F}_{\text{diff}}$  is opposed to  $\hat{v}_{\text{sc}}$ ). Positive  $F_{\text{diff}}$  should therefore not be confused with strictly westward flux, *it only implies that the differential ion flux projection onto s/c trajectory has a westward component*. The measured differential ion flux is plotted in Figure 5. General trend in the direction-corrected data (panel **b**) is eastward, with larger values on the dayside ionosphere ( $\text{SZA} < 70^\circ$ ). Concentrations of westward flux around terminator ( $70^\circ < \text{SZA} < 110^\circ$ ) occurs mostly around Titan's poles (see Figure 6), implying effects of interaction with Saturn's magnetosphere (e.g. ions flowing in and out).

Multiplying  $F_{\text{diff}}$  with electron charge we obtain the differential (total) ion current, plotted in corotational coordinates in Figure 6 and in altitude versus west longitude in Figure 7, separated by the SZA into day, terminator and night as described above. The differential ion current shows a pattern of direction reversal between dayside and nightside ionosphere, occurring over the terminator region (Figure 6). More accurately since we are measuring along the s/c trajectory, on the dayside the current has a component in the direction of Saturn's corotational plasma while on the nightside the current has a component in the opposite direction and the terminator region has a mixture of both. This is consistent with the convection patterns from the magnetospheric two-fluid MHD simulations of the plasma flow by [Ma *et al.*, 2011, personal communication] and may be similarly explained by the currents closing into the magnetospheric plasma in the terminator region, especially since the majority of the terminator flybys are concentrated around Titan's north pole (Figure 6, panels **c** and **d**). Similar picture is expected on the south polar region, with support from the ion outflow observed by Edberg *et al.* [2011], but the flyby coverage below 1400 km in this part of Titan's ionosphere is insufficient at present.

Close examination of the region where the ions follow the neutrals (below  $\sim 1100$  km) reveals strong polar neutral winds (Figure 8 and Figure 10) within an order of magnitude of 0.5-2.5 km/s on the dayside and up to 4 km/s on the nightside. The terminator flybys cover mostly the north polar region of Titan ionosphere [Shebanits *et al.*, 2013]. T70 is a special case across the North Pole with wind speeds estimated here to 5.3 km/s between 880-900 km altitudes (Figure 8). Cui *et al.* [2009] discussed the inconsistency between the ion transport modelled based on the ion drift velocity estimates of  $\sim 200$  m/s by Müller-Wodarg *et al.* [2008]; Crary *et al.* [2009] and the striking similarity of the measured ion composition in the dayside and nightside ionosphere. The neutral wind velocities presented here solve that issue as they would transport ions at altitudes  $\sim 1000$  km from dayside to nightside in about 1.5 h.

The measurement points near the closest approach (marked with arrows in Figure 9 and Figure 10) show s/c trajectories with  $< 5^\circ$  inclination with respect to the surface. In fact, all of the trajectories below 1100 km altitude have inclination  $< 15^\circ$ , the only exception is T70, the trajectory of which reaches  $20^\circ$  inclination at 1100 km altitude. Vertical components of the neutral winds have therefore less impact on the measurements than the horizontal components. For the differential ion flux (current) measurements between altitudes 1100-1400 km, the inclination of s/c trajectories is below  $25^\circ$  (below  $29^\circ$  for T70) and similar conclusion applies there: horizontal components of the flux (current) has more influence on the measured projection. The direction of the ion flux is governed by the direction of electric field and the ion-neutral collision frequency, it is expected to be primarily horizontal below 1350 km altitude [Cui *et al.*, 2010]. On the dayside, positive ions dominate and thus

the direction of  $\mathbf{F}_{\text{diff}}$  is expected to be aligned with the positive ion flux, but for the terminator and nightside regions the charge densities of positive and negative ions become comparable and it is currently not possible to separate the fluxes along the s/c trajectory.

### 3.1 Uncertainties

The derived differential ion flux and the neutral wind speeds are directly related to the total ion charge density and the measured electron density. A minimum detection threshold of  $200 \text{ cm}^{-3}$  was introduced to remove uncertainties in the measured electron densities.

It must be stressed that the presented measurements are all along Cassini's trajectory. As such they represent projections on the s/c velocity direction ( $\hat{\mathbf{v}}_{\text{sc}}$ ) and give therefore a minimum constraint on the derived quantities. The measurement error of the LP currents and densities is 10% due to the instrument noise level. The mean ion masses are ultimately derived from the relative abundancies (IBS and ELS) which are systematically affected by the ion velocities and the uncertainties are expected to be  $< 15\%$  [Crary *et al.*, 2009; Wellbrock *et al.*, 2013].

## 4 Summary and Conclusions

The investigation of the observed discrepancy between the apparent total ion charge densities and electron densities in the RPWS/LP data from 55 flybys of Titan's ionosphere below 1400 km altitude showed that it cannot be explained with effects other than the differential ion flux due to ion drifts along the spacecraft trajectory. Ion drift speed measured by Crary *et al.* [2009] and modelled by Müller-Wodarg *et al.* [2008] are insufficient to explain the measured differential ion flux presented in this study. Additionally, the previously derived ion drift speeds were also insufficient to explain the discrepancy between the measurements and the ion transport model by Cui *et al.* [2010] as well as the T70 analysis results by Ågren *et al.* [2012], which both required ion velocities on the order of a few km/s. Based on *in-situ* measurements of mean ion masses, neutral densities and magnetic field, Titan's ionosphere is divided by altitude into three regions:

1. Above 1600 km, dominated by the  $\mathbf{E} \times \mathbf{B}$ -drifting ions
2. 1100-1600 km (dynamo region), collisions with neutrals in the presence of electric and magnetic fields force the ions to drift in opposite directions ( $\perp \mathbf{B}$ ). Positive ions move faster than negative, inversely proportional to the ratio between their respective mass/charge parameters
3. Below 1000-1100km, ions follow neutral winds. Upper limit decreases with increasing electric field.

In the region 3 (below 1100 km altitude), the differential ion flux translates into neutral wind speeds that consistently average to 0.5-1.5 km/s on the dayside and 1.5-2.5 km/s on the nightside but can be as high as 5.3 km/s as seen during the T70 flyby (Figure 8).

North polar region of the ionosphere has the most variable measured ion drifts and strongest measured neutral winds, which supports the enhanced influence of the Kronian magnetospheric plasma flow in this region in agreement with the flow direction in the two-fluid MHD simulation by

*Ma et al.* [2011]. Similar effect is expected on the south polar region of Titan's ionosphere but cannot be verified presently due to poor flyby coverage.

Manuscript

## Figures

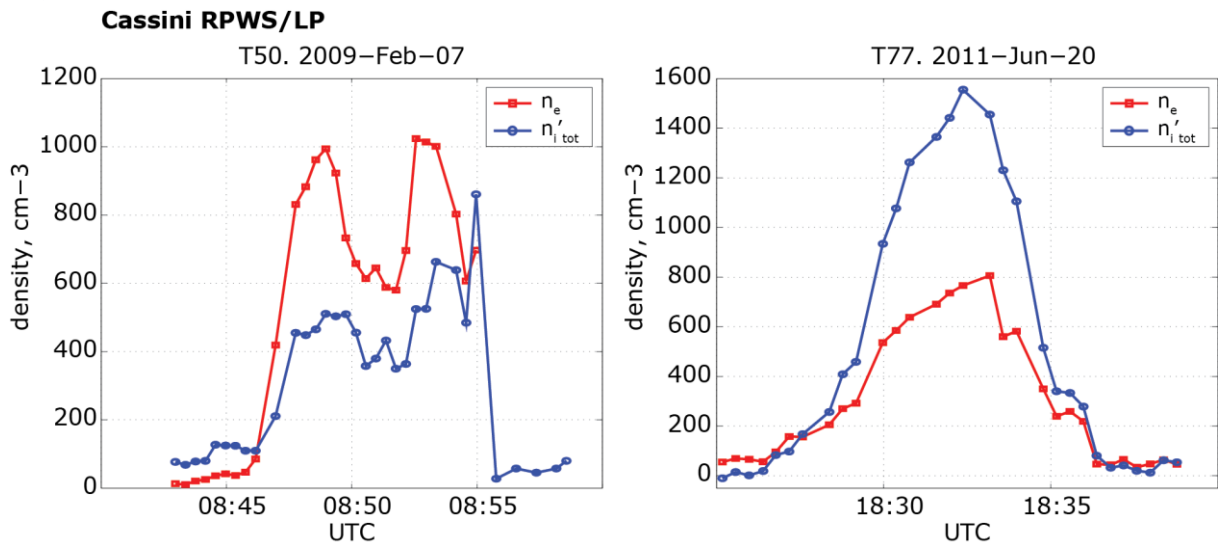


Figure 1. Ion drift effecting the total measured ion charge densities (compared to electron densities) during T50 and T77. T50 is an example of a tailwind ion drift and T77 of a headwind ion drift along the s/c trajectory.  $n'_{tot} = n_+ - Z_- n_-$  is the total ion density in stationary plasma (Equation ( 7 )).

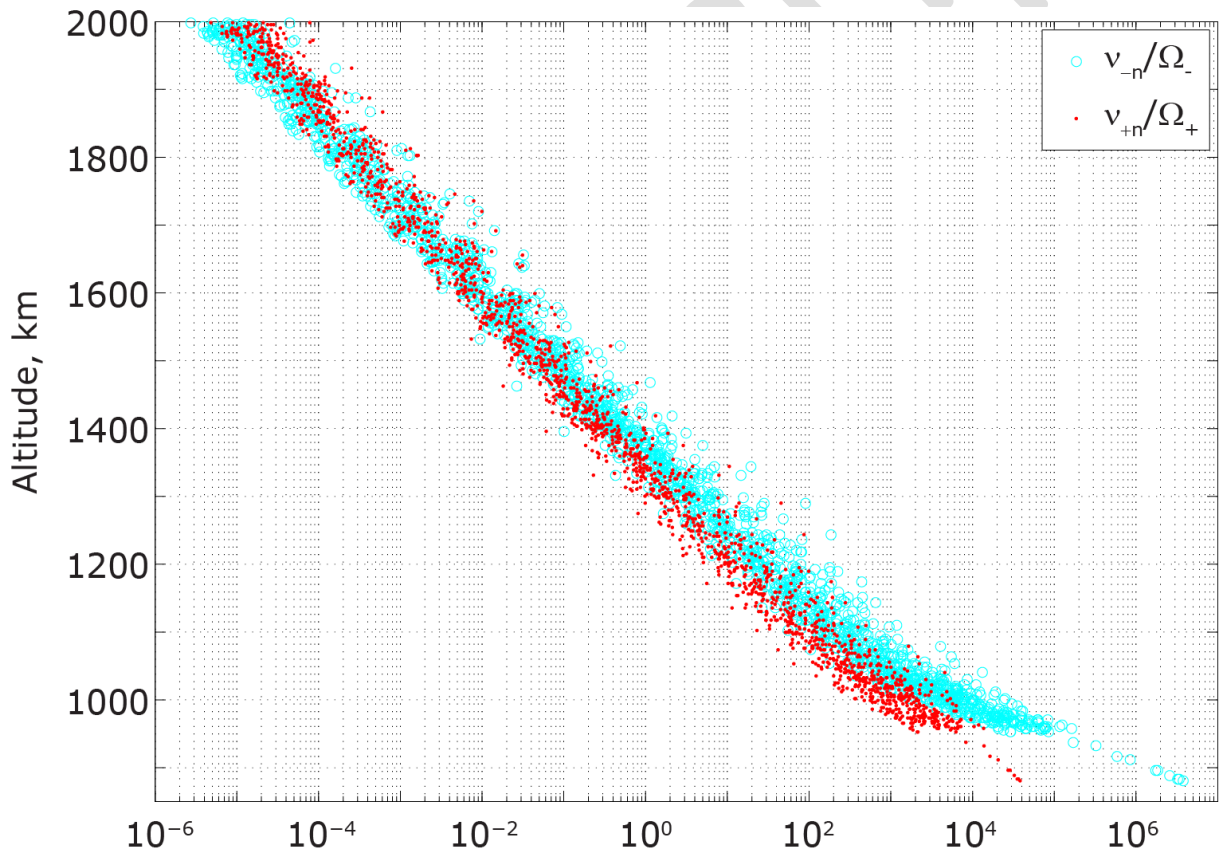


Figure 2. Collision to gyrofrequency ratios, derived from in-situ measurements, for positive (red dots) and negative (blue circles) ions. The difference in ratios below 1400 km altitude is due to gyrofrequencies, the collision frequencies are on the same order of magnitude.

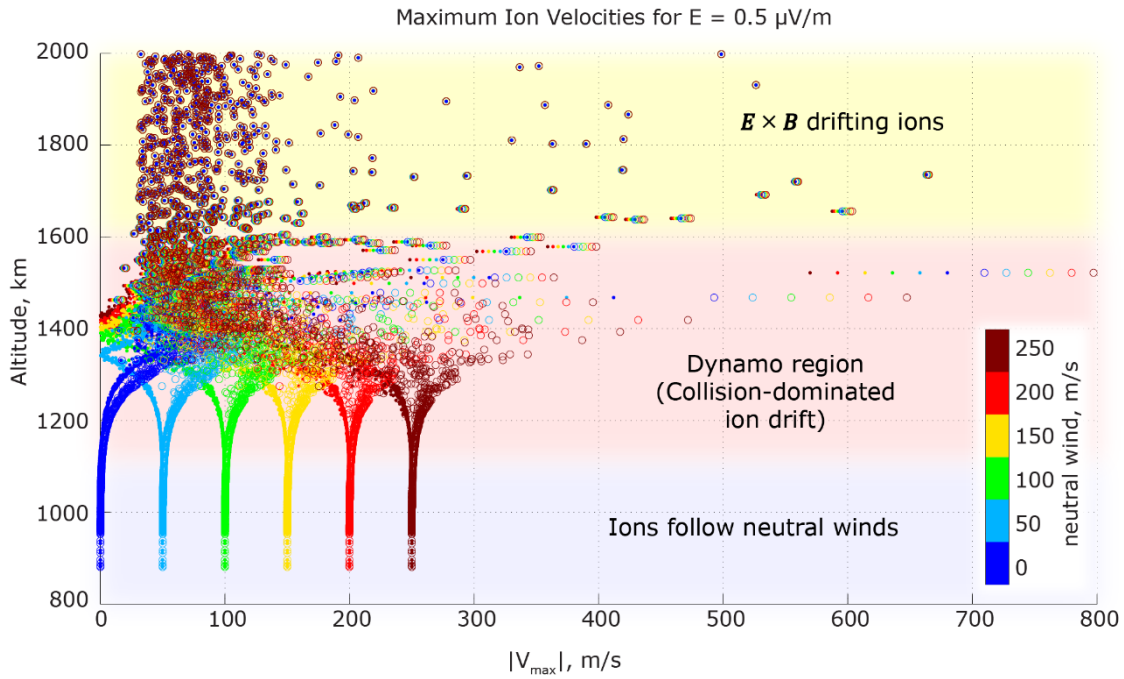


Figure 3. Color-coded: Maximum ion speed dependence on altitude and neutral winds for lower limit of  $E = 0.5 \mu\text{V}/\text{m}$ , calculated from Eq. (10) with  $E \parallel v_n$ . Dots and circles represent negative and positive ion velocities, resp. Simulated neutral winds of 0-250 m/s demonstrate how the ions follow the neutrals in the collision-dominated region. At 1300-1400 km altitude there may be a stagnation region ( $|V_{\text{max}}| = 0$ ) for either positive or negative ions (negative here), given the opposite directions of the neutral winds and ion drifts (also proposed by Cravens et al. [2010a]).

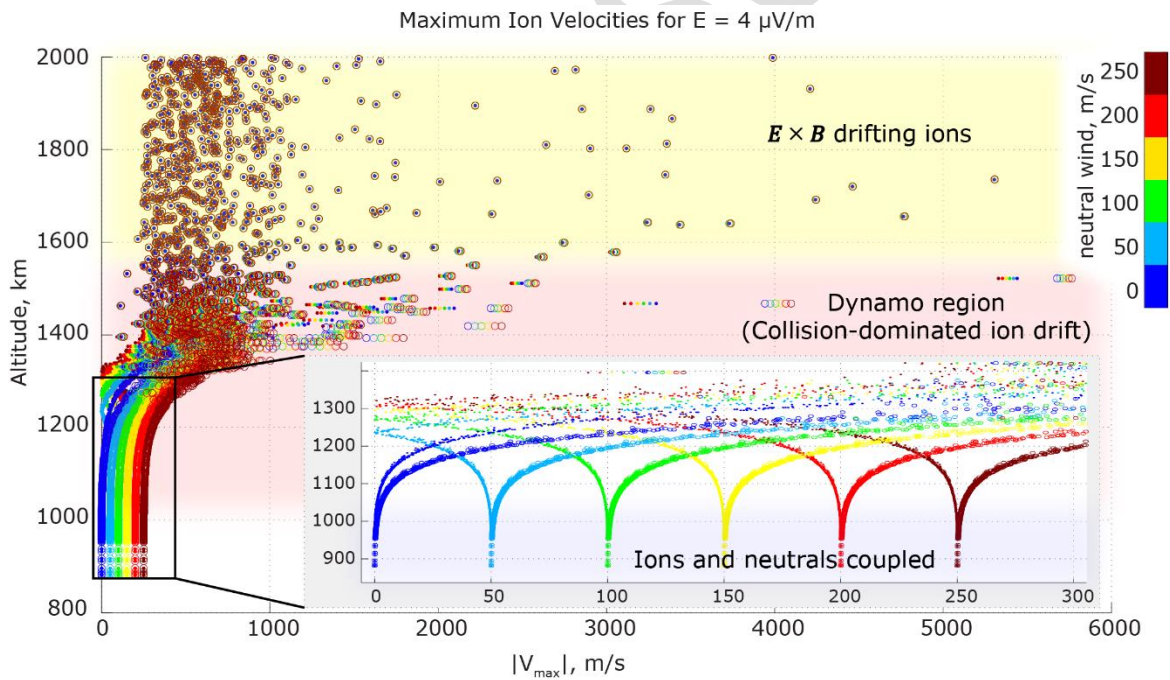


Figure 4. Same as Figure 3 but for  $E = 4 \mu\text{V}/\text{m}$ .

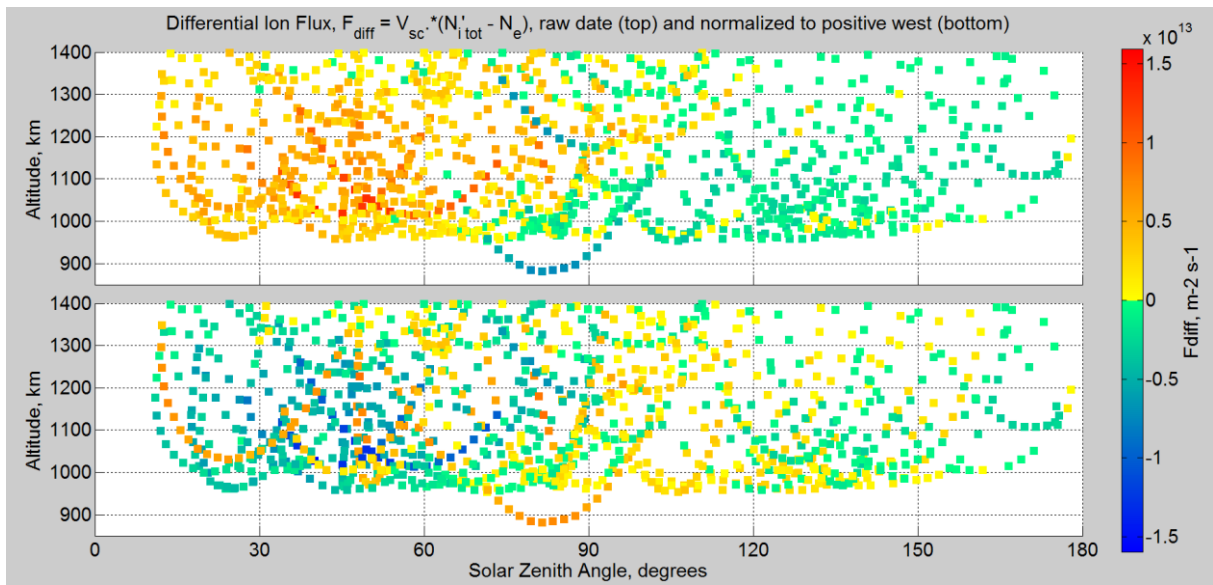


Figure 5. Differential Ion Flux plotted in Altitude vs Solar Zenith Angle, raw data (panel a) and normalized to positive direction west (panel b).

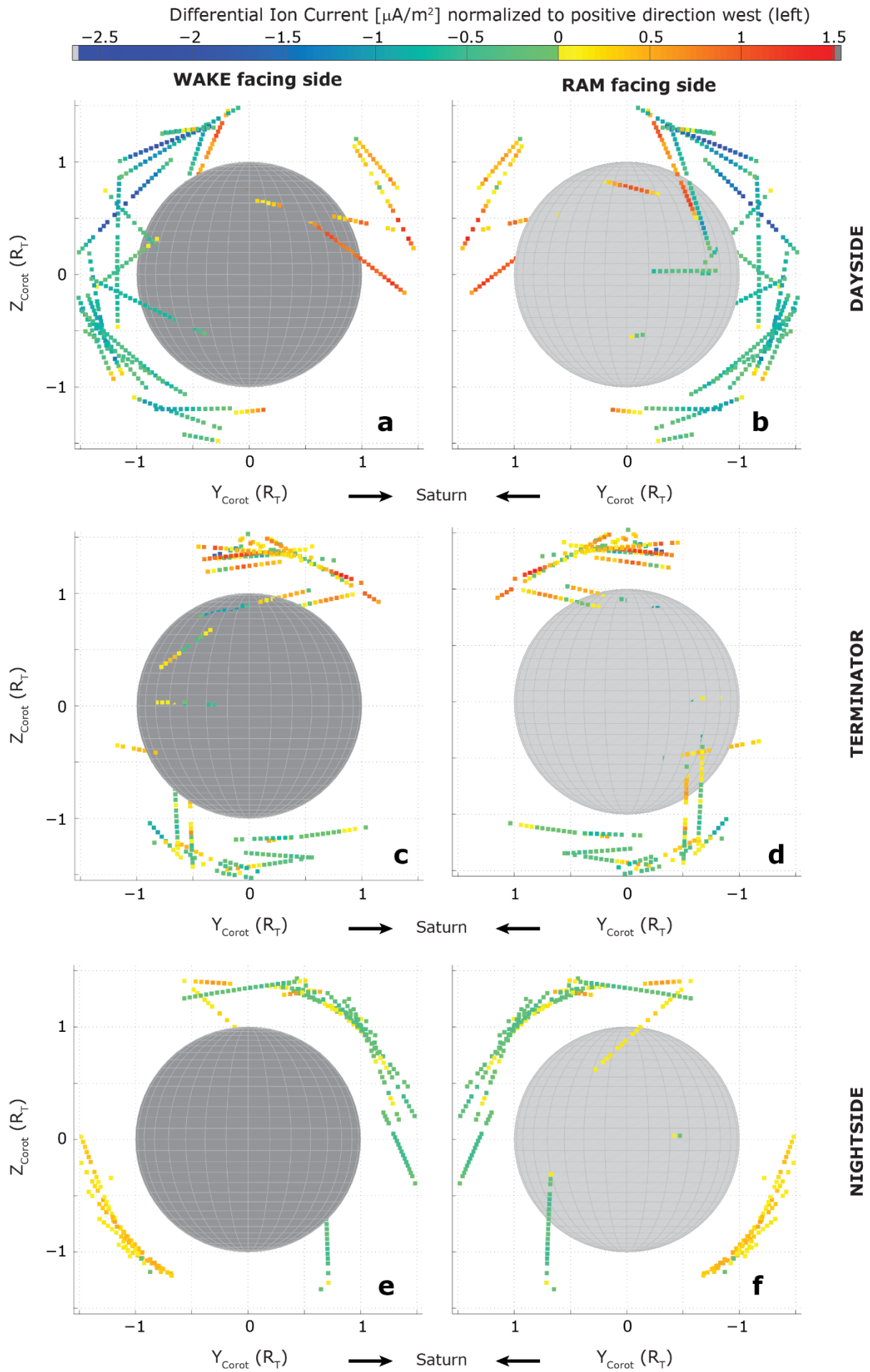


Figure 6. Differential Ion Current in Titan's ionosphere below 1400 km altitude, divided into dayside ( $SZA < 70^\circ$ , panels **a** and **b**), terminator ( $70^\circ < SZA < 110^\circ$ , panels **c** and **d**), nightside ( $SZA > 110^\circ$ , panels **e** and **f**), corotational plasma wake (panels **a**, **c** and **e**) and corotational plasma ram (panels **b**, **d** and **f**). Corotational coordinate axis in each panel are defined with  $\hat{x}$  along the Saturn's magnetospheric plasma flow,  $\hat{y}$  towards Saturn (out of the figure in panel **a**, into the figure in panel **b**), and  $\hat{z} = \hat{x} \times \hat{y}$ . Each data point corresponds to a measurement. Colour shows the direction of the flux mapped to Titan's reference frame, positive westward. Please note a different colour-scale than in Figure 5.

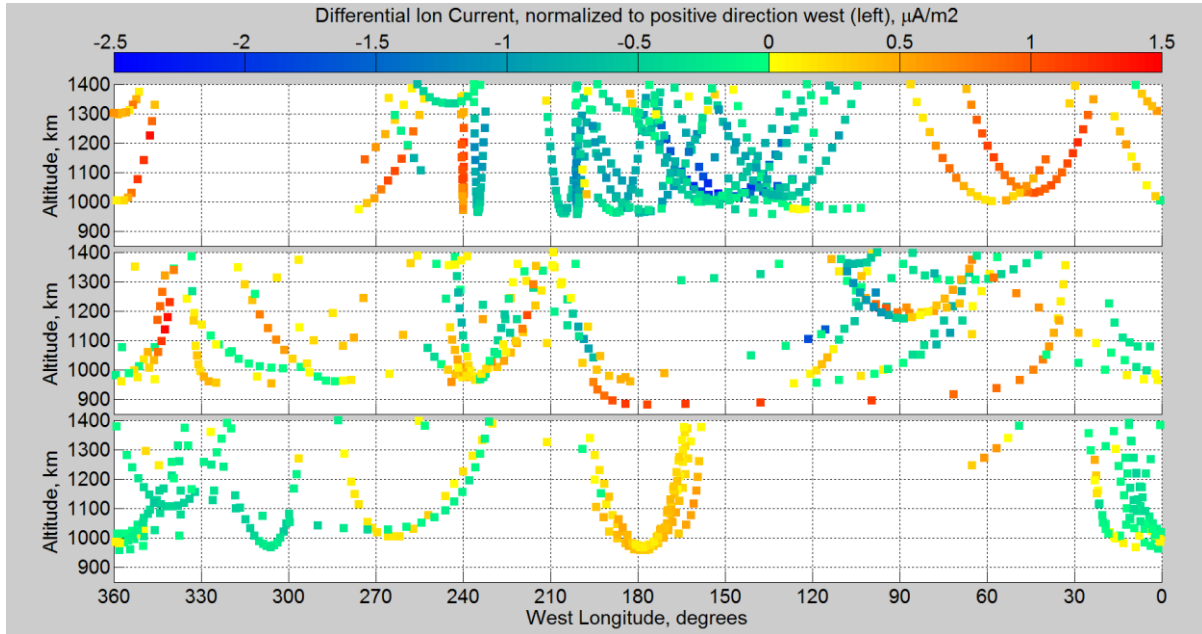


Figure 7. Same as Figure 6 but in altitude vs west longitude coordinates (Cassini always flies right to left), split into day (panel **a**,  $SZA < 70^\circ$ ), terminator (panel **b**,  $70^\circ < SZA < 110^\circ$ ) and night (panel **c**,  $SZA > 110^\circ$ ) regions. Shaded area indicates the region where the ions are following the neutral winds.

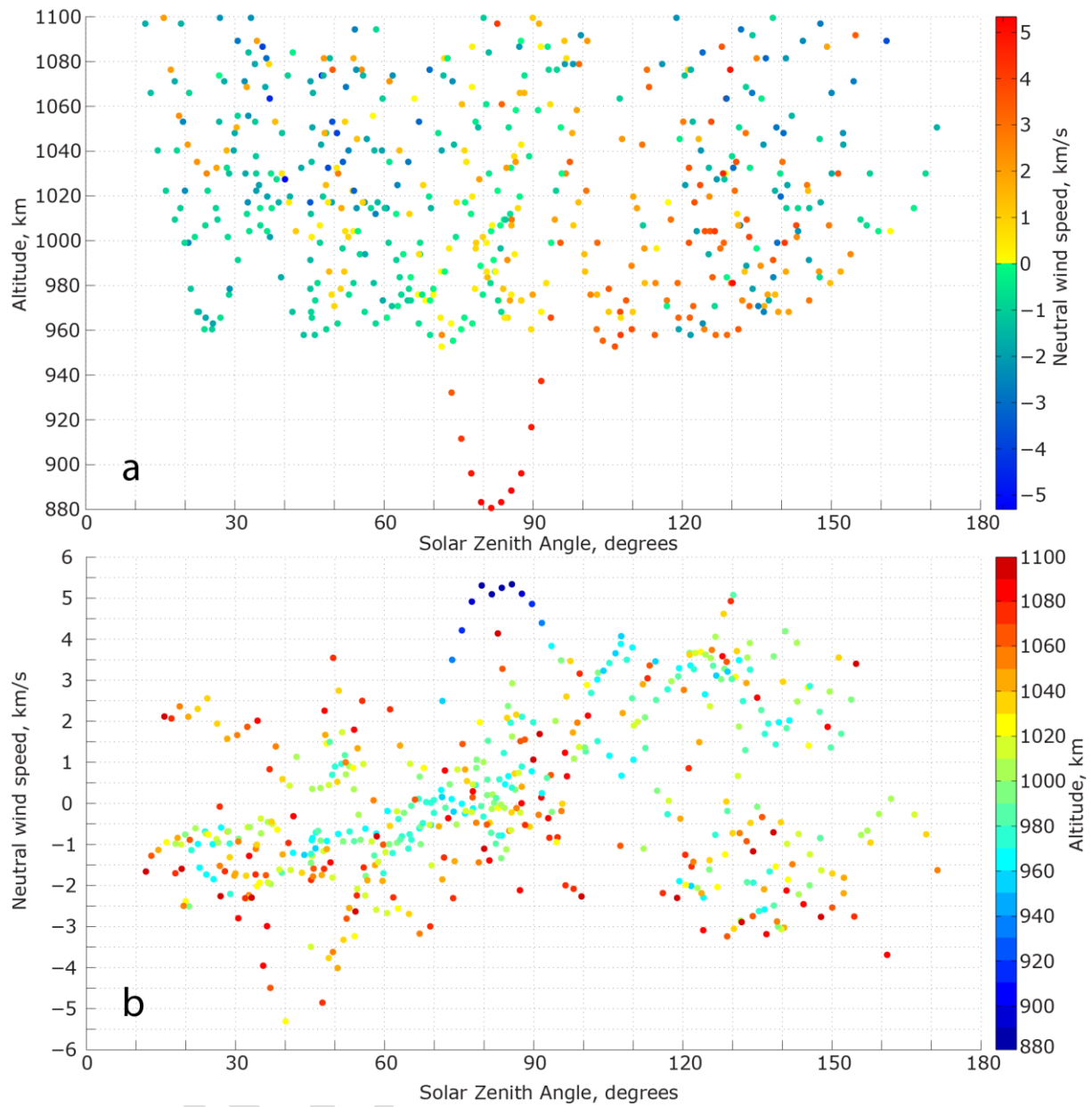


Figure 8. Measured neutral winds below 1100 km altitude, plotted in altitude vs SZA (panel a) and speed along the s/c trajectory (normalized to positive westward) vs SZA (panel b).

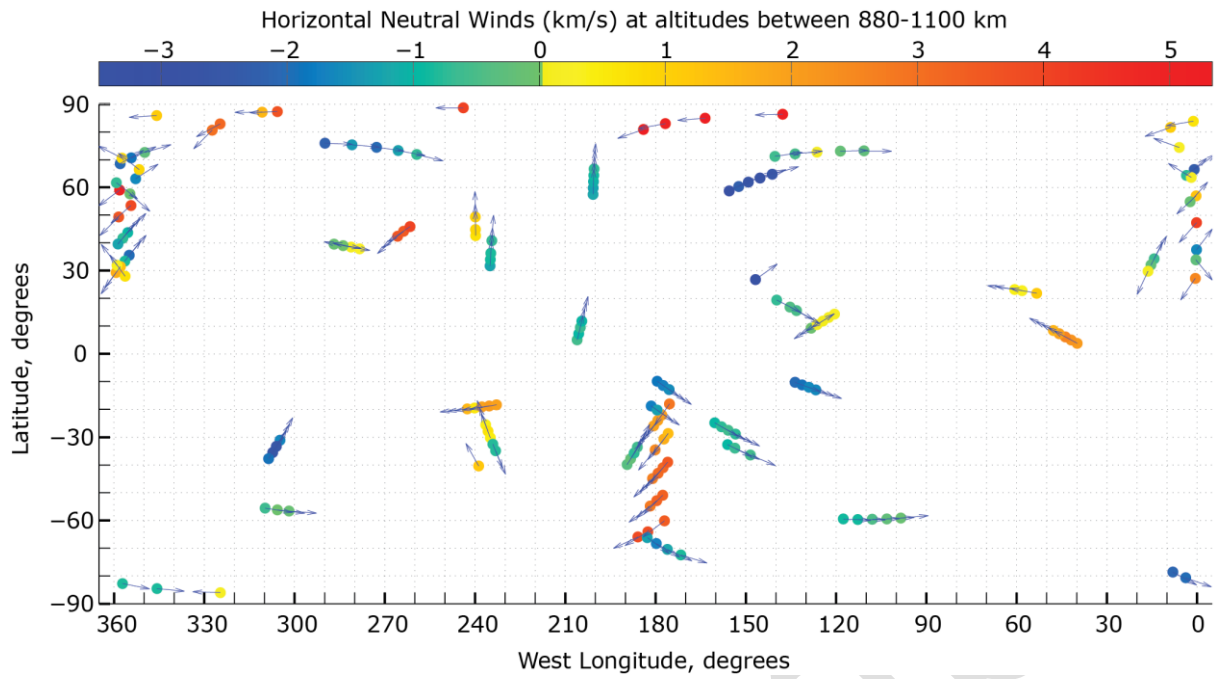


Figure 9. Map of neutral winds along the horizontal (within 5°) parts of the Cassini trajectories. Only datapoints in the immediate vicinity of CA are shown, in altitude range 880-1100 km. Arrows mark the direction of the winds, strength is colourcoded with positive direction westward.

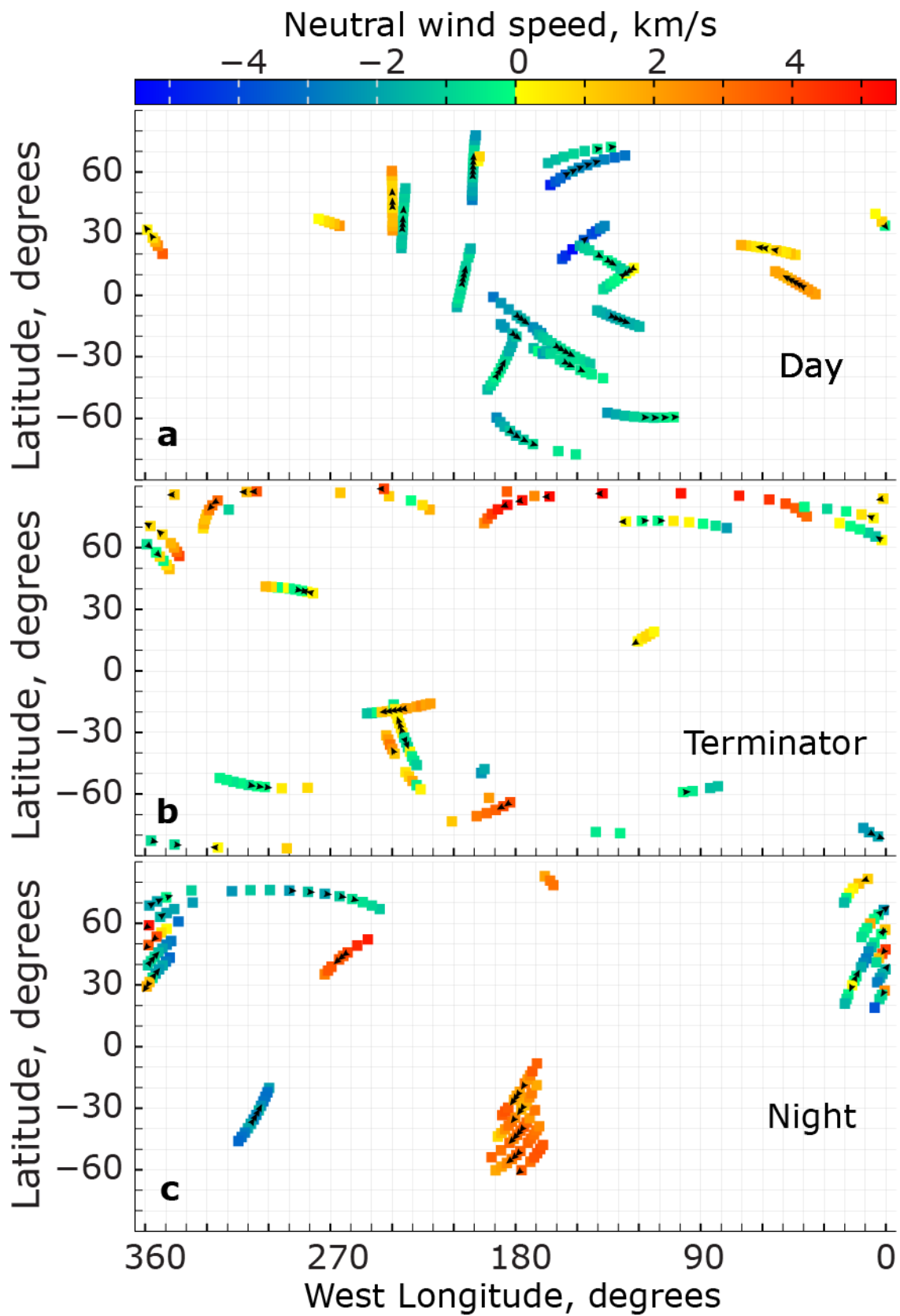


Figure 10. Neutral wind speed below 1100 km altitude for dayside (panel **a**), terminator (panel **b**) and nightside (panel **c**), mapped to Titan latitude and west longitude. Black arrows show the direction of the wind near the closest approach (horizontal within 5%).

## References

- Ågren, K., et al. (2011), Detection of currents and associated electric fields in Titan's ionosphere from Cassini data, *Journal of Geophysical Research*, 116(A4), doi:10.1029/2010ja016100.
- Ågren, K., N. J. T. Edberg, and J. E. Wahlund (2012), Detection of negative ions in the deep ionosphere of Titan during the Cassini T70 flyby, *Geophysical Research Letters*, 39(10), doi:10.1029/2012gl051714.
- Ågren, K., J. E. Wahlund, P. Garnier, R. Modolo, J. Cui, M. Galand, and I. Müller-Wodarg (2009), On the ionospheric structure of Titan, *Planetary and Space Science*, 57(14-15), 1821-1827, doi:10.1016/j.pss.2009.04.012.
- Banks, P. M., and G. Kockarts (1973), *Aeronomy*, Academic press.
- Coates, A. J., F. J. Crary, G. R. Lewis, D. T. Young, J. H. Waite, and E. C. Sittler (2007), Discovery of heavy negative ions in Titan's ionosphere, *Geophysical Research Letters*, 34(22), doi:Doi 10.1029/2007gl030978.
- Coates, A. J., A. Wellbrock, G. R. Lewis, G. H. Jones, D. T. Young, F. J. Crary, J. H. Waite, R. E. Johnson, T. W. Hill, and E. C. Sittler (2010), Negative ions at Titan and Enceladus: recent results, *Faraday Discussions*, 147, 293-305, doi:Doi 10.1039/C004700g.
- Crary, F. J., B. A. Magee, K. Mandt, J. H. Waite, J. Westlake, and D. T. Young (2009), Heavy ions, temperatures and winds in Titan's ionosphere: Combined Cassini CAPS and INMS observations, *Planetary and Space Science*, 57(14-15), 1847-1856, doi:DOI 10.1016/j.pss.2009.09.006.
- Cravens, T. E., et al. (2010a), Dynamical and magnetic field time constants for Titan's ionosphere: Empirical estimates and comparisons with Venus, *J Geophys Res-Space*, 115(A8), doi:Doi 10.1029/2009ja015050.
- Cravens, T. E., et al. (2006), Composition of titan's ionosphere, *Geophysical Research Letters*, 33(7), doi:Doi 10.1029/2005gl025575.
- Cravens, T. E., R. V. Yelle, J. E. Wahlund, D. E. Shemansky, and A. F. Nagy (2010b), Composition and Structure of the Ionosphere and Thermosphere, in *Titan from Cassini-Huygens*, edited by R. Brown, J.-P. Lebreton and J. H. Waite, pp. 259-295, Springer Netherlands, doi:10.1007/978-1-4020-9215-2\_11.
- Cui, J., M. Galand, R. V. Yelle, V. Vuitton, J. E. Wahlund, P. P. Lavvas, I. C. F. Muller-Wodarg, T. E. Cravens, W. T. Kasprzak, and J. H. Waite (2009), Diurnal variations of Titan's ionosphere, *J Geophys Res-Space*, 114(A6), doi:Doi 10.1029/2009ja014228.
- Cui, J., M. Galand, R. V. Yelle, J. E. Wahlund, K. Ågren, J. H. Waite, and M. K. Dougherty (2010), Ion transport in Titan's upper atmosphere, *Journal of Geophysical Research*, 115(A6), doi:10.1029/2009ja014563.
- Dougherty, M. K., et al. (2004), The Cassini Magnetic Field Investigation, *Space Science Reviews*, 114(1-4), 331-383, doi:10.1007/s11214-004-1432-2.

Edberg, N. J. T., K. Ågren, J. E. Wahlund, M. W. Morooka, D. J. Andrews, S. W. H. Cowley, A. Wellbrock, A. J. Coates, C. Bertucci, and M. K. Dougherty (2011), Structured ionospheric outflow during the Cassini T55–T59 Titan flybys, *Planetary and Space Science*, 59(8), 788-797, doi:10.1016/j.pss.2011.03.007.

Fahleson, U., Falthamm, C. G., and A. Pedersen (1974), Ionospheric Temperature and Density-Measurements by Means of Spherical Double Probes, *Planetary and Space Science*, 22(1), 41-66, doi:10.1016/0032-0633(74)90122-6.

Galand, M., R. Yelle, J. Cui, J. E. Wahlund, V. Vuitton, A. Wellbrock, and A. Coates (2010), Ionization sources in Titan's deep ionosphere, *J Geophys Res-Space*, 115(A7), doi:10.1029/2009ja015100.

Gurnett, D. A., et al. (2004), The Cassini radio and plasma wave investigation, *Space Science Reviews*, 114(1-4), 395-463, doi:10.1007/s11214-004-1434-0.

Lavvas, P., et al. (2013), Aerosol growth in Titan's ionosphere, *Proceedings of the National Academy of Sciences of the United States of America*, 110(8), 2729-2734, doi:10.1073/pnas.1217059110.

Ma, Y. J., et al. (2011), The importance of thermal electron heating in Titan's ionosphere: Comparison with Cassini T34 flyby, *Journal of Geophysical Research*, 116(A10), doi:10.1029/2011ja016657.

Magee, B. A., J. H. Waite, K. E. Mandt, J. Westlake, J. Bell, and D. A. Gell (2009), INMS-derived composition of Titan's upper atmosphere: Analysis methods and model comparison, *Planetary and Space Science*, 57(14-15), 1895-1916, doi:10.1016/j.pss.2009.06.016.

Mandt, K. E., et al. (2012), Ion densities and composition of Titan's upper atmosphere derived from the Cassini Ion Neutral Mass Spectrometer: Analysis methods and comparison of measured ion densities to photochemical model simulations, *J Geophys Res-Planet*, 117(E10), doi:10.1029/2012je004139.

Medicus, G. (1962), Spherical Langmuir Probe in Drifting and Accelerated Maxwellian Distribution, *Journal of Applied Physics*, 33(10), 3094-3100, doi:10.1063/1.1728574.

Morooka, M. W., J. E. Wahlund, A. I. Eriksson, W. M. Farrell, D. A. Gurnett, W. S. Kurth, A. M. Persoon, M. Shafiq, M. Andre, and M. K. G. Holmberg (2011), Dusty plasma in the vicinity of Enceladus, *J Geophys Res-Space*, 116(A12), doi:10.1029/2011ja017038.

Mott-Smith, H., and I. Langmuir (1926), The Theory of Collectors in Gaseous Discharges, *Physical Review*, 28(4), 727-763, doi:10.1103/PhysRev.28.727.

Müller-Wodarg, I. C. F., R. V. Yelle, J. Cui, and J. H. Waite (2008), Horizontal structures and dynamics of Titan's thermosphere, *Journal of Geophysical Research*, 113(E10), doi:10.1029/2007je003033.

Niemann, H. B., et al. (2005), The abundances of constituents of Titan's atmosphere from the GCMS instrument on the Huygens probe, *Nature*, 438(7069), 779-784, doi:10.1038/nature04122.

Olson, J., N. Brenning, J. E. Wahlund, and H. Gunell (2010), On the interpretation of Langmuir probe data inside a spacecraft sheath, *The Review of scientific instruments*, 81(10), 105106, doi:10.1063/1.3482155.

Rosenqvist, L., J. E. Wahlund, K. Ågren, R. Modolo, H. J. Opgenoorth, D. Strobel, I. Müller-Wodarg, P. Garnier, and C. Bertucci (2009), Titan ionospheric conductivities from Cassini measurements, *Planetary and Space Science*, 57(14-15), 1828-1833, doi:10.1016/j.pss.2009.01.007.

Shebanits, O., J.-E. Wahlund, K. Mandt, K. Ågren, N. J. T. Edberg, and J. H. Waite (2013), Negative ion densities in the ionosphere of Titan–Cassini RPWS/LP results, *Planetary and Space Science*, 84, 153-162, doi:10.1016/j.pss.2013.05.021.

Vuitton, V., P. Lavvas, R. V. Yelle, M. Galand, A. Wellbrock, G. R. Lewis, A. J. Coates, and J. E. Wahlund (2009), Negative ion chemistry in Titan's upper atmosphere, *Planetary and Space Science*, 57(13), 1558-1572, doi:DOI 10.1016/j.pss.2009.04.004.

Wahlund, J. E., et al. (2005), Cassini measurements of cold plasma in the ionosphere of Titan, *Science*, 308(5724), 986-989, doi:10.1126/science.1109807.

Waite, J. H., Jr., et al. (2004), The Cassini Ion and Neutral Mass Spectrometer (INMS) Investigation, *Space Science Reviews*, 114(1-4), 113-231, doi:10.1007/s11214-004-1408-2.

Waite, J. H., Jr., et al. (2005), Ion neutral mass spectrometer results from the first flyby of Titan, *Science*, 308(5724), 982-986, doi:10.1126/science.1110652.

Waite, J. H., Jr., D. T. Young, T. E. Cravens, A. J. Coates, F. J. Crary, B. Magee, and J. Westlake (2007), The process of tholin formation in Titan's upper atmosphere, *Science*, 316(5826), 870-875, doi:10.1126/science.1139727.

Wellbrock, A., A. J. Coates, G. H. Jones, G. R. Lewis, and J. H. Waite (2013), Cassini CAPS-ELS observations of negative ions in Titan's ionosphere: Trends of density with altitude, *Geophysical Research Letters*, doi:10.1002/grl.50751.

Young, D. T., et al. (2004), Cassini Plasma Spectrometer Investigation, *Space Science Reviews*, 114(1-4), 1-112, doi:10.1007/s11214-004-1406-4.